

INFORMATION TO USERS

This manuscript has been reproduced from the microfilm master. UMI films the text directly from the original or copy submitted. Thus, some thesis and dissertation copies are in typewriter face, while others may be from any type of computer printer.

The quality of this reproduction is dependent upon the quality of the copy submitted. Broken or indistinct print, colored or poor quality illustrations and photographs, print bleedthrough, substandard margins, and improper alignment can adversely affect reproduction.

In the unlikely event that the author did not send UMI a complete manuscript and there are missing pages, these will be noted. Also, if unauthorized copyright material had to be removed, a note will indicate the deletion.

Oversize materials (e.g., maps, drawings, charts) are reproduced by sectioning the original, beginning at the upper left-hand corner and continuing from left to right in equal sections with small overlaps. Each original is also photographed in one exposure and is included in reduced form at the back of the book.

Photographs included in the original manuscript have been reproduced xerographically in this copy. Higher quality 6" x 9" black and white photographic prints are available for any photographs or illustrations appearing in this copy for an additional charge. Contact UMI directly to order.

UMI

A Bell & Howell Information Company
300 North Zeeb Road, Ann Arbor MI 48106-1346 USA
313/761-4700 800/521-0600

NOTE TO USERS

The original manuscript received by UMI contains pages with indistinct and/or slanted print. Pages were microfilmed as received.

This reproduction is the best copy available

UMI

Electromagnetic and Optical Characteristics
of Lightning Measured in the Earth's Ionosphere

by

Benjamin Heath Barnum

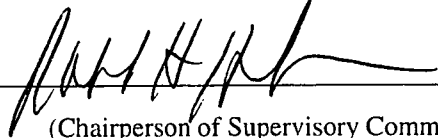
A dissertation submitted in partial fulfillment of
the requirements for the degree of

Doctor of Philosophy

University of Washington

1999

Approved by _____



(Chairperson of Supervisory Committee)

Program Authorized

to Offer Degree _____ Geophysics Program

Date _____ February 5, 1999

UMI Number: 9924072

UMI Microform 9924072
Copyright 1999, by UMI Company. All rights reserved.

This microform edition is protected against unauthorized
copying under Title 17, United States Code.

UMI
300 North Zeeb Road
Ann Arbor, MI 48103

In presenting this thesis in partial fulfillment of the requirements for the Doctoral degree at the University of Washington, I agree that the Library shall make it's copies freely available for inspection. I further agree that extensive copying of this dissertation is allowable only for scholarly purposes, consistent with "fair use" as prescribed by the U.S. Copyright Law. Requests for copying or reproduction of this dissertation may be referred to University Microfilms, 1490 Eisenhower Place, P.O. Box 975, Ann Arbor MI 48106, to whom the author has granted "the right to reproduce and sell (a) copies of the manuscript in microform and/or (b) printed copies of the manuscript made from microform."

Signature 

Date 5-Feb-99

University of Washington

Abstract

Electromagnetic and Optical Characteristics
of Lightning Measured in the Earth's Ionosphere

by Benjamin Heath Barnum

Chairperson of Supervisory Committee: *Robert H. Holzworth*
Space Physics, Department of Geophysics

This dissertation is an experimental study of the upward coupling of lightning electromagnetic waves to the lower ionosphere which was investigated by a rocket flight over a very active thunderstorm near Wallops Island Virginia. The trajectory took the rocket over the thunderstorm to an altitude of 400 km. Along with electric and magnetic field measurements, simultaneous data were obtained from a host of ground instruments including a lightning 3-D mapping system called LDAR, the National Lightning Detection Network and ground optical flash data.

We look at optical flash data and compare cases which were simultaneously recorded by the rocket and ground optical instruments. The optical flashes show the difficulties of distinguishing in-cloud and cloud-to-ground lightning. In a second part of the optical study using the ground based optical measurements, no relation is found between the stroke brightness and the NLDN estimated peak current. The optical study should have important applications to the interpretation of satellite based lightning studies. We also show that the use of the measured rocket VLF electric fields can be used as an aid in distinguishing between cloud-to-ground and in-cloud lightning rocket measured optical flashes.

Lightning produced field aligned electric pulses, which had also been reported on previous rocket experiments, were measured up to 240 km altitudes. The nature of the pulse is carefully analyzed, and the conclusion is that the electric pulse is probably composed of large amplitude vertically polarized waves at higher frequencies which do not produce a unipolar electric field. The pulse is produced by cloud-to-ground strokes but generally not by intra-cloud lightning. This is because much larger vertical electric fields are produced by cloud-to-ground lightning stroke channels.

The electron density profile of the F region ionosphere is deduced from the dispersion of whistler waves measured by the rocket. The results compare very well with the on-board Plasma Probe instrument and ionosonde measurements taken in Bermuda at the time of flight. This is the first time that this method has been used in the lower ionosphere.

The correlation between the electric field of whistler waves in the ionosphere and the ground NLDN measured stroke current is computed for frequencies between 500 Hz to 20 kHz. We find that the highest correlation with NLDN estimated currents is at the lower frequencies. Based on this result and the previous work of Y. Li, [Li, 1993], it should be possible to estimate lightning stroke currents from an orbiting satellite.

In a collaborative effort with Professor Nagano at the Electrical Engineering Department at Kanazawa University, Japan, a new 3-D lightning simulation model is compared with measured data from the rocket. The model calculates the electromagnetic fields from lightning in the ionosphere. The computed wave fields are larger than the measured whistler wave amplitudes, but the model used an estimated ionospheric density. In a later study, we plan to update these results with the new ionosphere density profile estimated in this thesis.

TABLE OF CONTENTS

List of Figures	v
List of Tables	viii
Chapter 1: Introduction	1
Chapter 2: Thunderstorm III Instrumentation	7
2.1 The Thunderstorm III Rocket Experiment	7
2.2 Electric Field Sensors	8
2.3 University of Washington Optical Lightning Detector	11
2.4 Particle Detectors	13
2.5 VLF Search Coils	14
2.6 Fluxgate Magnetometer	14
2.7 Star Imager	15
2.8 Danish Technical University (TUD) Lightning Imager	15
2.9 Utah Plasma Frequency Probe (PFP)	16
2.10 Rocket Flight Chronology	16
2.11 Supporting Ground Instruments	17
2.11.1 National Lightning Detection Network	18
2.11.2 SPANDAR	19
2.11.3 Lightning Detection and Ranging (LDAR)	19
2.11.4 Basic Theory of Operation	21
2.11.5 Ground Electric Field Mills	23

Chapter 3:	The Thunderstorm	25
3.1	Thunderstorm Meteorology and Development	27
3.2	Convective Available Potential Energy (CAPE) and Lightning Flash Rates Based on Cloud Top Height	29
3.2.1	The Wallops Thunderstorm Meteorology	31
3.2.2	SPANDAR radar data	33
3.3	Thunderstorm Electric Fields and Charge Structure	36
3.4	Summary of Cloud-to-Ground Lightning Flashes	39
Chapter 4:	Whistler Waves	41
4.1	Introduction	41
4.2	Theory of Whistler Waves	42
4.3	Changes in Whistler Wave Amplitude with Altitude in the Ionosphere	46
4.4	Electromagnetic Coupling in the Lower Ionosphere	48
4.4.1	Low Altitude D Region Lightning Transients	51
4.4.2	The Effects of Sub-Ionospheric Propagation on Lightning Whistlers	56
4.4.3	ELF Tails from Distant Lightning	58
4.5	Study of Ionospheric Dispersion of Whistlers	61
4.6	In-Situ Determination of the Refractive Index	67
4.7	ELF Energy in Whistler Waves	70
4.8	Whistler Stimulated Lower Hybrid Waves	71
4.9	Correlation of Whistler Wave Amplitude and NLDN Peak Currents	76
Chapter 5:	Field Aligned Electric Pulses	80
5.1	Properties of the Field Aligned Electric Pulse (FAP)	81
5.2	In-cloud and Cloud-to-Ground Lightning Stimulation of the Pulse	88
5.3	Conclusion	88

Chapter 6:	VHF Location of Thunderstorm Lightning Stepped Leader Activity and Lightning Channel Formation During Thunderstorm-III	91
6.1	Introduction	91
6.2	Overview of the LDAR VHF System	93
6.3	Characteristics of Lightning VHF Radiation Producing Triggers	94
6.4	Location of LDAR Electrical Activity	96
6.5	LDAR Stepped Leader Velocities	99
6.6	Location of LDAR VHF Activity Relative to Radar Reflectivity	102
6.7	Comparison of Intracloud and Cloud-to-Ground Lightning Fields Measured in the Ionosphere	103
6.8	Conclusion	108
Chapter 7:	Lightning Optical Experiment	110
7.1	Introduction	110
7.2	Ground and Rocket Optical Instruments	112
7.2.1	Basic Theory of Operation	113
7.3	Scattering and Intensity of Lightning Optical Signal	116
7.4	Analysis of Ground and Rocket Optical Cloud-to-Ground Strokes	119
7.4.1	Estimate of Stepped Leader Velocity from Optical Data	119
7.4.2	Optical Pulse Analysis of CG Strokes	121
7.5	Cloud-to-Ground M Events	123
7.6	Case Study of Cloud to Ground Lightning	128
7.7	Comparison of Rocket Optical, VLF and NLDN flash rates	131
7.8	Optical Brightness and the NLDN Current of Cloud-to-Ground Flashes	132
7.9	Conclusion	135

Chapter 8: 3-D Lightning Wave Simulations 138

- 8.1 Full-Wave Modeling of Lightning EM Fields 139
- 8.2 Model Results and Comparison with Thunderstorm III Measurements . . . 140
 - 8.2.1 Simulations at Different Altitudes at Constant Range 142
 - 8.2.2 Simulations at Different Ranges at a Fixed Altitude 143
- 8.3 Conclusion 145

Chapter 9: Conclusion 147

Bibliography 149

Appendix A: Appendix A: Rocket Optical Instrument 159

LIST OF FIGURES

2.1	The Thunderstorm-III Rocket Payload	10
2.2	Thunderstorm III Rocket Flight	18
3.1	Preflight Upper Air Sounding at Wallops Island	32
3.2	SPANDAR Radar summary of the Wallops Island Thunderstorm	34
3.3	Simple Thunderstorm Dipole Charge Structure	37
4.1	Polarization of Ex and Ey Electric Fields for Whistler Mode Waves	44
4.2	Index of Refraction for Whistler Mode Waves	45
4.3	Change in Lightning VLF Waves Amplitude with Altitude	47
4.4	Change in Lightning VLF Waves with Altitude	49
4.5	Low Altitude (84 km) Lightning Recovery Field	54
4.6	Lightning Stroke Showing the effects of Waveguide cutoff from the North- east Thunderstorm Cell	57
4.7	Distant Lightning Stroke from Florida storm	58
4.8	ELF tail waveforms in strokes from North Carolina	60
4.9	Determination of the whistler dispersion parameter D	63
4.10	Measured Whistler Dispersion D	64
4.11	IRI95 Model Dispersion vs. Measured Whistler Dispersion D	65
4.12	Electron Density Profile During Thunderstorm III	67
4.13	In-Situ measurements of the index of refraction n	69
4.14	Positive CG Lightning with large amplitude ELF waves	71

4.15	An Example of Lower Hybrid Wave Stimulated by the passage of a Whistler	73
4.16	Lower Hybrid Wave Frequencies Calculated for Thunderstorm III	75
4.17	Calculation of NLDN stroke current and VLF whistler electric fields'	77
4.18	Correlation of Whistler Amplitude and NLDN Peak Current	78
5.1	Field Aligned Electric Pulse from lightning strokes	82
5.2	Electric Pulses produced by distant lightning strokes	84
5.3	Electric Pulse measured Electric and Magnetic fields.	85
5.4	Electric Pulse Change with Altitude	86
5.5	Effect of CG and IC lightning strokes on the parallel electric field	89
6.1	LDAR VHF Trigger Activity During the T-III Rocket Flight.	96
6.2	LDAR VHF Triggers Preceding a -CG Flash	97
6.3	LDAR High Altitude VHF Triggers	98
6.4	Histogram of LDAR Stepped Leader Trigger Speed changes with Altitude	100
6.5	SPANDAR 40 dBz radar reflectivity contours and LDAR VHF Locations .	103
6.6	Example of In-cloud pre-stroke lightning activity preceding a CG return stroke	104
6.7	Example of IC Lightning Strokes at High Altitudes	106
6.8	Example of CG Lightning Stroke	107
7.1	Percent of light exiting upper surface of a cylindrical cloud vs. height of source	118
7.2	Rocket VLF Electrical and Optical measurements of a CG stroke	120
7.3	Ground Optical data of a Cloud-to-Ground stroke near Wallops Island VA. .	122
7.4	Summary of Ground and Rocket Optical pulse durations (FWHM)	123
7.5	Ground and Rocket optical CG stroke and associated IC event	124
7.6	M-Event occurring during a multiple stroke CG Flash.	125
7.7	A two stroke CG flash, with an M event during the second stroke	126

7.8	Optical Flash of Negative CG Lightning and CG triggered IC activity . . .	130
7.9	Relationship between Lightning stroke brightness and NLDN peak current .	134
8.1	Computer Simulation of Lightning Whistler Wave	141
A.1	Rocket Optical Instrument	161
A.2	Rocket Optical Circuit Diagram	162

LIST OF TABLES

2.1	T-III Electric-Field Channels	11
2.2	T-III AC Fluxgate Magnetometer Channel List	14
2.3	Electric Field Mill Locations at Wallops Island	24
3.1	Summary of NLDN CG Flash Order and Average Flash Stroke Currents	40
4.1	D-Region Transient Vertical Electric Field Decay Observations	55
6.1	LDAR Stepped Leader Velocities with Altitude	101
6.2	Cloud-to-Ground Channel Lengths determined by LDAR	107
7.1	Summary of Lightning Flash Rates	132
8.1	Summary of Kanazawa Model E_x Electric Fields Compared with Thunderstorm III at different altitudes	143
8.2	Change in Whistler Electric Field E_x with Range	144

ACKNOWLEDGMENTS

The author wishes to express sincere appreciation for the support of the Department of Geophysics. The graduate students of the Space Sciences Department who were always ready to tackle any problem that led to new ideas and thinking. Many hours were spent discussing data, analysis and approaches with my office mates who have give their full support in my effort. John Williams has been tireless in looking over my ideas and editing, Andrew Johnson has given valuable advice about data analysis and modeling, Kirsten Lorentzen has given a lively challenge to many of the ideas we have discussed. No project of this size gets very far without the aid of extensive computer analysis. Jeff Ross has dedicated many hours of his time to the data analysis and software development during this project. To get data, good instruments must be designed, and to this effort John Chin has made a huge contribution to this rocket experiment in his design of the optical instruments and countless hours during the rocket integration. His senior expertise has made possible what other engineers deem impossible. Professor Michael McCarthy and Professor John Sahr agreed to be on my reading committee. They have been supportive in their suggestions and discussions. I am grateful to have them as committee members. Deepest appreciation to Professor Holzworth for support and leadership throughout these years and his guidance in the Graduate process. Through all of the midnite hours, Katy has kept me motivated and made suggestions as I wrote. To my mother, who always showed us by her example the value of ideas and learning, and to Ted, who works by the quote over his desk from Sherlock Holmes: "Assume nothing Watson!".

Chapter 1

INTRODUCTION

I have been struck by lightning and I am alive. **Gretel Ehrlich**, *A Match to the Heart, one Woman's Story of Being Struck by Lightning* -1984.

This thesis documents the principal scientific work analyzing the effects of lightning on the lower and middle ionosphere, using the data from the Thunderstorm III rocket experiment, launched over an active thunderstorm off the coast of Wallops Island, Virginia. This experiment is the continuation of recent research using rockets to study the effects of thunderstorms on the lower ionosphere. In the following chapters, we will look at the results from the Thunderstorm III rocket experiment.

The Thunderstorm III rocket experiment had the most sophisticated and diverse array of instruments ever flown over a thunderstorm. This rocket flight was the continuation of the research done by its predecessor, Thunderstorm II which was launched in 1988 [Kelley *et al.*, 1990; Li, 1993]. These types of direct rocket over-flights of thunderstorms were first begun in a series of research campaigns made in 1981 through 1985 by Cornell University and Penn State University in conjunction with several other universities and NASA. Some of the main rocket campaigns were ThunderLo and ThunderHi and WIPP [Kelley *et al.*, 1985; Siefiring, 1987; Li, 1993]. It was already known that lightning produces up-going electromagnetic waves in the ionosphere known as whistler waves [Cain *et al.*, 1961; Helliwell, 1964]. Surprising results from Thunderstorm II showed that the whistler waves could also stimulate other types of plasma mode waves in the ionosphere.

The data from these flights showed that lightning produced unexpectedly large vertical

transient electric fields in the lower ionosphere which were aligned parallel to the Earth's magnetic field, \vec{B}_0 . This field aligned electric pulse lasted several milliseconds and preceded the arrival of the 1 to 10 kHz whistler wave energy at the rocket [Kelley *et al.*, 1990].

Thunderstorm III was instrumented to directly measure these pulses. The rocket payload carried particle instruments to detect precipitating electrons, or electrons that would be accelerated by the pulses. The electric and magnetic field instruments used higher sampling frequencies and a new 4 MHz high sample rate digital waveform capture instrument was specially designed to record the high frequencies that might make up these pulses.

Further research indicated that lightning could also cause electrons in the magnetosphere to precipitate and thereby change the conductivity in the lower ionosphere. There is also evidence that lightning could directly affect the electron density in the lower ionosphere, causing changes in sub-ionospheric radio propagation at low frequencies [Voss *et al.*, 1984; Dowden and Adams, 1993].

In the ionosphere, lightning generates strong electromagnetic waves known as whistler waves. There is direct evidence that suggests these waves may induce electrons to precipitate from the magnetosphere to the lower ionosphere [Goldberg *et al.*, 1987; Voss *et al.*, 1984]. Models suggest that lower ionosphere electrostatic and electromagnetic waves from lightning may also cause heating of the electrons and localized changes in the electron density [Taranenko *et al.*, 1993]. The most dramatic discovery of upward coupling of thunderstorms into the lower ionosphere were the confirmations of upward discharges known as Sprites and Jets [Sentman and Wescott, 1993]. Ongoing ground based campaigns are currently underway to investigate a number of new phenomena related to these types of discharges, including Extremely Low Frequency emissions (ELF), and a current pulse from the discharge region of the Sprites¹ [Dowden *et al.*, 1996; Marshall *et al.*, 1998].

Thunderstorm III rocket over flew two active thunderstorms and was equipped with

¹ Sprite activity has now been confirmed during daytime thunderstorms, and from negative and positive polarity cloud-to-ground lightning. Mark Stanley NMIT personal communication

electric and magnetic field instruments, optical detectors, imaging system and electron particle instruments. The rocket apogee was within 100 km of two storm cells each with high lightning flash rates, resulting in more than 700 individual NLDN (National Lightning Detection Network) located strokes being detected during the 10 minute flight. A great deal is known about many of the lightning strokes in the thunderstorm that was over flown. The lightning stroke currents, location, and precise time down to ± 1 ms are known. From the ground based instruments, the location of the electrical activity in the thunderstorm and the approximate lightning channel paths of some of the strokes has been determined. Electric fields were measured using a sampling frequency of 4 MHz, and magnetic and electric fields were recorded continuously at a rate of 40 kHz. The amount of high quality data that was recorded on the rocket during the 10 minute flight consists of 6 CD ROMs recorded from 4 separate high speed telemetry links.

In Chapter 6 the thunderstorm lightning electrical activity is looked at using a VHF 3-D time of arrival mapping system called LDAR (Lightning Detection and Ranging). This system detects the formation of lightning channels by using the radiation that is produced during the movement of electrical charge in the thunderstorm. LDAR gives a detailed look at the location of the overall electrical activity in the thunderstorm which can be directly related to the meteorologic and radar images of the storm. The LDAR data also show the formation in in-cloud lightning channels and, in some cases, the cloud-to-ground lightning channels. These data gave valuable information about the orientation and length of the lightning channel which we argue in Chapter 5, is directly related to the occurrence of the so called electric pulse [Kelley *et al.*, 1990]. In the processes related to lightning channel formation, the LDAR data show that the initial lightning channel, known as the stepped leader, appears to propagate at higher velocities at lower altitudes. A similar result was recently reported by D. Proctor using a similar 3-D VHF system in South Africa [Proctor, 1997]

The rocket experiment measured hundreds of upward propagating whistler waves. In Chapter 4 the wave amplitudes, and changes with altitude are compared with the ground

based measurements of lightning strokes. The effects of sub-ionospheric propagation of the lightning electromagnetic wave energy are also seen to change with distance and with the polarity of the lightning stroke. Several forms of whistler stimulated emission were measured during the rocket flight, believed to be lower hybrid electrostatic waves and something unexpected, which seem to be previously unreported harmonic emissions related to the height of the lower ionosphere.

One of the big differences between Thunderstorm II and Thunderstorm III was the magnitude of the measured electric fields from lightning strokes. The fields that were measured on Thunderstorm III were only about one tenth the magnitude of the Thunderstorm II fields. It seemed likely that the differences in the electric fields were the result of much higher electron densities in the ionosphere during the Thunderstorm III flight. A problem developed with the determination of the ionosphere electron density profile during the Thunderstorm III experiment. The onboard instrument which was designed to directly measure electron density failed at an altitude of 240 km, well below the F region peak density. In Chapter 4 the rocket measured lightning whistler waves are used to reconstruct the electron density profile. The method proved very successful, and the results compared very well to the measured densities near 240 km. The reconstructed electron density helps explain some of the differences in the electric field amplitudes between the experiments.

We also look for a relationship between the measured whistler wave amplitudes at different frequencies and the National Lightning Detection Network (NLDN) estimated lightning stroke currents. In an earlier comparison made by Yaqi Li [Li, 1993], a correlation between the whistler amplitudes at 1 to 3 kHz was found with the NLDN currents. The results of this study also show a similar relationship.

In Chapter 7, the results of the first ever simultaneous measurements of lightning strokes made by the optical sensor located at Wallops Island and the Thunderstorm III rocket. To date, there have been no other such studies published. Our results show that many of the in-cloud lightning strokes are often not detected optically on the ground but can appear very

bright at the rocket. Secondly, we show that many of the cloud-to-ground lightning strokes were followed by in-cloud strokes which were not seen by the ground optical sensor. The following in-cloud flash was often much brighter optically than the cloud-to-ground lightning at the rocket because it occurred in the mid and high levels of the thunderstorm cloud.

Current research efforts are underway to try and relate thunderstorm severity such as precipitation rate and radar reflectivity, to the observed optical flash rates from orbiting optical detectors [Baker *et al.*, 1995]. We measure the lightning optical flash rate at the rocket and compare it to the stroke rates calculated from the National Lightning Detection Network (NLDN) and the rate based on the number of lightning whistler waves measured by the rocket electric field instruments. The rocket flash rates are 3 to 5 times higher than the NLDN stroke rates, presumably because of additional in-cloud lightning flashes seen at the rocket. Based on the meteorologic data, we estimated a standard index used to compute thunderstorm severity, known as CAPE (Convective Available Potential Energy). The conclusion is that the CAPE index is a crude estimator of lightning flash rate, and not one that can be related directly to space observed flash rates of thunderstorms. This chapter should be particularly useful for the analysis of lightning flash rates using satellites. It is suggested that electric or magnetic field measurements of the whistler waves, in conjunction with the optical flash measurements made by satellites, might allow a way to better discriminate between lightning flashes from cloud-to-ground and in-cloud lightning.

Earlier thunderstorm rocket experiments reported an unpredicted field aligned electric pulse in the ionosphere caused by lightning strokes [Kelley *et al.*, 1990, 1985]. The field aligned pulse was powerful enough to accelerate electrons in the ionosphere to 30 times their normal thermal velocity. This pulse was also seen in the electric field data on Thunderstorm III. How this pulse changes in form with altitude and what types of lightning produce this stroke are examined in Chapter 5.

In Chapter 8, a new 3-D full wave electromagnetic computer code, developed at the electrical engineering department of Kanazawa University, Japan was used to model the

lightning stroke electric fields at different altitudes above the storm [*Miyamura et al.*, 1996]. This is the first ever full wave simulation made of lower ionosphere electromagnetic waves from lightning with direct comparison to measured data .

The model was used to compute the whistler electric fields at different altitudes in the ionosphere using the NLDN measured location and lightning stroke currents of observed events during the rocket flight. The measured and modeled wave electric fields are compared, and it is shown that the electron density profile plays a critical role in the modeling results when applied to the upward coupling of lightning electromagnetic waves. The model is capable of simulating the lightning whistler waves that were measured on the rocket and the sub-ionospheric waveforms, including tweek atmospherics. Suggestions for further improvements to the model are made, as are adjustments to the model inputs based on the revised electron density profile. The research using the computer model is continuing in a collaborative effort between the US and Japanese research groups.

Chapter 2

THUNDERSTORM III INSTRUMENTATION

2.1 The Thunderstorm III Rocket Experiment

This chapter will describe the instrumentation of the Thunderstorm III sounding rocket which was launched over an active thunderstorm during the evening of September 1, 1995 at a local time of 9:13 p.m.. The rocket made measurements in the lower ionosphere between 100 and 400 km altitude near Wallops Island, VA.

The main goal of the flight was to investigate the lightning generated electromagnetic pulse in the ionosphere. Electric field measurements were made from DC, Extremely Low Frequency (ELF ≤ 3 kHz), Very Low Frequency (VLF 3-30 kHz) up to High Frequency (HF 1.2 MHz). The Thunderstorm III had a specially designed set of experiments to measure the lightning precursor pulses that had been detected on Thunderstorm II [Kelley *et al.*, 1985, 1990]. The rocket experiment looked for direct evidence of electron precipitation and wave particle interactions due to lightning over active thunderstorms. Wave induced particle precipitation had been previously reported by other researchers but never directly correlated with lightning [Imhof *et al.*, 1985; Goldberg *et al.*, 1987].

This thesis emphasizes the investigation of the ELF and VLF whistler waves produced by lightning. In particular we wish to relate the types of lightning responsible for the observed wave energies, and to estimate the energy of the VLF and ELF waves at different altitudes in the lower ionosphere. We will also investigate the electron density and propagation of the whistler waves in the lower ionosphere and the properties of the electric pulse. In this section we will emphasize the instruments that have been used in our study.

The ground based instruments such as LDAR have been invaluable in the understand-

ing of the lightning events which took place during the flight and will be described in the following chapters. Here we focus on the rocket instruments which recorded optical, magnetic and electric fields. All of the recorded experiment data have been assigned an arbitrary time based on the rocket launch time. The convention used in this thesis, unless otherwise noted, is that times are given in seconds relative to the launch time of 01 hours 13 minutes and 0.0 seconds Universal Time Coordinate (UTC). For example, rocket apogee was at 311 seconds, or 01:18:00 UTC.

2.2 Electric Field Sensors

The electric-field measurements on Thunderstorm III were made using a set of 6 booms mounted on the rocket payload as shown in Figure 2.1. The set of 6 booms gives 3-axis electric field measurements. The internal electronics measured from DC to 2 MHz using the double-ended probe technique. This method uses two opposing spheres, where each measured the voltage difference from the sphere to the payload ground. The electric field amplitudes are found by taking the difference between the two spheres divided by their separation. At DC to VLF frequencies the input impedance to the preamplifiers, which were located in the spheres, is roughly 10^{12} ohms. This is much larger than the local ionospheric plasma impedance, of about 10^8 ohms. The ionospheric plasma is effectively a voltage source driving the sphere pre-amplifiers in each sphere. The plasma is resistively coupled to the spheres from DC to roughly 100 kHz in the Low Frequency (LF), LF is 30 kHz to 300 kHz. At higher frequencies, a correction to the separation term is necessary to account for the higher plasma impedance [Siefring, 1987].

All 6 booms have internal pre-amps and use the “boot-strapping” technique in which the coax cable shield from the spheres is driven with the same voltage as the inner conductor which minimizes the cable capacitance. Each of the 3.0 inch diameter aluminum sphere probes were coated with Aerodag, a carbon paint to give them uniform conductivity and minimizes the photo-conductivity of the aluminum.

Continuous data were transmitted for the VLF channels which were digitally sampled at 40 k samples/sec., giving a Nyquist frequency of 20 kHz. The VLF signals were directly coupled from the sphere preamplifiers as described above, and the signal was filtered by a 3 pole Butterworth filter with a high frequency rolloff below 20 kHz before being digitized. All channels had the 3 dB rolloff below 20 kHz, but the 3 pole Butterworth filter did not prevent some aliasing from occurring. In some of the recorded lightning strokes there is significant signal amplitude above 20 kHz which enters into the VLF data channels. In the spectrograms of the electric field data, the aliased signals from the US Naval transmitter stations, NSS (20.4 kHz) and NAA (24 kHz), can be seen in most of the VLF electric field spectrograms. In the case of the Z axis electric field channel, VLF_{26} , the 3 dB point was at 18.5 kHz. An input signal at 25 kHz would have an amplitude of 0.36 times the original signal appearing as a digitized aliased signal. An input signal at 35 kHz the signal would have 0.14 times the value of the original amplitude. Lightning strokes often have significant amplitude above 20 kHz, so the occurrence of some aliased frequencies in the VLF data is not surprising using the 3 pole Butterworth filters.

The higher frequencies were digitized and stored in the Scratch and Shift (SNS) high speed waveform instrument. This instrument could only capture about 1.25% of the total flight data because of the limited telemetry bandwidth.

The electric fields were found by taking the differences between opposing sphere pairs. The x-axis ac electric field, referred to as $VLFH_{12}$ or as $VLFH_X$, in the TM data, is found by taking the voltage on sphere 1 minus the voltage on sphere 2 and dividing the voltage value by the total separation between the spheres, which was 3 meters. The electric field along the rocket payload axis, parallel to the earths magnetic field \vec{B}_o , is given by $VLFH_{26}$, or as it is sometimes labelled in the figures, $VLFH_Z$. A positive voltage on this channel corresponds to an electric field which is directed downward, or parallel to the earths magnetic field at Wallops Island. The rocket had an onboard Attitude Control System (ACS) which kept the payload aligned to the local magnetic field within ± 5 degrees.

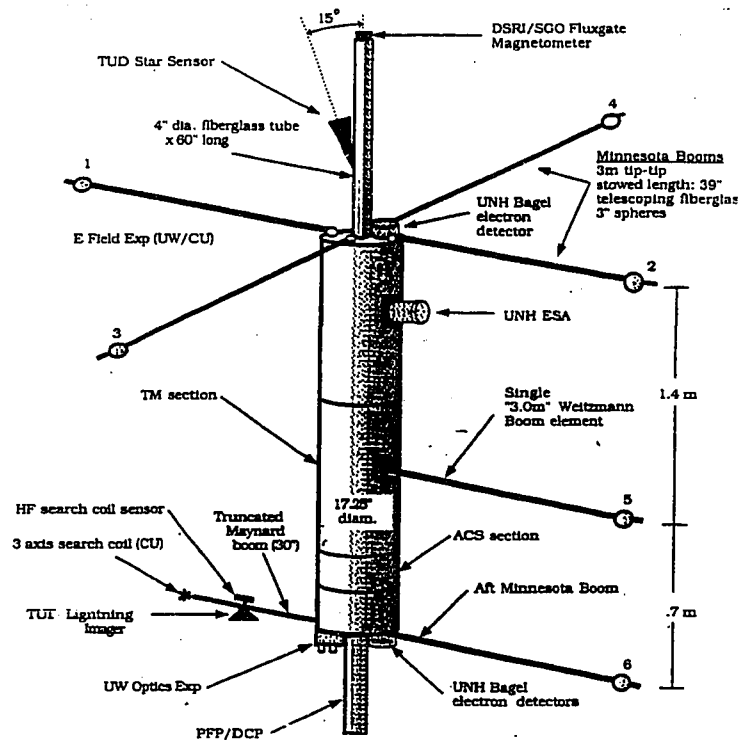


Figure 2.1: The deployed configuration of the Thunderstorm-III experiment is shown. The electric field probe spheres 1-4 are deployed from the forward deck and measure the E-field components perpendicular to \vec{B} . The parallel electric-field is measured from the voltage differences between spheres 2 and 5, or 2 and 6, which give two different measurement ranges. The DSRI fluxgate is located in the forward mast. UW optical experiment, STAR Imager and the PFP are on the aft deck.

The passband of the VLF portion of the sphere probe electronics covered from 10 Hertz to nearly 20 kHz. The whistler data analyzed in this thesis used electric field data from the high gain VLF channels prefixed by "VLFH_{nn}". The channel gains and passbands are summarized in the table 2.1.

The telemetry data can be converted into electric fields in Volts per meter by:

$$VLFH_{xx} = \left(\frac{TM_{out} * \text{Full A/D Range}}{(\text{Gain}) * (\text{Sphere Sep}) * (2^{\text{No. Bits}} - 1)} \right) \quad (2.1)$$

The bit resolution of the high gain VLF channels is 0.023 mV/m per bit on data Link 6.

Table 2.1: T-III Electric-Field Channels

Channel	TM Link	Gain	Bandwidth (Hz)	Sample Rate(Hz)	No. Bits	distance (meters)	A/D range
$VLFH_{12}$ X	6	31.56	10-19.3k	40k	12	3.0	-4.51 -+ 4.50
$VLFH_{43}$ Y	6	31.64	11-20.3k	40k	12	3.0	-4.51 -+ 4.50
$VLFH_{26}$ Z	6	31.65	9-18.5k	40k	12	2.78	-4.52 -+ 4.52

In addition to the electric field measurements made by the electric field booms, a second set of data were collected from the DC Probe experiment. The DC Probe experiment made relative electron density measurements by placing a small bias voltage on one of the boom probes and measuring the current that flowed between the probe sphere and payload ground. The current will be proportional to the electron density. Usually this type of measurement is best made along with another instrument which can make an absolute determination of the electron density at some of the rocket altitudes. The advantage of the DC Probe method is that it can measure lower electron densities than other types of instruments. The disadvantage is that the DC Probe makes relative measurements and needs a second instrument to provide an absolute electron density measurement. The absolute electron densities were measured by the Plasma Frequency Probe instrument on the rocket.

2.3 University of Washington Optical Lightning Detector

The UW optical instrument provided an optical trigger of lightning strokes for Cornell University's SnS high speed waveform digitizer. The instrument employs 3 voltage biased silicon photodiodes, each with an area of 1 cm^2 . The silicon photodiodes are each mounted into a circular aperture well with a diameter of 1.5 cm and depth of 0.28 cm. The field of view of each uncollimated detector was $\pm 80^\circ$. Two of the detectors use broad-band color glass filters to cover different portions of the lightning emission spectrum. The white light (WL) sensor covers the full response of the Hamamatsu silicon photodiode, from 520 nm to

the Near Infrared (NIR) at 1.1 nm. It was hoped that if a Sprite type event occurred that the method of broadband color discrimination would be able to distinguish these events from normal lightning strokes based on differences in brightness in the filtered channels. At the time of flight, the optical emission characteristics of Sprites were unknown, but that they appeared much more red than normal lightning strokes. The optical circuits were newly designed for the Thunderstorm III payload. The detector was extremely sensitive, within an order of magnitude of photo-multiplier (PMT) type systems. The minimum detectable signal in the lab test of the white light sensor showed that it could detect a photo-current as low as several picoamps, equivalent to an input power of about a picowatt.

The digitized telemetry data is converted back to the original instrument output voltage by

$$V_{out} = \left(TM_{out} * \frac{5.0 \text{ V}}{4095 \text{ bits}} \right)^2 * 0.625 \quad (2.2)$$

The output voltage can be converted to optical irradiance L_p in W/cm^2 at the detector by using

$$L_p = V_{out} / R_{fb} * W_p / I_p * 1 / a_{det} \quad (2.3)$$

Here R_{fb} is the feedback resistance used in the current to voltage circuit of the sensor which was 100 M ohms. The area of the detector, a_{det} is 1 cm^2 , and W_p / A_p is the photo-watts per ampere constant of the Hamamatsu silicon detector which is approximately 2.0 watts per ampere at 600 nm wavelength, near the peak wavelength of lightning emissions.

Note that the Link 3 digitization used 8 bits and the Link 6 data was digitized using 12 bits giving 4095 levels, shown in the equation above. Originally, the launch of the rocket was proposed to be delayed until astronomical twilight at rocket apogee. This constraint meant that the summer launch times would be well past 10 PM local time. By the end of the rocket campaign in September, the intensity and position of the storm took precedence over this launch restriction. As a result of the early launch time of 9:13 PM EDT, the rocket optical sensor was in sunlight above 200 km altitudes. This reduced the amount of data considerably, down to about less than 100 seconds out of 500 seconds of flight data.

2.4 Particle Detectors

Three low energy electron particle detectors were flown on the spacecraft, two Bagel detectors located on the front and aft payload sections and an Electrostatic Analyzer (ESA). These instruments were provided by the Space Physics Department at the University of New Hampshire, under the supervision of Professor Craig Kletzing. These instruments were to look for Lightning Induced Electron Precipitation (LEP) which had been reported by [Imhof *et al.*, 1985; Goldberg *et al.*, 1987], and to look for electrons which would be accelerated by the lightning field aligned electric pulses which had been measured on Thunderstorm II. By making the measurements directly over the thunderstorms, it was hoped that LEP or the accelerated electrons from the electric pulses could be directly correlated with the lightning strokes from the thunderstorm. Prior to the rocket flight, neither of the above cited reports of LEP had directly correlated lightning strokes with the observed electron precipitation.

The ESA was mounted on a Weitzman type boom which extended radially from the payload midsection. The ESA measured electrons at all pitch angles and the forward and aft Bagels measured magnetic field aligned particles only.

The Bagel detector is a hemispherical particle instrument designed to increase the entrance aperture size. The instrument has dE/E of about 12% and a total geometric factor of approximately $0.1 \text{ keV/cm}^2\text{-ster}$. The ESA is a more standard "top hat" design, with a dE/E of 15% and a geometric factor of $5 \times 10^4 \text{ keV/cm}^2\text{-ster}$. These instruments scanned over energy ranges of 1 eV to 12 keV.

The results of the particle detector experiments did not show any evidence of LEP. In fact, no electron precipitation was observed at all during the flight of Thunderstorm III. It may be that LEP is only observed in conjunction with strong multi-hop whistler activity, and these were not seen during the experiment. Particle acceleration caused by the field aligned electric pulses from lightning were not observed in any of the particle detectors.

Table 2.2: T-III AC Fluxgate Magnetometer Channel List

Axis	TM CH	BW (Hz)	Samp per s	No. Bits	Calibration Constant	Payload Orientation
AC X(2)	3	300-3k	8333	16	0.0286 nT/bit	+X=270°
AC Y(3)	3	300-3k	8333	16	0.0324 nT/bit	+Y=0°
AC Z(1)	3	300-3k	8333	16	0.0316 nT/bit	+Z=Nose

2.5 VLF Search Coils

A vector magnetic-field detector consisting of three ferrite-core search coils made 3 axis vector magnetic-field measurements. The search coil instrument was designed by the Electrical Engineering department at Cornell University. The search coils have passbands from approximately 300 Hz to 7 kHz, however the frequency response over the passband is not flat and this makes direct comparison of the VLF Search Coil data to the VLF electric field data more difficult. The peak frequency response is near 6 kHz with the 3 dB frequencies at 3.7 kHz and 8.5 kHz. The search coils were digitized at 40 kHz on the Link 6 telemetry channel. The lack of good calibration data from this instrument makes a full wave field measurement of \vec{B} and \vec{E} impossible. Some good waveform data was obtained from this instrument which were useful for comparison to the electric field data and to the AC fluxgate data described in the next section.

2.6 Fluxgate Magnetometer

A sensitive AC/DC fluxgate magnetometer was provided by Professor Fritz Primdahl at DSRI (Danish Technical research institute, at Sodonkylän Geophysical Observatory. This instrument provided 3 axis vector magnetic-field data from DC to 10 Hz and 300 to 3 kHz on the AC channels. The axes are labeled 1,2,3 and Z,X,Y, respectively. The instrument bandwidths and calibration constants are given in the Table 2.2.

The original fluxgate instrument failed during the summer launch window and had to be replaced. The new fluxgate had a digital latching problem which resulted in small amplitude high frequency spikes in the output waveform. Despite the latch problem, the instrument was able to provide very useful information during the flight, especially when the low frequency AC magnetic fields were larger than 1 nT.

2.7 *Star Imager*

A new instrument which provides precision Euler angles was test flown on the Thunderstorm III payload. The Star Imager was able to determine payload inertial attitude within 20 arc-seconds provided the spin rate of the rocket is less than 0.025 Hz. The payload had a sufficiently low rotation frequency only after the apogee despin at $t=311$ seconds. The instrument was mounted on the forward payload mast. It used a CCD camera supported by an on-board 486 computer which compared the image fields to a star constellation catalogue database. The instrument was built and supplied by the Department of Electrophysics of the Danish Technical University (TUD). This is the same Star Image to be used on the Danish microsatellite ØRSTED.

2.8 *Danish Technical University (TUD) Lightning Imager*

An aft-mounted CCD camera provided a series of images of the lightning flashes below the payload during the entire flight. The 390 by 288 pixel images are JPEG compressed, with compression ratio dependent upon the number of images with lightning flashes visible. During periods of high lightning activity the compression ratio increased at the expense of additional loss in the image information. The imager system had an image integration time of 430 milliseconds, which is slow in terms of the speed and duration of most lightning events. Some of the longer duration IC lightning activity was imaged by the TUD system.

2.9 Utah Plasma Frequency Probe (PFP)

Electron density measurements were made by the PFP during the flight. This instrument can make ionosphere electron density measurements in regions with electron densities greater than 7×10^3 per cc, which is about 220 km altitude at Wallops Island at night. The instrument had been flown successfully on a number of rocket experiments. The calibration and design of this instrument was under the direction of Professor Mark Jensen at Utah State. The PFP instrument was located on the aft rocket deck and uses a short 0.5 m antenna. The antenna is swept in frequency while monitoring the antenna impedance. The frequency where impedance is maximum and non-reactive is closely related to the local plasma frequency [Jensen and Baker, 1992]. The instrument had been flown successfully on Thunderstorm II.

The probe only worked for a short time during the upleg of the Thunderstorm III flight. The current to the instrument fluctuated and at 153 seconds after launch the Utah PFP instrument data went to all zeros. It is not known what caused the failure of the probe or how reliable the data was up to $t=153$ seconds. At 225 km altitude, the PFP estimated the electron density at 7×10^4 cc, which is 30% lower than the IRI95 estimated profile. At 265 km, the PFP estimated the electron density at 4×10^4 cc, which is nearly double the IRI95 model estimate. The PFP gives an absolute electron density measurement, which can be used to calibrate the relative electron density measurements made by the DC Probe instrument. We will examine in detail the question of what the electron density profile was in Chapter 4 and we will show that the PFP data up to the time of failure is probably reliable, at least as reasonable as the IRI95 model electron density profile.

2.10 Rocket Flight Chronology

During the evening of September 1st, 1995, a very active thunderstorm moved over Wallops Island and out over the Atlantic. There was a second active thunderstorm about 20 km to the

Northeast of Wallops Island Figure 2.2. Thunderstorm III was launched over these storms at 01:13:00 GMT from pad 2¹. The first stage Nike rocket boost ended at $t=5$ seconds and the Black Brandt motor burned out at $t=44$ seconds. The payload separation and nose cone eject were completed by $t=71$ seconds and the initial despin and payload alignment to the B-field were done by $t=95$ seconds. The electric field booms were deployed at $t=82$ seconds and all instruments were operational at the time of the attitude control system (ACS) initial alignment. The upleg spin rate of the payload was $180^\circ/\text{second}$, and at rocket apogee, the spin rate was reduced to $6^\circ/\text{second}$. The lower spin rate enabled the Star Imager to acquire data during the downleg. A consequence of the lower spin rate was an increase in the number of ACS firings during the downleg which reduced the usable data. The PFP instrument data went to all "zeros" at $t=152.9$ seconds and no further data was obtained from the instrument. It is not known if there were problems prior to $t=152.9$ seconds but the current bus showed a large increase at $t=115$ seconds and a drop at $t=153$ seconds. It is not known if the instrument was giving reliable data until $t=152.9$ seconds or not. A consequence the early evening launch was that the optical instrument was not in astronomical sunset above 220 km altitude. This caused a substantial portion of the optical lightning activity to not be recorded. Even so, many events were measured by the University of Washington optical experiment during the early portion of the upleg and final downleg of the flight.

2.11 Supporting Ground Instruments

There were several ground based systems that have been crucial in the data analysis. The National Lightning Detection Network (NLDN) provided the locations of cloud-to-ground lightning strokes down to millisecond time resolution. NASA Wallops had an on-site meteorological radar system called SPANDAR, and a ground electric field mill (EFM) system. NASA Wallops had a newly operational Lightning Detection and Ranging (LDAR) system which recorded incloud electrical activity, this system is the subject of chapter 6. Lightning

¹ 37.838 North Latitude, 75.482 West Longitude

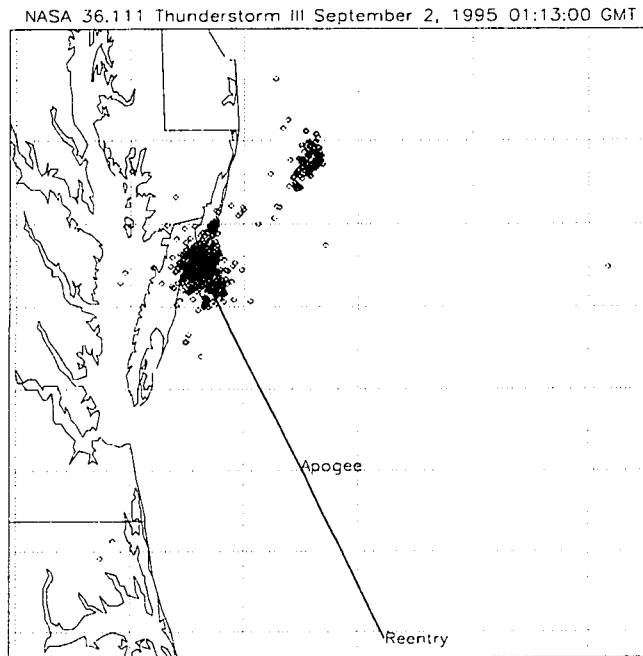


Figure 2.2: Thunderstorm III was launched from NASA Wallops Island VA. at 9:13 p.m. EDT. The rocket apogee was at 398 km at $t=312$ seconds after launch. Reentry and loss-of-signal occurred at $t=598$ seconds at 98 km. More than 1700 NLDN recorded CG lightning strokes occurred during the flight.

optical data was recorded from the roof of the NASA telemetry building at Wallops using an older version of the rocket optical sensor. The ground sensor had been flown extensively on high altitude balloon payloads.

2.11.1 National Lightning Detection Network

The National Lightning Detection Network (NLDN) is a nationwide system which is designed to detect cloud-to-ground lightning. The system gives the 2-D location (latitude and longitude) and the estimated peak current of the lightning strokes. Lightning location estimates are calculated by the system along with the location uncertainty. During the flight of Thunderstorm III, NLDN provided the CG data at one millisecond time resolution which

allowed individual CG stroke times and locations to be determined.

The system has been modified since its original design and now uses a combination of time-of-arrival (TOA) and magnetic loop direction finding (DF) antennas to locate CG lightning. NLDN only records cloud-to-ground lightning. Lightning strokes which occur in the thunderstorm but do not strike ground, known as intracloud lightning, are not recorded by the system. The NLDN system is able to characterize the lightning signals based on their rise time. At low frequencies, cloud-to-ground (CG) strokes have faster rise time than intracloud (IC) lightning. This allows the system to discriminate CG from IC lightning. The peak lightning currents are estimated based on the signal strengths, which are believed to be accurate to within 30% [Orville *et al.*, 1987].

2.11.2 SPANDAR

The SPANDAR meteorological radar uses a 6 meter diameter steerable dish antenna located on Wallops Island. The radar operates in the X band radar frequency at 10 GHz. The radar can be circularly or linearly polarized. During the rocket flight, the radar was operated in the linear polarization, which is better for studying the structure of the thunderstorm. The system can develop range-azimuth or range-height integrated radar images of thunderstorms. These images show the extent and the locations of the core convective regions of the storm which have higher radar reflectivity from the liquid water and ice in the storm cells. The radar system can also measure the relative Doppler wind velocities in the storm (see Chapter 3, figure 3.2).

2.11.3 Lightning Detection and Ranging (LDAR)

The LDAR system had just come into service during the summer of 1995, after many upgrades to the original design. Many of the changes are unique to the NASA Wallops system. NASA has a similar system in operation at Kennedy Space Center (KSC) in Florida, but this system does not have some of the digital hardware and software upgrades imple-

mented at Wallops and is based more on the original system [Poehler and Lennon, 1979]. The LDAR system detects the 80 MHz VHF pulsations which occur during the initial formation of incloud and CG lightning channels. The system then computes the 3-D locations of the pulsations and stores the data for display and analysis. The system sensitivity and the area of coverage of the system can be set according to the location of the thunderstorm activity under study.

Prior to a cloud-to-ground (CG) or an intracloud (IC) lightning flash in a thunderstorm, smaller amounts of charge are moved within the cloud near the main charge levels by the step leader process. When these charges move, the ionization of the air along the path of the charges is a strong source of VHF radio energy. The movements of the VHF sources sometimes occur in a path-like series between regions of charge in the thunderstorm or from the lower level charge regions of the storm extending toward ground, such as for a stepped leader preceding a first CG stroke. Researchers have identified two distinct types of VHF activity during the development of IC and CG events, these are Q noise and pulsed emission. Q noise occurs in short bursts of VHF pulses. These pulses appear over a positive half cycle interval lasting from 10 to 400 μs . The Q noise bursts usually occur along an existing ionized channel and are believed to be caused fluctuations in the channel current. In contrast, pulsed emissions only last about 1 μs and do not have the ragged "spiky" appearance in their waveform, and are quite distinct from Q noise. [Proctor, 1988]. The LDAR system used at Wallops was designed to detect the pulsed type emissions only, but not the Q noise bursts.

The LDAR system at Wallops Island is designed so that only the pulsed emissions are recorded and Q bursts are rejected (C. Etheridge personal communication, 1997). This is done by the signal processing software which puts the received pulses into 376 μs long windows. The LDAR software then checks the digitized pulse in the window and compares the signal rise time and duration compared to the known characteristics of pulsed emissions.

LDAR computes the time of occurrence of the pulsations, their locations in the storm

and the grouping of the pulses. If there is a series of discharges in the same region and close in time the pulse are grouped into a "multi-trigger" event.

2.11.4 Basic Theory of Operation

The LDAR system uses a group of 3 remote receiving stations which form a network around a central station located at the SPANDAR facility. All 4 sites have VHF receivers which are tuned to 70 MHz with a +/-10 MHz bandwidth. When the VHF signal at the central station exceeds a set threshold, data from the 3 remote stations is accepted and then cross-correlated to determine the difference in time of arrival. The remote signals are corrected for the known time delay to the central station and the computer performs the signal correlation between the remote and central sites to get the Difference Time of Arrival (DTOA) of the signals. The VHF signals are put into 2048 consecutive time bins, each bin is 50 nanoseconds long, so the window is a total of 0.1024 ms long. The peak signals in the window are used in the signal cross-correlation between the different receiving antenna locations. The rise time of the peak signal must occur in 0.2 μ sec, otherwise the particular peak is rejected as a valid LDAR trigger. This may occur if multiple pulses are received simultaneously (Charlie Etheridge, personal communication, 1997).

The location of the triggers are found by solving a set of hyperbolic equations for X, Y and Z, using the the computed DTOA between the different receivers. The computed solutions then give the locations of the pulses in the correlation window. The hyperbolic equations for the DTOA systems have been detailed by [Proctor, 1971], and have been used in systems such as LDAR and SAFIR.

Two data files are output by the system, one is a listing of all of the triggers, the other is the list of grouped multiple (≥ 2) triggers. The uncertainty in the location of the triggers is not included in the data files. The estimated uncertainty in the sources made by Rustan et al. for the KSC LDAR system was a 100 meter uncertainty owing to the size of the correlation window of 376 μ s, assuming a discharge propagation velocity of 10^5 m/s. Two other types

of location uncertainty result in the system due to the discrete sampling interval and to calibration errors. These errors are typically 100 meters in the E/W direction, 600 meters in the N/S direction and 400 meters in altitude. Worst case errors can be up to 3 times larger depending on the location geometry [Rustan *et al.*, 1980]. The uncertainty in the LDAR system at Wallops is assumed to be similar to that of the KSC LDAR, but NASA has not released a technical report on the WFF LDAR system at this time.

When a trigger occurs within a given time and distance of the preceding trigger, it may be associated into a multiple trigger event by the LDAR system. During channel development preceding CG strokes, or during the movement of charge between upper and lower regions of the thunderstorm, a series of triggers will often form along the path between the charge region toward ground or between the incloud centers of charge. These triggers appear grouped in location and in time. These groupings can usually be automatically identified by the LDAR computer software. The grouping scheme can be set in the software and is done as follows: 1) is the trigger time within x milliseconds of the preceding trigger? 2) is the trigger within \pm km of the last trigger within the time window? Usual settings for the grouping are \pm 5km distance and a time window of 300 milliseconds.

The software is designed so that triggers can be limited to a user selected region and to be above a minimum threshold. This feature is useful for studying the electrical activity from a particular thunderstorm cell. During the launch of Thunderstorm III, the region was set so that only activity from the thunderstorm that passed over Wallops Island were processed, while activity from the storm located to the Northeast (North of latitude 38.1 degrees) was not recorded in the database. Also, the sensitivity was decreased by increasing the attenuation of the receivers to more than 15 dB.

LDAR gives a more complete look at the electrical activity in the storm. The VHF (80 MHz) pulsations occur during the formation of incloud and CG lightning channels. This system provides invaluable information about the locations of electrical activity in the thunderstorm in real time. The LDAR VHF activity also shows where charge movement is tak-

ing place in the storm preceding and after lightning strokes. Because of its importance to this study, we will devote Chapter 6 to the results of the LDAR data taken during Thunderstorm III.

2.11.5 *Ground Electric Field Mills*

NASA Wallops operates a network of electric field mills positioned around the facility that are used to warn of conditions of large electric fields associated with thunderstorms. The system measured the DC electric fields at 7 locations around the base facility. The field mills are manufactured by Thunderstorm Technology of Huntsville, Alabama. The mills can measure the electric fields from ± 1 V/m to 32 kV/m from DC to 10 Hz frequencies. The data has low time resolution (0.2 samples/second) and during the rocket experiment was only recorded on strip chart paper. We will try to use the data to make some estimate of the charge deposited by lightning strokes from the storm and a gross estimate of the magnitude of the total charge in the main thunderstorm cell near Wallops Island. For a complete analysis of the charge structure of a thunderstorm, a larger array of field mills would be needed [Krehbiel *et al.*, 1979]. Still, we will make an estimate of the charge removed in a lightning stroke based on the field change in the Electric Field Mill data in chapter 3. Overall the data from the network did not have good correlation with the NLDN recorded strokes. There were only a few cases of clear changes in the electric field data that could be related to cloud-to-ground lightning activity. The thunderstorm was within 10 km of Wallops Island and the close proximity of the thunderstorm caused several of the field mills to be saturated.

For reference, the locations of the NASA Wallops Electric Field Mill (EFM) system is given in the following table. All of the location values are current as of 1997, and are given relative to the WGS 84 Datum, along with the height correction to the reference geoid. Future research using the field mill system at Wallops Island should consider obtaining digital recordings of the data rather than the strip chart records. A calibrated reference station

Table 2.3: Electric Field Mill Locations at Wallops Island

Station	Latitude(deg. min. sec.ss)	Longitude	Ellipsoid Ht(m)
Runway East	37 56 37.993 N	75 27 22.137 W	-25.6
Runway North	37 56 38.516 N	75 28 51.382 W	-25.4
Building N162	37 55 40.130 N	75 28 23.354 W	-25.2
Launch Pad 2	37 50 24.234 N	75 29 00.443 W	-34.7
Launch Pad 5	37 51 11.638 N	75 28 03.424 W	-34.2
Helo Pad	37 52 19.465 N	75 26 30.587 W	-33.8
SPANDAR	37 51 16.417 N	75 30 40.925 W	-34.1

would also be useful as a check on the system calibration. Additional field mills for better measurement geometry, rather than the current system, would improve the calculated thunderstorm charge estimates. Currently, all of the mills are located on the NASA Wallops facility, and if any of the 6 mills becomes saturated, the charge configuration model solutions are not possible without supplemental information.

Chapter 3

THE THUNDERSTORM

GRADUATE: *What causes thunder and lightning?*

COSMOGRAPHER: *Thunder results from the touching of currents of air which run into each other with great force, and lightning is air which has set itself on fire and lights up. This comes about in the following way: the wet vapor, as explained, rises and as it approaches the upper air, the currents from one part clash against another, and from the collision derives the noise of thunder. This motion heats up the air to such an extent that it is converted into the substance of fire, which causes the explosion or lightning which we see when there is thunder. Although this happen all at once, we see the lightning sooner than we hear the thunder because sight is quicker than hearing. Also it is said that the collision of the watery cloud as it rises and meets its opposite, which is fire, causes thunder and lightning. **Pedro de Medina.** The Libro de Cosmographia, 1538.*

Thunderstorm convective activity is believed to be directly related to the charging and therefore the lightning flash rates. For this reason, the details of what is known about the thunderstorms that were over-flown by the rocket experiment, will be given. The extensive array of ground instruments at NASA Wallops Island gives a very detailed look at the most active thunderstorm cell of the two storms that were over-flown. Doppler radar images were made by SPANDAR, two sets of weather balloon data were taken just prior and 11 hours after the rocket experiment, and ground electric field data were recorded. These data, when combined with the optical and LDAR measurements give a very complete picture of this thunderstorm, which had a very high lightning flash rate, exceeding 1 cloud-to-ground

stroke per second.

In this chapter the necessary background needed for the discussion of thunderstorms and lightning processes will be covered. A summary of the ground based measurements of the estimated lightning stroke peak currents during the experiment for the Wallops thunderstorm are summarized based on the NLDN data.

Radar data from the SPANDAR Doppler radar system is compared with the meteorologic soundings made just prior to the rocket launch. The radar data will be compared to the LDAR VHF data in Chapter 6, showing the locations of thunderstorm electrical activity in relation to the thunderstorm core region seen in the radar profile.

It is hoped that, by giving all of the detailed data that are available for this storm this study and later thunderstorm over-flights can be used to relate space based optical measurements of lightning flash rates to meaningful atmospheric parameters related to storm severity.

Using the balloon meteorological data that were measured at the time of the rocket launch, a standard index of atmospheric instability known as the Convective Available Potential Energy (CAPE) is calculated. We argue that CAPE can have large uncertainties in its computed estimate. Later in Chapter 7, we will argue that CAPE is not a reliable indicator of lightning flash rates or storm severity.

In terms of the lightning flash rates, this storm was vigorous, although the peak NLDN lightning currents were not exceptionally large. We want to know if the flash rate of lightning can be related in some way to the measured meteorological parameters of the storm. In particular, can the rocket measured optical lightning flash rates be related to the thunderstorm severity? The storm severity can be based on size, radar reflectivity and the available convective energy of the storm determined by balloon soundings or updraft speeds in the storm.

What is found later in Chapter 7 is that the flash rates determined by the rocket will be quite different than those measured by the NLDN system. This is generally because the

National Lightning Detection Network only records cloud to ground (CG) lightning but the rocket records all flashes including in-cloud lightning strokes. Even so, rocket measured flash rates give a comparable estimate of thunderstorm electrical activity and its severity. The problem comes in relating the rocket optical data to quantifiable meteorologic indices used to determine thunderstorm severity.

The Wallops thunderstorm had a high lightning flash rate and fairly severe weather. The National Weather Service issued a strong rain and a flash flood warning for this thunderstorm in the afternoon of September 1st, 1995. The storm had persisted through most of the day, traveling eastward across the state of Virginia and finally, by 9 PM EDT, it reached the Eastern Shore, near Wallops Island. The storm then moved out to the Atlantic Ocean and dissipated by local midnight, about 3 hours after rocket launch .

3.1 Thunderstorm Meteorology and Development

Moisture in the air and available energy cause the strong convective instabilities of thunderstorms. A displaced air parcel which maintains its temperature above the surrounding air temperature will have a lower density and it will rise. The rate at which the air temperature of the local atmosphere changes with altitude is known as the atmospheric lapse rate. A displaced air parcel in this local environment, will cool according to the adiabatic lapse rate. This rate may vary considerably from the temperature lapse rate of the surrounding air. An atmosphere with a lower lapse rate than the adiabatic lapse rate, is said to be unstable. This is because the displaced air parcel will continue to rise until it reaches a level where its temperature is equal to that of the surrounding air. As long as the displaced air parcel maintains its temperature above the surrounding air temperature, it will have a lower density and it will rise. During the ascent the parcel will cool at the adiabatic lapse rate, about $10^{\circ}C/km$. As it cools, it cannot hold as much water in the vapor state, and becomes more saturated meaning the relative humidity (RH) of the air parcel continues to increase until the air cools to the dew point (RH=100%). The water in the air parcel then releases more heat

or energy from the latent heat of condensation of the water. It will then cool at the saturated adiabatic lapse rate, which is $6^{\circ}\text{C}/\text{km}$ [Fleagle and Businger, 1981]. Depending on the local atmospheric lapse rate, the air parcel will either become stable at some higher altitude (cloud top) or continue to rise until stopped by the base of the tropospheric inversion region known as the tropopause. The tropopause has a strong temperature inversion caused by the increasing ozone in the atmosphere at these altitudes. The ozone is heated by the absorption of solar UV and this then dramatically alters the lapse rate from cooling with altitude to a profile where the atmosphere actually increases in temperature with height.

In the unstable case, as the air parcel continues to rise, it will eventually cool to the freezing point of water, 0°C . As the water freezes, more energy is released from the water, into the nearby air parcel making it warmer and more buoyant, this further contributing to the instability. At temperatures below freezing in the cloud, collisions between super-cooled water and ice crystals will produce graupel, a form of soft hail¹. This process is known as riming, and the collisions between water and ice particles are believed to be important in the convective charging process in thunderstorms [Williams, 1985].

The main region of charging, based on the models of convective charging, is believed to exist where there is strong convection along with large amounts of super-cooled water graupel and other forms of ice crystals in combination. The region where this region happens in a thunderstorm The region, referred to as the charging region, is usually defined by the altitudes at which the air temperatures are between -10°C to -20°C . In Chapter 6, the electrical activity of the Wallops storm will actually occur at somewhat lower altitudes than predicted by these charging models. Some researchers believe that larger convection within the storm will also result in greater charging and higher lightning flash rates [Williams *et al.*, 1992; Baker *et al.*, 1995; Solomon, 1997]. Empirical data suggests that there is a fifth power relation between flash rate and the thunderstorm height [Williams, 1985]. This relation will

¹ liquid water can exist below freezing as small droplets in the absence of condensation nuclei [Fleagle and Businger, 1981]

be compared with the measured cloud height and flash rates for the Wallops thunderstorm in the following section when we look at the SPANDAR data.

The instability of the atmosphere can be estimated if the temperature and the dew point have been measured at a variety of different altitudes in the atmosphere. Such measurements are routinely made at 0 and 12 hours GMT at meteorological stations around the world. The atmosphere soundings give a profile of temperature and relative humidity with height using a free ascending, disposable balloon, known as a radiosonde. NASA Wallops Island is a World Meteorological Organization (WMO) weather site, and routinely makes these atmospheric soundings. The sounding preceding the flight of Thunderstorm III is shown in Figure 3.1. In the figure, the humidity data from the 0 UTC and the 12 UTC soundings following the rocket launch are used to reconstruct the atmospheric profile.

3.2 Convective Available Potential Energy (CAPE) and Lightning Flash Rates Based on Cloud Top Height

One method for estimating the amount of convective activity is the Convective Available Potential Energy or CAPE index. The CAPE has been suggested as a good indicator for thunderstorm severity and electrical activity [Williams *et al.*, 1992]. If the convective instability is related to thunderstorm charging, the lightning flash rate should also be related to CAPE. In the case of the Wallops thunderstorm, NLDN has recorded very high lightning flash rate (F), more than 80 per minute. Based on this high lightning flash rate, we would expect a large CAPE index. There is not an explicit, empirical relation as yet, relating CAPE to lightning flash rates, though such a link has been suggested [Williams *et al.*, 1992]. What we will show in this section is that the index can have some very large uncertainties that make it difficult to apply, even when good meteorological data are available. We also look at the lightning flash rate predictions using an empirical model relating cloud top height to lightning flash rate.

We will make an estimate of CAPE for the thunderstorm at Wallops Island as a compar-

ison to other thunderstorm CAPE values. The lightning flash rates for the Wallops thunderstorm can be well quantified, so CAPE can be compared with the flash rate for this storm to see if the index proves useful as an indicator of lightning severity. Ideally, if space-measured optical flash rates can be used to estimate storm severity, then there should be a relation between CAPE and flash rates of the storm.

As will be seen in this section, there can be several areas of uncertainty when using the CAPE index and applying it to the lightning flash rate F . The CAPE is given by:

$$CAPE = g \int_{z_{cb}}^{z_{top}} \frac{\theta(z) - \overline{\theta(z)}}{\theta(z)} dz \left(\frac{J}{Kg} \right) \quad (3.1)$$

where g is the gravitational acceleration, $\overline{\theta(z)}$ is the potential temperature of the environment and $\theta(z)$ is the potential temperature of the lifted air parcel. z_{top} is the height at which the parcel temperature equals the surrounding environment temperature and z_{cb} is the start of the integration at cloud base. CAPE can be calculated from the balloon sounding data using each of the measured values of temperature and humidity lifted up to their equilibrium level with the surrounding air.

Critical in the calculation of CAPE is the estimate of the relative humidity and temperature in the lower atmosphere. Typical World Meteorological Organization (WMO) data records 30 levels for the first 10 km of altitude in most atmospheric balloon data soundings. It is the measurement of the relative humidity that is often subject to a fair amount of uncertainty. Standard balloon radiosonde hygrometers use the changes in resistivity of an exposed salt, usually barium fluoride (BaF_2). The resistance of barium fluoride is known to change in a linear way with humidity. The time response of this type of hygrometer is about 2 seconds for a change of 63% in the relative humidity (RH), which is equivalent to a 5 meter change in balloon altitude at the suggested NOAA ascent rate of 300 meters per minute. The measurement range becomes limited at very low temperatures below about $-40^\circ C$, so no RH measurements are made below this temperature. The measured average standard deviation in the measured relative humidity at $0^\circ C$ is 15%. The electric hygrome-

ter can become less sensitive with time and exposure to a moist environment, and therefore must remain sealed until it is flown. Calibration of these sensors is rarely checked after they leave the manufacturer. Even so, WMO usually records only a fraction of the sounding data, 30 levels for the first 10 km of altitude in most soundings. What we wish to stress here is that the CAPE index is sensitive to small changes in the atmospheric profile data. These variations can be very large compared to the measurement uncertainties in the radiosonde atmospheric profiles.

3.2.1 The Wallops Thunderstorm Meteorology

The storm cell over Wallops Island had persisted since late afternoon when it was located over the Blue Ridge highway in Western Virginia. The storm produced very severe weather while over these mountains. One anecdotal story given by one of the NASA project engineers was that he was forced out of his camping site because of strong rains and local flooding which ended his Labor Day weekend trip. The same storm cell continued eastward and crossed the Chesapeake Bay to the Eastern Shore region of Virginia, where it passed directly over Wallops and out to the Atlantic before it dissipated.

About 1 hour prior to launch of Thunderstorm III, an upper air balloon sounding was made from Wallops Island. The results of the sounding which give temperature and relative humidity (RH) with altitude, are shown in Figure 3.1. From the sounding data, cloud base is at the lowest altitude that reaches 100 percent RH, which was at 2.2 kilometers. Freezing level was at 3.5 kilometers. One feature in the data is the multiple levels of saturation in the atmosphere. The estimated height of the tropopause based on the sounding was between 12 and 13 kilometers. The anvil top of the thunderstorm based on the SPANDAR Doppler radar vertical cross-sections, was at 41 k Ft or 12.5 km. This storm cell had developed to the full height possible given the conditions in the troposphere. The thunderstorm was capped-off by a temperature inversion at 12.5 km, about 3.5 km below the estimated tropopause height at 16 km, where the temperature reaches a minimum which forms the

boundary between the troposphere and the stratosphere. Above the tropopause, the temperatures increase with altitude in the stratosphere, an effect of increasing ozone and UV absorption at these altitudes [Fleagle and Businger, 1981]. The estimated cloud base, z_{cb} ,

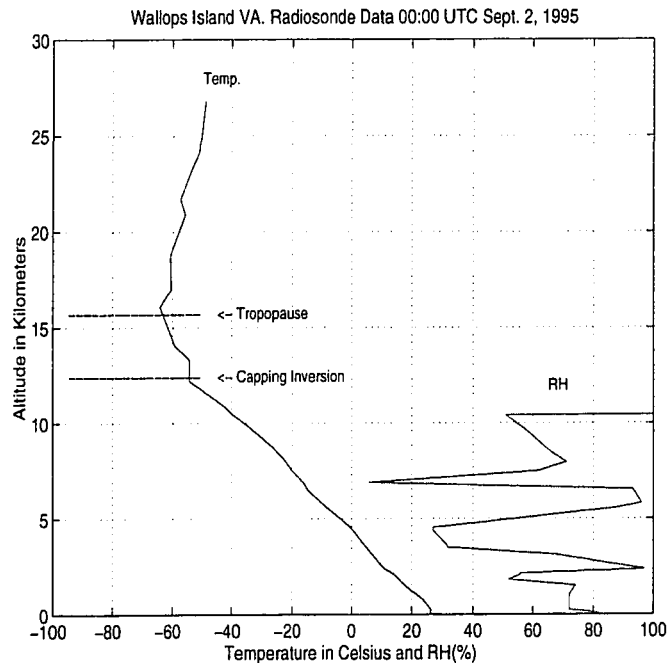


Figure 3.1: Upper air sounding of temperature and relative humidity made by a balloon (radiosonde) launched one hour before the launch of Thunderstorm III

based on the first saturated level in the sounding data ($RH=100\%$) was at the 768 mb level or at 2.36 km altitude. The computed CAPE index using this level as the cloud base was 200 J/kg. If the cloud base is estimated by taking a surface parcel of air, using the measured temperature and humidity from the radiosonde data, and finding the height at which it reaches saturation, i.e. $RH=100\%$, the estimated CAPE changes considerably. This method of estimating cloud base is known as the Lifted Condensation Level (LCL). Using the LCL cloud base, the computed value of CAPE increases dramatically to 1657 J/kg.

There is no independent estimate available for the cloud base level at the time of flight

at Wallops. Most studies using CAPE will have a similar problem of the combined uncertainties in cloud base and the humidity profile which result in large changes in the computed CAPE index. A second problem is that humidity measurements from upper air soundings rarely go up to the tropopause level where thunderstorm anvils typically cap-off, or even up 12.5 kilometers altitude, as is the case for the Wallops thunderstorm radiosonde data. The CAPE calculations are only integrated up to the last measured humidity level, which is often lower than the actual anvil top of the thunderstorm by at least 2.5 km. This variation in the computed values of CAPE illustrates the problem of using this index to relate the lightning flash rates to the thunderstorm meteorology. CAPE estimates, as shown here, can vary widely depending on the sounding data. The index is very sensitive to the cloud base z_{cb} and to the variations in the radiosonde profile [Solomon, 1997]. CAPE has been suggested as an indicator of electrification and lightning flash rates [Williams *et al.*, 1992].

Based on the cloud top height estimated from the sounding and the SPANDAR data, we can make an estimate of the lightning flash rate F . Using the model of Price and Rind (1992), the maximum flash rate F in strokes per minute is given by:

$$F = 3.44 \times 10^{-5} Z^{4.9} \quad (3.2)$$

Where Z is the cloud top altitude in km. Using Equation 3.2, the lightning flash rate is estimated to be 8 strokes per minute, roughly a tenth of the actual rate!

3.2.2 SPANDAR radar data

The SPANDAR Doppler radar facility is located at NASA Wallops Island. The system has a 10 meter steerable dish which emits an X-band polarized radar signal at 10.6 cm wavelength. SPANDAR is able to sweep in azimuth and elevation thereby making vertical cross section pictures of the storm. These types of radar systems are very useful for detailed storm analysis. The radar reflectivity of the thunderstorm shows the location of the storm cores, which are regions of high radar reflected signals. The core regions are associated with the most severe convective activity. In addition to graupel, rime ice and water, hail may form in

the severe up drafts in the core regions of the storm. The radar reflectivity is given in dBz, or, dB above zero. The 0 dBz level is defined roughly as the equivalent radar reflectivity of 1 drop of water in a cubic meter volume of space. Radar reflectivity levels of 30 dBz are associated with strong rain and levels of 45 to 50 dBz with the the presence of hail [Battan, 1973]. Two sets of elevation radar data taken about 1 minute prior to the rocket launch are shown in Figure 3.2. The upper panel shows the Doppler wind velocities of the Wallops thunderstorm, and the lower panel shows the radar reflectivity. This is an elevation cut through the thunderstorm with the radar beam directed to the Southeast. The SPANDAR

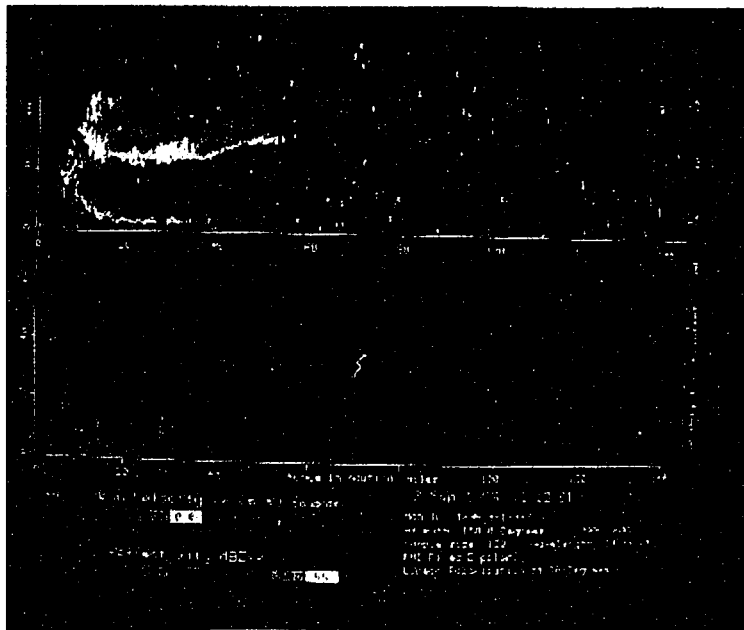


Figure 3.2: The Doppler wind velocity profile and the radar reflectivity of the thunderstorm near Wallops Island are shown in the two panels of this figure for vertical profiles (in kFt) looking southeast into the storm. Each of the profiles extends up to 21 km altitude and out to 260 km range. This radar profile was taken about 30 seconds prior to launch. The regions of high wind shear are also regions where the LDAR VHF electrical activity was greatest.

Doppler radar system was able to give azimuth and elevation data of the Doppler wind ve-

locity and reflectivity of the storm cell. At the time of rocket launch, the storm had just passed into the region where the radar system could image most of the storm. Within a few kilometers of the radar dish, the system cannot recover fast enough between transmit and receive in order to make any measurements thus creating a blind spot. Despite this, most of the storm was imaged. The radar data shows the Doppler cloud top to be slightly above 12.5 kilometer capping inversion shown in the temperature profile in Figure 3.1. At the lower levels are regions of strong wind shear separating levels of inflow and outflow into the thunderstorm main core region. It is interesting that these regions of strong Doppler wind shears are roughly coincident with the electrically active regions of the storm that are detected by LDAR, as shown in Chapter 6.

The SPANDAR data shows that the radar estimated cloud top of the Wallops thunderstorm was at 12.5 km, where a small temperature inversion caps off the cloud top just below the tropopause. Based on the cloud top height shown by the SPANDAR radar, the empirical scaling law prediction for the lightning flash rate can be estimated using equation 3.2. The cloud-to-ground lightning flash rate was more than 80 strokes per minute. The rate using equation 3.2 is only 8 strokes per minute calculated in the previous section. This is the danger of using simple scaling relations such as cloud height and the computed index CAPE to predict the intensity of thunderstorm electrical activity reflected in the lightning flash rates. With CAPE, we find that the computed values can vary widely with the choice of cloud base height. The lower value that has been calculated from the first estimate of cloud base gives a value below which cloud electrification would be expected. The higher estimate of CAPE, should produce strong electrical activity, since it is well above the 400 J/kg threshold suggested for thunderstorm electrification [Solomon, 1997; Baker *et al.*, 1995].

It is true that when thunderstorm convective activity is severe enough to drive the cloud top heights up to the tropopause level, the thunderstorm will have a well developed core electrical region which can generate vigorous lightning flash rates. The use of environmental parameters such as cloud top height, Z_{et} , and CAPE, based on radionsonde data, do not

give good indications of lightning flash rates. In the case of CAPE, the calculation of the index can have such large variations that, at least in the case of the Wallops thunderstorm, we must question its usefulness as a predictor of thunderstorm electrification and activity. It would be an interesting study to look for a correlation between the GOES IR satellite measured cloud top heights and the OTD and LIS satellite optical flash rates, and compare the flash rates to the NLDN rates.

3.3 Thunderstorm Electric Fields and Charge Structure

The "fair weather" electric field is normally directed downward and has a magnitude of -100 V/m [Volland, 1984]. During the passage of the thunderstorm at Wallops Island, the ground electric field was directed upwards and had a vertical magnitude of more than $+10$ kV/m at some of the field mill stations in the EFM network. Such large fields are typical from nearby thunderstorms which have large regions of negative and positive charges. In this section, the basic charge configuration and simple field equations are given. Based on the equations, we can estimate the dipole charge of the Wallops storm, and make an estimate of the charge neutralized in a cloud to ground stroke. The field equations given are simplified, but here we only wish to illustrate the static, inductive and radiation fields components, and how they change with distance.

The electrical structure of thunderstorms is often approximated as a "Wilson Dipole", named after C. T. R. Wilson who developed the simple model to explain his observations of thunderstorm electric fields [Wilson, 1925]. In the Wilson Dipole model, the lower thunderstorm regions carry net negative charge and the upper cloud regions carry net positive charge. Recent measurements of the electric fields inside thunderstorm show a more complicated structure, but one that is fairly well modeled using the Wilson Dipole approximation [Stolzenburg *et al.*, 1998b; Rustan *et al.*, 1980]. The simple charge model is a lower region of negative charge in the thunderstorm with an opposite positive charge above it as shown in Figure 3.3. The static electric field of a thunderstorm having a positive over nega-

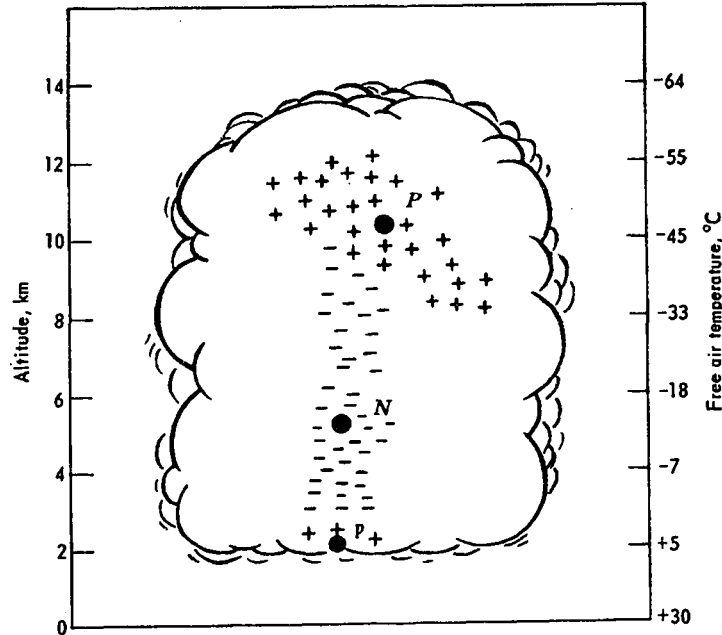


Figure 3.3: In the simple Wilson Dipole, the thunderstorm charge structure is modeled as positive charge P, over a lower negative charge region N [Uman, 1984]. Some models also include small screening charge regions, denoted by the small letters. Even though this is a very simplified picture of the charge structure, it has proven remarkably good at modeling the measured electric fields [Rustan *et al.*, 1980].

tive charge configuration described by the Wilson dipole model can be calculated from the individual charges and their image charges, since they are over the earth or ocean which is a conducting surface. The field from a single charge, and its image is [Uman, 1984]:

$$E = \frac{2QH}{4\pi\epsilon_0(H^2 + D^2)^{3/2}} \quad (3.3)$$

Where the charge Q is at a height from the ground H at a distance D . The charges in the thunderstorm form an electric dipole moment which can be described by the equation:

$$M = 2 \sum_i Q_i H_i \quad (3.4)$$

where the total dipole moment M is summed over the different charges. Note that if we

were looking at the change in dipole moment dM , such as from a lightning discharge. Only the charges that were added or removed by the lightning stroke would be summed in equation 3.4. The electromagnetic equations for the field at the ground are

$$E = \frac{[M]}{4\pi\epsilon_0 D^3} + \frac{1}{4\pi\epsilon_0 c D^2} \left[\frac{dM}{dt} \right] + \frac{1}{4\pi\epsilon_0 c^2 D} \left[\frac{d^2 M}{dt^2} \right] \quad (3.5)$$

Here c is the velocity of light and the charge moment expressions in brackets are evaluated at their retarded values at time $(t - D/c)$. The equation for the ground magnetic fields B are

$$B = \frac{\mu_0}{4\pi D^2} \left[\frac{dM}{dt} \right] + \frac{\mu_0}{4\pi D} \left[\frac{d^2 M}{dt^2} \right] \quad (3.6)$$

In equation 3.5, the first term is the electrostatic term. Notice that the electrostatic fields decrease as $1/D^3$. The second term is the inductive term, which appears when there is a current. The electric and magnetic inductive fields decrease as $1/D^2$. The last term is the radiation field, and the E and B fields decrease as $1/D$. Later in chapter 4 we will show cases where distant lightning strokes in Florida, have sufficient radiative energy to be measured at the rocket above Wallops Island, Virginia. We will also see cases of nearby lightning strokes with electrostatic fields that can be measured by the rocket at the base of the ionosphere.

During a negative cloud-to-ground lightning stroke, negative charge is brought to ground and neutralized. The net field change from the charge removal can be modeled by placing an equivalent positive charge at the height of the original negative charge. This model of a negative CG stroke gives a negative change in the ground electric field. This type of field change was measured by the EFM system at Wallops during negative CG strokes. For example, beginning at $t=540.592$ seconds, NLDN recorded two -CG strokes near Wallops Island. The ground optical system recorded the flashes and the second of the two strokes had a longer optical duration (see Chapter 7, Figure 7.7). The first stroke in the 2 stroke flash, had a peak current of -24.8 kA and the second stroke at $t=540.666$ s, had a peak current of -33.1 kA. The ground field mills nearest the flash (Pad2) recorded a negative field change of

-6.8 kV/m and -7.5 kV/m for the first and second strokes respectively. At the main base at Wallops Island, less than double the distance from these strokes (relative to Pad2), the measured field changes were -1.5 kV/m for both strokes measured at building N162. Notice that the stroke had less than 1/5 the field decrease compared to the change at Pad2, showing the rapid decrease in electrostatic field changes with distance from lightning strokes.

3.4 Summary of Cloud-to-Ground Lightning Flashes

The thunderstorm over Wallops Island had a very high lightning flash rate, often exceeding an average of 1 stroke per second during the rocket flight. The lightning CG flashes had stroke multiplicities as large as 15 strokes in a single flash. The average stroke peak current was 22 k Amps, with the largest CG stroke having a peak current of +92 k Amps. A summary of the lightning flashes is given in Table 3.1. The lightning flash rate F , measured in flashes per minute, is summarized in Table 7.1 in Chapter 7.

One of the features noticed in this study of the CG activity, was that in multiple stroke flashes the stroke of maximum peak current was often not the first stroke in the multiple stroke sequence. This was also reported in lightning flash statistics from Brazil, where only 50.4% of first strokes had maximum peak currents [*Pinto et al.*, 1996]. It is not known why this is, but apparently other researchers have found similar features in the data from thunderstorms in some Florida storms as well (Osmar Pinto personal communication, 1998.). As will be seen in chapter 6, most of the CG strokes originated from the electrically active region at 4.5 km altitude.

During this study of the NLDN lightning data, it was suggested that the time between strokes was related to the the stroke current, i.e. a longer inter-stroke time produces a larger current in the following stroke. This idea seems reasonable since more time would be available for the lightning channel to tap into new regions of charge during inter-stroke junction (J changes). No such relation was found between the peak current and the inter-stroke time in the analysis of the NLDN stroke data. Most strokes typically follow the same channel

Table 3.1: Lightning Flash order summary and NLDN peak currents. Each of the rows is a summary of lightning flashes of multiplicity M . Each column gives the average peak current and standard deviation in k-Amps for each stroke in the flash series. There were 233 single strokes recorded by NLDN, but only 5 lightning flashes with multiplicity $M=6$.

Number	M=1	M=2	M=3	M=4	M=5	M=6
1:233	22.3std6.3	30	-	-	-	-
2: 43	25.6±1.2	22.5±7.3	-	-	-	-
3: 25	26.7±7.6	25.8±6.7	25.3±6.2	-	-	-
4: 20	25.5±7.8	24.8±6.4	26.7±11.4	22.5±6.2	-	-
5: 14	25.4±8.6	28.5±9.8	26.2±9.1	24.5±9.3	22.9±6.7	-
6: 5	22.3±7.1	26.2±7.1	25.9±8.9	21.9±5.9	20.8±6.4	20.4±5.1

within 40 ms [*Uman*, 1984]. If the inter-stroke interval exceeds 80 ms the channel usually is not conductive enough for the Dart to follow it to ground. In this case, a new step leader forms a new path or a branch off of the old channel to ground [*Proctor*, 1988].

Chapter 4

WHISTLER WAVES

4.1 Introduction

The lightning VLF wave energy which travels up to the earth's ionosphere, directly interacts with the electrons in the ionospheric plasma. The electromagnetic energy from a lightning stroke would normally be reflected or absorbed in the lower ionosphere, but the addition of the earth's magnetic field allows these waves to couple into a type of plasma wave known as the whistler mode [Ratcliffe, 1959]. The electrons in the earth's ionosphere are not completely free to move in all directions, but are limited by the effects of the earth's magnetic field \vec{B}_0 . The electron motion perpendicular to the earth's magnetic field is circular about the magnetic field line of force. This motion has a natural frequency known as the electron gyro frequency Ω . The wave frequencies in the whistler mode are limited to those below the electron gyro frequency, and the wave electric and magnetic fields are polarized mostly perpendicular to the local magnetic field. In the lower ionosphere, the vertical electron density gradient, ∇n , causes the whistler waves to be directed nearly vertically so that the wave vector, \vec{k} is directed along ∇n , i.e. $\vec{k} \parallel \nabla n$. At Wallops Island, the angle between the vertical direction (∇n) and the local geomagnetic field \vec{B}_0 is approximately 20 degrees.

Under certain conditions, whistler waves can become ducted along the field lines all the way to the conjugate hemisphere. These ducted whistlers can then reflect between magnetically conjugate points, each reflection being termed a "hop", or several reflections between hemispheres are called "multi-hop" whistler waves. The whistler waves measured during Thunderstorm III, did not have any cases of "multi-hop" whistler waves.

Whistler waves are dispersive, meaning that different frequency components of the wave

travel with different velocities through the ionosphere. This changes the "burst" of electromagnetic energy from lightning, the pulse transforms from an impulsive event in the lower atmosphere to a frequency dispersed wave which becomes more stretched in time as it passes through the ionosphere (see Figure 4.4).

The whistlers waves that were recorded by the Thunderstorm III instruments are not ducted waves because they do not follow the magnetic field lines of force out to the conjugate hemisphere and back. These whistler waves are known as unducted fractional hop whistlers. Most whistlers are unducted, but sometimes they are observed with ducted multi-hop whistler activity [*Kelley et al.*, 1990].

4.2 Theory of Whistler Waves

The complex index of refraction n in a magneto-ionic medium is given by the Appleton Hartree equation. This equation assumes that the medium is composed of electrons, ions and neutral particles. These particles are assumed to have no thermal motion which means that the motion of the ions, which are much heavier than the electrons, can be neglected from the equation. Later in this chapter, we will look at regions in the ionosphere where the ion motion must be accounted for in order to explain the observed wave modes. The index of refraction then is given by [*Ratcliffe*, 1959]:

$$n^2 = 1 - \frac{X}{1 - iZ - \frac{1}{2} \frac{Y_T^2}{(1-X-iZ)} \pm \left(\frac{1}{4} \frac{Y_T^4}{(1-X-iZ)^2} + Y_L^2 \right)^{1/2}} \quad (4.1)$$

where

n is the complex index of refraction = $(\mu - i\chi)$

$X = \omega_p^2/\omega^2$, $Y = \Omega/\omega$, $Z = \nu_{en}/\omega$,

$Y_L = Y \cos(\theta)$, $Y_T = Y \sin(\theta)$

$\omega_p = 2\pi F_p = (Ne^2/\epsilon_0 m)^{1/2}$, is the electron plasma frequency.

N is the electron density, e is the electron charge,

m is the mass of the electron and ε_0 is the permittivity of free space, and

ν_{en} is the electron-neutral collision frequency.

ω is the wave angular frequency $=2\pi f$

\vec{B}_0 is the static background magnetic field vector

$\Omega = |\vec{B}_0| e/m$ is the electron gyro frequency.

\vec{B}_0 is the static background magnetic field vector

θ is the angle between \vec{B}_0 and the z vertical axis. The solutions of the Appleton-Hartree

equation allow several different modes of electromagnetic waves. In the direction of the magnetic field \vec{B}_0 , there are two modes, the right circularly polarized R and left circularly polarized L wave modes. In the transverse direction there are two wave-modes known as the X and the O mode waves. In equation 4.1, the O and R mode waves are the solutions for the minus sign, the X and L modes for the positive sign solutions.

The whistler mode waves are the branch of solutions of equation 4.1 for the lower minus sign at frequencies below the electron gyro frequency Ω . The whistler waves are right hand circular polarized waves, and the polarization of the whistlers is given by:

$$R = E_x/E_y = \frac{-i}{Y_L} \left\{ 1/2 \frac{Y_T^2}{(1-X-iZ)^2} \mp \left(\frac{1}{4} \frac{Y_T^4}{(1-X-iZ)^2} + Y_L^2 \right)^{1/2} \right\} \quad (4.2)$$

For many of the whistler waves measured on Thunderstorm III, the whistler polarization was very close to a value of $R=1$ with a right handed polarization, meaning the electric field vectors rotate about B_0 counterclockwise when looking in the anti-field direction. An example of a whistler wave is shown in Figure 4.1. In this example, the waves at the beginning of the whistler, being of higher frequencies, are only sampled a few times in one rotation of the electric field wave vector. The lower frequency waves which arrive later, and because they are sampled many times in one wave period, unlike the higher frequency waves, they appear nearly circular in the figure.

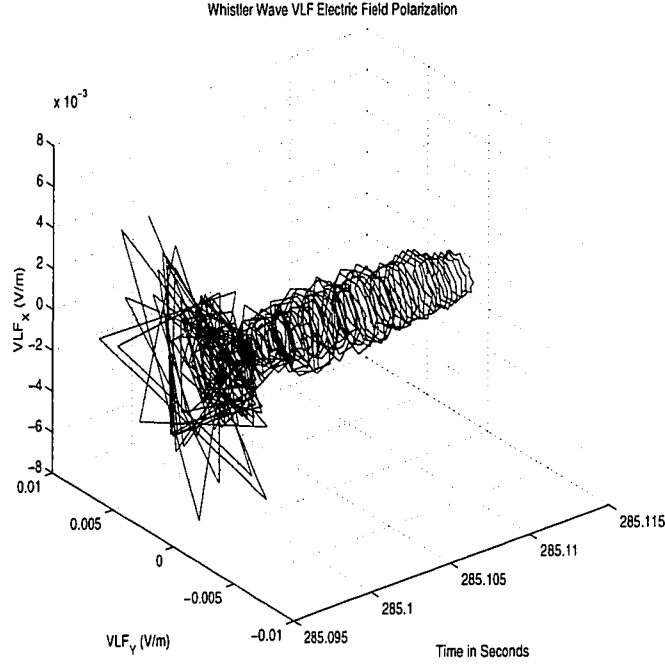


Figure 4.1: The electric field of the lightning whistler waves is circularly polarized about the earth's magnetic field \vec{B}_0 . The instantaneous wave electric field amplitude changes direction in time, rotating counterclockwise about the rocket vertical axis which points in the $-\vec{B}_0$ direction.

The solutions to equation 4.1 are complicated but some simplifications can be made under conditions of propagation in the ionosphere at ELF and VLF frequencies. When the whistler wave direction is sufficiently close to \vec{B}_0 , the tangential terms in the Appleton-Hartree equation can be considered small enough to be omitted without significantly affecting the calculated index of refraction n . This is known as the Quasi-longitudinal or 'QL' approximation. The conditions for the QL approximation are:

$$\frac{Y_T^4}{4Y_L^2} = \frac{Y^2 \sin^4(\theta)}{4 \cos^2(\theta)} \ll |(1 - X - iZ)^2| \simeq |X^2| \quad (4.3)$$

Then the simplified form using the QL approximation reduces equation 4.1 to [Helliwell, 1964]:

$$n^2 = 1 - \frac{X}{1 - iZ \pm |Y_L|} \quad (4.4)$$

Equation 4.4 can be further simplified if the effects of the electron-neutral collisions can be ignored. Note that the imaginary term in Equation 4.4 is due to the collision term Z , which gives a loss of the wave energy. If the wave frequency is much greater than the collision

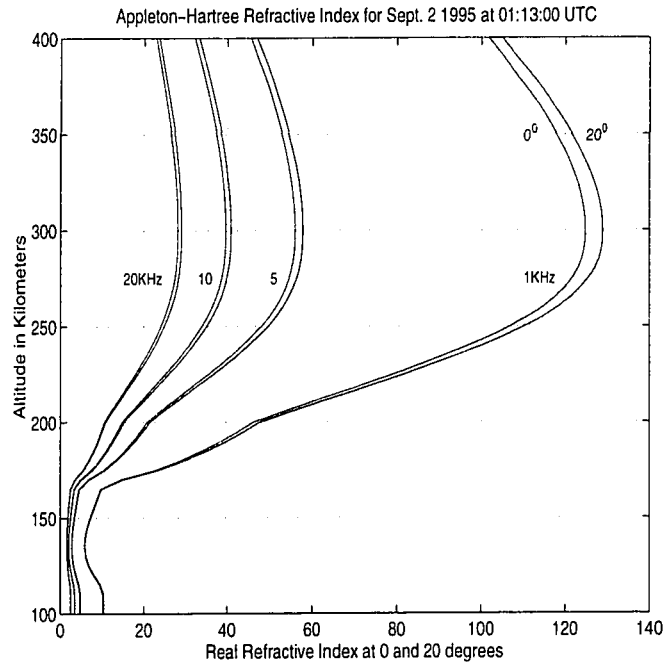


Figure 4.2: The index of refraction for whistler waves calculated using the Appleton-Hartree equation. The conditions are for the time of flight of Thunderstorm-III based on the IRI95 electron density model. The index of refraction n is calculated for $\theta = 0$ and 20 degrees from the magnetic field B_0 .

frequency, then the electrons are unlikely to collide and lose energy during the passage of the whistler wave. Neglecting the effect of collisions is certainly valid in the F region and even at 150 km except at the lower ELF frequencies. The electron-neutral collision frequency ν_{en} drops to about 1000 collisions/sec (c/s) at 150 Km, and to less than 100 c/s at 260 Km below the F layer.

For the nighttime conditions at Wallops Island at the time of flight of Thunderstorm III, the index of refraction of whistler waves is shown in Figure 4.2. The calculated index of

refraction n , used the electron density profile based on the International Reference Ionosphere 1995 (IRI95) density model. Two angles of wave propagation have been calculated for the up-going whistler waves. The wave vector \vec{k} , is not aligned to the magnetic field B_0 because of the strong electron density gradient in the lower ionosphere. The deviation of the wave vector \vec{k} may be as large as the local dip angle, which is about 20 degrees at Wallops Island. This causes a small increase in n . In section 4.6 we will compare the computed index of refraction to the *in situ* index based on the ratios of the measured amplitudes of the whistler magnetic and electric fields.

4.3 Changes in Whistler Wave Amplitude with Altitude in the Ionosphere

The lightning wave amplitude decreases noticeably with altitude of the rocket typically from 20 mV/m at 100 km to less than 5 mV/m at 400 km altitude. The average peak electric fields are shown in Figure 4.3. This plot summarizes the mean whistler wave amplitudes measured from NLDN located lightning strokes. The mean has not been normalized by the stroke currents, and the plot summarizes the data from more than 150 lightning strokes. There is a marked decrease in the peak whistler wave amplitudes upon entry into the base of the F region of the ionosphere at 260 km. In the F region, the peak VLF whistler amplitudes were less than 10 mV/m, averaging 5 mV/m. This was true even from the very largest +CG recorded during the flight, which had an NLDN estimated current of 92 kA, yet only a peak electric field amplitude at 380 km of 5 mV/m.

The wave amplitude should decrease with increasing electron density according to Magneto-Ionic theory. The electric and magnetic fields are related by:

$$n = c|B|/|E| \quad (4.5)$$

Here, c is the velocity of light, $|B|$ and $|E|$ are the magnitude of the magnetic and electric fields of the waves. Note that the values of n , B and E depend on frequency. This relation will be used later on to determine the refractive index of the ionosphere using the measured

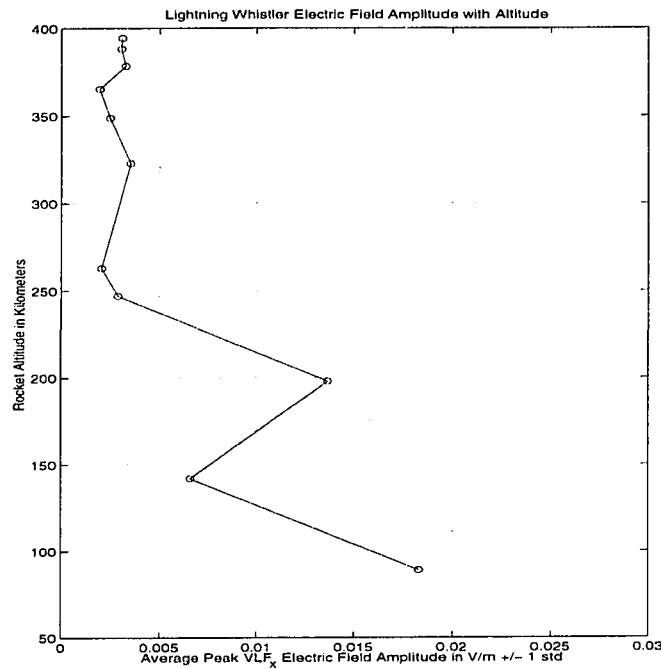


Figure 4.3: Data from more than 150 lightning strokes originating from the Wallops Island thunderstorm are summarized. The mean peak whistler amplitude with altitude and the standard deviation are shown. Notice the decrease in peak amplitude when the rocket enters the F region at 260 km

values of the VLF and ELF electric and magnetic fields. Because of the wave dispersion in the ionosphere, it will be important to know the time and frequency of the waves when applying this method in order to determine n . The Poynting flux \vec{S} is given by [Jackson, 1980]:

$$\vec{S} = \frac{1}{2\mu_0} \vec{E} \times \vec{B} \quad (4.6)$$

In the case of unducted whistlers, which the waves recorded by Thunderstorm III seem to be, there is no loss of energy along the path to the rocket except the losses from electron-neutral collisions at the very lowest altitudes in the ionosphere. The electric field amplitudes will also change if the electron density in the ionosphere changes. As the electron density increases, the wave amplitudes will decrease, even if the Poynting flux is conserved. This

can be derived from equations 4.6 and 4.5 along with the simplified form for the index of refraction which can now be written as [Helliwell, 1964]:

$$n = \frac{\omega_p}{(\Omega\omega)^{1/2}} \quad (4.7)$$

the change in the VLF electric field with altitude z can be written as:

$$E(z)^2 = \left(\frac{S^2 c \mu_0^2 \omega |\vec{B}_0|}{n_e(z)} \right)^{1/2} \quad (4.8)$$

Equation 4.8 shows that the whistler wave electric fields should decrease with altitude as the $(n_e)^{-1/4}$ and the wave amplitude will also change depending on the wave frequency as the $(\omega)^{1/4}$. The measured electric fields being studied here range from 10^2 Hz to 2×10^4 Hz, which means that the field amplitudes should vary from their free space amplitudes by as much as a factor of 10 at the highest frequencies. From the base of the ionosphere at 90 km to 300 km, the electron density increases from 10 to 2×10^5 per cc. The amplitude of the whistler mode waves will decrease by more than 1/35 of the free space amplitude at the 90 km injection altitude into the ionosphere. The ratio of both of these effects on the wave amplitude will be an approximate decrease in wave amplitude with altitude by 70% when the wave reaches middle F region altitudes of 300 km. This is approximately what is seen in the peak whistler wave amplitudes on Thunderstorm III. In the E-region the peak wave amplitudes are typically between 15 to 30 mV/meter and decrease to less than 10 mV/meter in the F-region at 300 km, as seen in Figure 4.4.

4.4 Electromagnetic Coupling in the Lower Ionosphere

The wave form of lightning changes with altitude and distance from the thunderstorm. The electromagnetic energy which reaches the rocket in the E and F regions must couple into whistler mode waves in the low density plasma at the base of the nighttime E region. The coupling of the wave frequencies is greatly affected by the conditions at the base of the

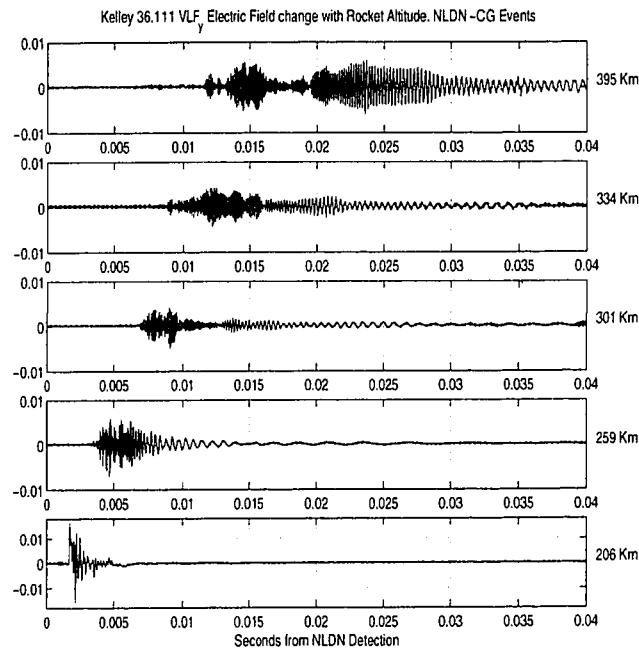


Figure 4.4: Each of the rocket measured VLF electric fields is plotted at the time of the NLDN recorded stroke. Notice that the time delay to the rocket increases and the dispersion of the wave also increases with rocket altitude. The peak wave amplitude decreases from ~ 15 mV/m at 200 km to ~ 5 mV/m at 300 km due to the increasing electron density.

ionosphere, and by the sub-ionospheric propagation of the lightning electromagnetic fields. If the lightning occurs near the point of coupling, the wave energy is not changed by losses caused by distance, such as waveguide losses, but it is affected by the local orientation of the lightning channel and by the height and the electron density gradient at the base of the E region. Each of these conditions change the coupling process from EM waves into the whistler mode waves.

In the next section, the effects of the distance the wave energy travels before entering into the ionosphere will be shown to influence the observed wave energy measured by Thunderstorm III. The distance traveled enhances the relative VLF energy, shifting the maximum wave energy to the lower ELF frequencies. A second interesting effect was observed in the

whistler waves at lower rocket altitudes caused by the physical height of the nighttime ionosphere. The height of the nighttime ionosphere allows certain VLF and ELF wavelengths to propagate differently below the ionosphere and has a very direct impact on the whistler mode wave energy at the rocket.

At altitudes of 90 to 150 kilometers, the electric field waveforms of lightning vary in appearance. Some lightning strokes appear as a short pulse with very little dispersion in frequency and last only a few milliseconds, other strokes have a more dispersed waveform with several oscillations [Siefiring, 1987]. The measured electric fields from many of the lower altitude lightning strokes had a strong field aligned component which was unipolar, or a combination of a unipolar pulse and oscillating electric fields. These field aligned electric pulses are the topic of Chapter 5.

The energy in the lightning wave transients at low altitudes, is made up of the electrostatic and electromagnetic components below the base of the nighttime E region, and only electromagnetic waves above¹. Below the base of the nighttime E region ionosphere, the electromagnetic wave components are made up of horizontal and vertically polarized waves. At VLF frequencies, from 3 kHz to 30 kHz, these two circularly polarized components are known as the O mode and the X mode waves. On entry into the base of the ionosphere, the vertically polarized X mode wave becomes evanescent, and attenuates rapidly with altitude. The O mode wave couples into the horizontally polarized whistler mode [Ratcliffe, 1959].

Earlier rocket flights suggested that the X mode wave was present up to about 120 km, where it rapidly decayed due to the presence of a strong Sporadic E layer [Siefiring, 1987]. There is no evidence that there was a sporadic E layer during Thunderstorm III, and the X mode waves were probably present up to higher altitudes during this flight.

The electrostatic fields if they are measured by the rocket, should be very small in the E

¹ Unless the electromagnetic whistler mode waves couple into Lower Hybrid frequency electrostatic waves. These were observed on Thunderstorm-II [Baker, 1998]

region, being rapidly attenuated by the increasing conductivity. Below the E region, there should be a measurable transient electrostatic field which decreases rapidly in duration and amplitude in the upper mesosphere and the D region with altitude [Hale, 1996]. The electrostatic field should show an initial decrease in the vertical electric field at the rocket in response to the removal of negative charge in the thunderstorm. The recovery of the electric field back to the new DC field level will depend on the local conductivity, but may be slightly less than the local relaxation time [Holzworth and Chiu, 1982].

Earlier data from the Thunderstorm II and Thunder Hi and Lo rocket flights, found evidence of a field aligned electric pulse. The amplitude of these pulses was as large as 30 mV/m [Kelley *et al.*, 1990]. This field aligned pulse can last up to a millisecond or more. A pulse in the ionosphere of several mV/m will produce a significant current flow upward (or downward) to the base of the F region ionosphere. The field in these pulsations is sufficient to accelerate the local electrons to many times their normal temperature [Siefving, 1987]. These pulses will thus change the overall velocity distributions of the electrons in the E region ionosphere. The electric pulse will be examined in Chapter 5.

4.4.1 Low Altitude D Region Lightning Transients

The flight trajectory of the rocket included measurements from below the base region of the nighttime E region, down as low as 70 km before loss of telemetry occurred. The lightning transients measured in this region show some combined features of electrostatic and electromagnetic pulses. There are only about 10 seconds of data from this altitude from 95 down to 70 km which begins the final reentry into the atmosphere. We will examine the what we believe to be the electrostatic field changes of the lightning pulses in order to make an estimate of the electron density in the lower D region. An attempt was made to look for a perturbation of the density in a multiple stroke lightning flash, using the decay of the electrostatic field. The results did not show any significant differences in the transient decay times between different strokes in the flash. The differences in decay times were all

within the uncertainty ($\pm 5\%$) in the curve fitting used to determine the decay times from the transients.

Based on the rapid rate of increase in the conductivity at the base of the D region, we should be able to determine the approximate earth-ionosphere waveguide height and compare this to the estimates made in section 4.4.2 based on the lightning sferics, known as tweeks.

In the D region, the electron density changes rapidly with altitude in a transition region at 85 to 110 km at nighttime. At the transition, the gradient in electron density is a good reflector of VLF and ELF wave energy, and forms the upper part of the earth-ionosphere waveguide. Small changes in the electron gradient can effect how well VLF waves propagate in the waveguide [Wait, 1967]. Thunderstorms are known to cause perturbations to this region, by lightning induced electron precipitation from ducted whistlers [Imhof *et al.*, 1985], or strong electron density changes caused by the electromagnetic pulse from the lightning stroke itself [Taranenko *et al.*, 1993; Dowden and Adams, 1993]. Direct measurements of the lightning transient wave fields in the D region are interesting for several reasons in this study, these are: 1) How large are the electrostatic field components from nearby lightning? 2) Can the electron density be estimated based on the recovery time of the electrostatic field decay? and 3) Are there measurable perturbations in the electron density between successive strokes?

Lower altitude measurements at 90 down to 70 km altitude do show a vertical electric field with an electrostatic field decay consistent with the electrostatic decay fields expected from the removal of charge from nearby thunderstorms. These fields show a large increase in decay times at lower altitude as the electron density decreases below the nighttime D region ledge at 90 km.

The transient decay field is shown in Figure 4.5. Here, the rocket has descended below the E layer and is now in the lowest part of the D region, just below the steep electron density increase from 90 to 120 km. The electrostatic field is now apparent in the wave

fields (see lower panel in Figure 4.5) as a slow 2 millisecond recovery which is imposed on the electromagnetic wave oscillations. Notice that the magnitude of the field offset and recovery measured at the rocket is negative, which corresponds to an electric field directed upward along B_0 . This is because VLF_{26} , the vertical field channel instrument described in Chapter 2, takes the voltage difference between the upper vertical probe VLF_2 , which is at a lower potential, minus the lower probe VLF_6 , which is at a higher potential. Thus the actual electric field shown in Figure 4.5 is in the positive (upward) direction, or, $VLF_{26} = -E_z$. The measured electric field, $\vec{E}_z = -VLF_z$, is consistent with the fields expected from a -CG, namely a positive, upward directed \vec{E}_z . When the negative charge is removed from the Northeast thunderstorm cell, located at 38.34 North, -74.5 West, a strong positive electric field change is observed, this appears in the instrument at the rocket as a negative change in VLF_z . The electrostatic field then recovers back to zero, with a decay time depending on the integrated conductivity at 84 km [Volland, 1984].

In the D region, the waveforms from lightning events measured by thunderstorm III do show a combination of electromagnetic and electrostatic wave components as shown in Figure 4.5. The measured vertical electric field of the lightning transient has strong ± 35 mV/m VLF wave components superimposed on a slowly decaying electrostatic field. The electrostatic field, really a "quasi-DC" field, decays in a time somewhat less than the local relaxation time equal to $\tau = \sigma / \epsilon_0$. The electrostatic wave field decays within several milliseconds after the CG return stroke. This decay would take even longer to relax at lower altitudes, up to several seconds in the stratosphere [Volland, 1984]. Based on the decay time of these electrostatic fields, it should be possible to estimate an upper limit to the local conductivity and electron density. This was done for several of the lightning strokes at this altitude. The time for the pulse to decay to $\tau = 1/\epsilon$ was found to be about 1.2 milliseconds at 84 km altitude and increased to more than 90 milliseconds at 70 km. Below this altitude, no further data could be recovered because of the effects of reentry. If we use a simple model to estimate the electron density at these altitude we can make an estimate of the local elec-

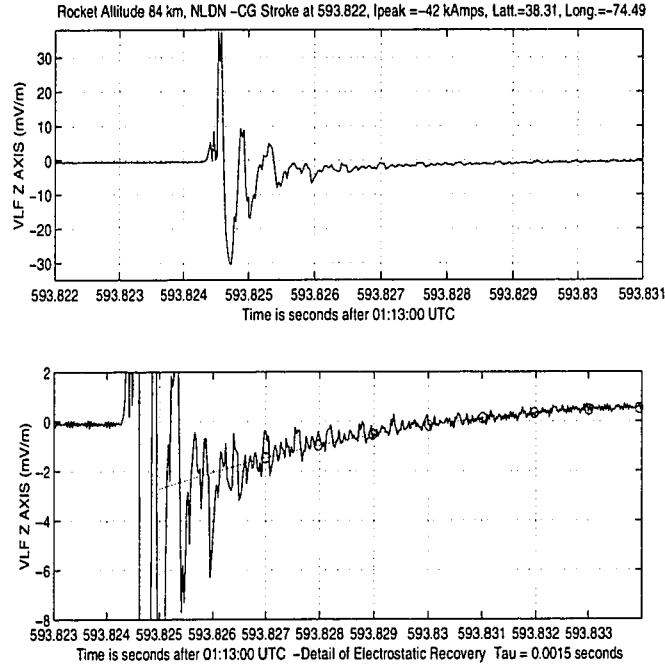


Figure 4.5: Lightning transient electrostatic fields measured at 84 km altitudes.

Top panel: the lightning stroke vertical electric field has an electromagnetic wave superimposed on a transient electric field.

Lower panel: the vertical scale has been reduced and the time axis shifted slightly to show the detail of the transient recovery field. An exponential curve has been fit, and the field transient has a calculated decay time of 1.15 ms.

tron density based on the transient field decay times. The equation for the \vec{B}_0 parallel AC conductivity is :

$$\sigma_0 = \frac{n_e e^2}{m_e (\nu_e - i\omega)} + \frac{n_i^+ e^2}{m_i^+ (\nu_i^+ - i\omega)} + \frac{n_i^- e^2}{m_i^- (\nu_i^- - i\omega)} \quad (4.9)$$

the superscripts, (+), (-), in the equation are for the positive and negative ion components and the subscripts e and i are for the electron and ion components. For the conductivity at 85 to 75 km, on the time scales of the local recovery field times $\tau > 1$ m sec, we can drop the imaginary terms ω in the equation and assume that the conductivities are "quasi-

DC". This approximation is valid since the electron-neutral collision frequencies ν_e is about $10^7 s^{-1}$, giving an average collision time $10^{-7} s$, which is much shorter than the transient field times we are looking at at these altitudes. The lightning transients have frequencies of roughly $\omega < 10^3$. The ion-neutral collision frequency ν_i is less than the electron-neutral collision frequency in the E and D regions. At 75 km ν_i is about $10^5 s^{-1}$. Therefore the DC approximation is valid since $\omega \ll \nu_e \ll \nu_i$, and the DC approximation of equation 4.9 can be used dropping the imaginary term $i\omega$ from the denominator.

Based on the transient electrostatic decay times τ , an upper limit for the parallel conductivity can be estimated in the D region and Mesosphere altitudes. The estimates of the electron densities are more difficult and uncertain because of the estimated collision frequencies. There is a second problem at mesospheric altitudes, which is that the transient decay times cannot be assumed to be dominated by the parallel conductivity σ_0 . At these lower altitudes, the Pederson or perpendicular conductivity components become comparable to the parallel component.

Table 4.1: The decay times of the local transient vertical electric fields were used to estimate the electron density and vertical DC conductivities at altitudes below the nighttime E-region "ledge" at 90 km. A large increase in the decay times was observed between 85 and 70 km as the electron densities decrease at the mesosphere altitudes.

Altitude	cases	τ (ms)	σ_0 (S/m)	N_e (cc)
84-81 km	2	1.15	7.7×10^{-9}	1200(-)
72-68 km	1	90.12	9.8×10^{-11}	16 (-)

Measurements of transient lightning fields at these lower altitudes are important, yet remain some of the least measured lightning events. The electrostatic field components from the nearby lightning storms show the expected field change at the rocket along the E_z field direction. These fields are completely absent above 110 km altitudes. Distant lightning storms, such as the storms in North Carolina, did not produce this type of measurable tran-

sient field decay. The magnitude of the electrostatic fields is only 10 mV/m, which is far less than the fields that have been estimated to produce the breakdown causing Sprites. These measurements were not made directly over the thunderstorm but are within 150 km of the lightning strokes. The transient electrostatic fields would be expected to be larger directly over the storm.

4.4.2 The Effects of Sub-Ionospheric Propagation on Lightning Whistlers

The wave frequencies making up a lightning stroke are modified with the distance they travel from the stroke by attenuation in the region between the earth and the lower ionosphere. The region can be thought of as the surface of the earth forming a lower conductive boundary and the ionosphere forming an upper conductive wall of a natural waveguide. Lightning electromagnetic waves which propagate in this waveguide, will have to satisfy the boundary conditions at the top and bottom walls of the guide.

One of the observed properties of waveguides is the cutoff wavelength. Cutoff occurs in a regular waveguide when the half wavelength is larger than the the distance between the top and bottom of the guide. If the wave has a longer wavelength or lower frequency, it is strongly attenuated. In a normal waveguide this distance is fixed, but in the earth-ionosphere waveguide, the distance varies depending on the electron density of the lower ionosphere. At ELF frequencies, at approximately 1.5 kHz, the cutoff wavelength results in a type of wave known as a tweak atmospheric or spheric. The tweak frequency wavelength is where the half wavelength is just slightly less than the height of the earth-ionosphere waveguide. This distance from the ground to the base of the D region ionosphere is typically 90 km at night. At the waveguide cutoff frequency, which is usually about 1.4 to 1.6 kHz depending on the height of the initial electron density "ledge" in the E region, the velocity of the electromagnetic waves decreases. The ray path of the electromagnetic wave as it approaches cutoff steepen, and the wave speed decreases. A nearby lightning stroke should show a delay at the cutoff frequencies, and at the multiples of the cutoff, as the wave partially reflects

between the earth and the ionosphere. Because the ray angle of these waves has changed from horizontal to more nearly vertical, the coupling into the lower ionosphere plasma and the whistler mode should be enhanced. This effect is observed in some of the light-

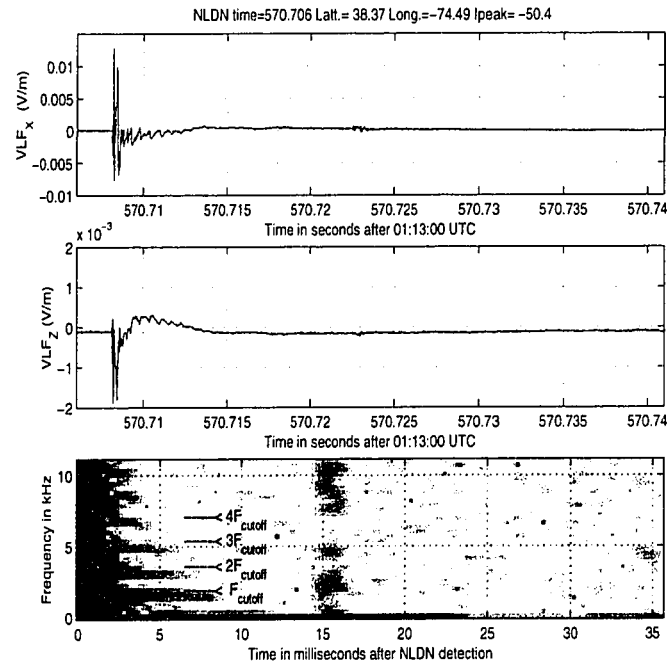


Figure 4.6: The -CG lightning stroke, was measured at a rocket altitude of 140 km. The lightning spectrogram shows harmonic lines which occur at multiples of the earth-ionosphere waveguide cut-off frequencies. This same effect was observed in some of the measured strokes during the up leg of the rocket flight. The harmonics of the waveguide cutoff have also been measured in sub-ionospheric studies by [Shvets and Hayakawa, 1998].

ning strokes at measured at lower altitudes by Thunderstorm III, an example is shown in Figure 4.6. When these waves finally reach the region near the rocket, some of the wave energy will couple upward to the ionosphere. The whistlers from distant lightning strokes have interesting properties which can be understood in terms of their sub-ionospheric propagation. Distant source whistlers can be used to find the height of the lower ionosphere and approximate density.

Lightning sferics which have propagated in the sub-ionosphere from Florida and then entered the ionosphere near the rocket in Virginia also show characteristic harmonic frequencies of the earth-ionosphere waveguide. In this case shown in Figure 4.7, the peak wave power is at 1.47 kHz. Above the cutoff frequency, harmonics of the wave cutoff frequency are visible in the electric field spectrogram. These harmonics appear as higher frequency waves "ringing" on the electric field waveform between $t=111.555$ to 111.565 seconds.

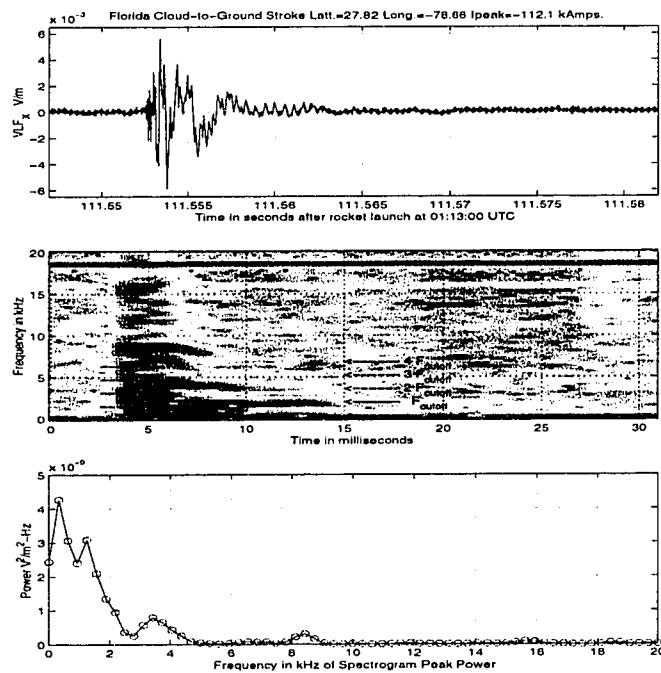


Figure 4.7: A powerful -100 k-Amp lightning stroke was received by the Thunderstorm III rocket from a stroke in Florida. The peak ELF frequency in this stroke was at 1.47 kHz, which is near to the earth-ionosphere waveguide cutoff frequency. This waveguide cutoff gives the approximate height and density of the nighttime ionosphere.

4.4.3 ELF Tails from Distant Lightning

The earth-ionosphere waveguide cutoff has been seen to alter the wave power spectral density of lightning whistlers in the previous section. There is another effect which is the re-

sult of the higher attenuation of the VLF wave frequencies traveling in the sub-ionospheric waveguide and the lower ELF frequency waves which traveling in a different wave mode that is not restricted by the dimensions of the earth-ionosphere waveguide. These waves are known as "0th mode" TM waves. The difference in attenuation for different frequencies of waves, which travel large distances, results in lightning power spectral densities which have much higher relative intensity at the ELF wave frequencies, often as large or larger than the VLF fields. The resulting waveforms have often been observed in ground measured waves and are known as ELF slow tails [Hepburn, 1957].

For CG lightning strokes which have a sufficient amount of ELF wave energy, there will be a slow oscillation "tail" consisting of 1 or 2 cycles following the higher VLF waves. The ELF tail will have an initial first cycle peak which is delayed depending on the receiver's distance from the lightning source. This delay typically follows a linear relation for distances greater than 2000 km, but at shorter distances, such as the two cases shown in Figure 4.8 the delay time is proportional to the square of the distance [Wait, 1960; Taylor and Sao, 1970]. Normally the ELF waves measured at the ground for ELF slow tail lightning strokes are vertically polarized [Shvets and Hayakawa, 1998]. In Figure 4.8, the horizontal wave fields have been plotted because the vertical fields have become very small and they are traveling as horizontally polarized whistler mode waves in the ionosphere. Lightning strokes which produce larger relative amounts of ELF wave energy are often positive CG strokes, but negative strokes also produce the observed ELF tails as well [Reising *et al.*, 1996]. If the ELF waves are generated in the stroke channel, then the stroke currents must last longer than average stroke currents, on the order of several milliseconds, to generate ELF waves. Positive CG strokes have been associated with continuing currents [Rust *et al.*, 1985] and measured distant slow tails waveforms from positive strokes have been recorded in Antarctica which have been directly related to observed Sprite activity [Reising *et al.*, 1996]. There still are no direct observations of strokes with continuing currents that have enhanced ELF wave energy. There are recent reports that ELF wave pulses within 1 to 5

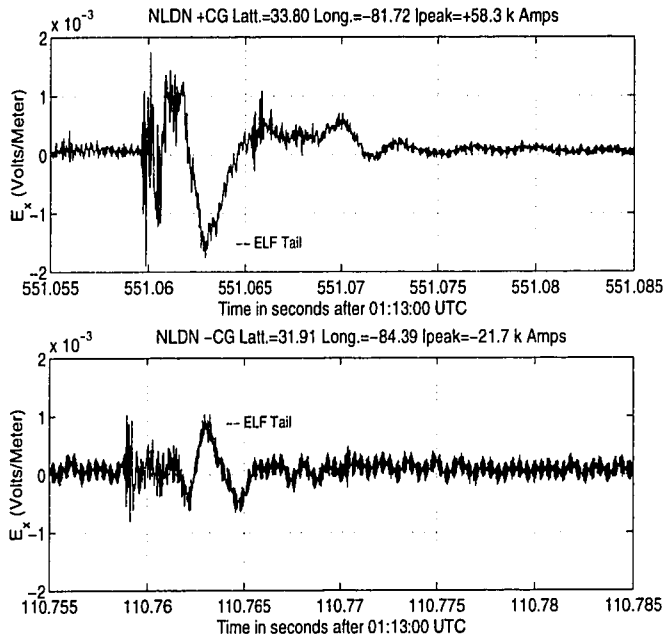


Figure 4.8: These lightning strokes traveled more than 600 km from N. Carolina to Virginia before entering the ionosphere. The lightning stroke in the top panel was measured at an altitude of 173 km and the stroke shown in the lower panel was measured at 196 km. In each case, distance has reduced the amount of VLF wave energy, and the ELF frequencies at 400 Hz are now dominant. These ELF waves propagate with a slower velocity than the higher frequencies. The single cycle ELF oscillation at 400 Hz is known as an ELF slow tail. In the cases shown, the slow tails occurred for a positive (top) and a negative (lower) CG stroke.

ms of the VLF CG waves have also been directly linked with the formation of the the Sprite channels. The Sprites have been observed to form immediately following negative as well as positive CG strokes².

It is believed that the slow tail ELF is the result of continuing currents in the lightning stroke. This argument stems from the observation of ELF wave cycles immediately following the higher frequencies in lightning strokes that are observed within 100 km distances. The observations of Sao et al. that ELF tails can come from apparent multiple stroke flash

² Mark Stanley, NMIT personal communication November 1998.

sources suggests that the ELF waveform is due to the continuing currents in the CG lightning channel [Sao *et al.*, 1970]. This could be further verified if ground optical observations could support the inference of continuing currents in these strokes. In the cases of apparent continuing currents observed by the ground optical instrument at Wallops Island during Thunderstorm III, there was some ELF enhancement in the negative CG stroke whistler at the rocket (see Chapter 7, Figure 7.6. It is possible that a particular lightning channel configuration is needed along with the continuing current, but it seems that the assumption that there are continuing currents should be further investigated. J. R. Wait suggested that horizontal lightning channels from intracloud lightning strokes could be sources of ELF slow tails. He suggests that the horizontal channels would have very different directional characteristics which would be apparent in observations made simultaneously at different locations [Wait, 1960]. Although it has been generally believed that strong ELF wave energy in CG strokes was the direct result of continuing currents, there seems to be some reasons to question this based on the ELF signature from the co-located Sprites which also have a similar unique ELF signature [Marshall *et al.*, 1998].

4.5 Study of Ionospheric Dispersion of Whistlers

In this section, we will show how the low frequency (VLF and ELF) whistler wave dispersion can be used to reconstruct the approximate electron density during the flight. This density information is critical to understanding some of the puzzling features seen in the electromagnetic fields below the F-region such as the field aligned pulsations and the small wave amplitudes that were recorded during Thunderstorm III.

Whistler waves are dispersive and this feature can be used to look at the density properties of the lower ionosphere, (and magnetosphere for that matter). The arrival time of each whistler wave frequency will be delayed according to the group velocity of the waves. It is the delay time of each of the frequency components that depends on the electron density along the propagation path up to the rocket. Thus, each lightning whistler wave packet

makes an integrated sounding of the electron density properties below the rocket.

The Thunderstorm III whistler waves were not ducted, but the frequency dispersion of the VLF whistlers can be used to estimate the electron density of the lower E and F regions at the time of flight. By comparing the amount of wave dispersion at different altitudes, it will be shown that we can determine the electron density in the E and F region ionosphere. Normally, multi-hop whistler waves are used to determine the equatorial electron density and path along the field lines. The technique is to look at the frequency of minimum time travel, known as the nose frequency, and the dispersion of the waves during the 'ring-down' portion of the whistler. The nose frequency occurs at $.25\Omega$ and this can be used to determine the L-shell or magnetic field line of force that the whistler encountered, since the nose occurs at the lowest gyro frequency encountered along the path between hemispheres. The dispersion can then be used to estimate of the electron density along the field line [Helliwell, 1964].

The method of using the dispersion to determine the electron density in the lower ionosphere involves inverting the integral in equation 4.10 This is possible to do only because we have measured values of the dispersion at different altitudes with the Thunderstorm III rocket. The successful application of this method has not been done before in the lower ionosphere, and this method is only possible using sounding rocket measured fractional hop whistlers. Previous attempts to determine the lower ionosphere density have not been successful, owing to the long paths taken by multi-hop whistlers. [Brown, 1965].

The dispersion D_0 is defined here as [Helliwell, 1964]:

$$D_z = \int_{z_1}^{z_2} \frac{f_0}{\sqrt{f_g}} ds^{1/2} \quad (4.10)$$

The equation assumes the wave frequencies are much lower than the local electron gyro frequency, f_g , and that the propagation of the whistlers is quasi-longitudinal. These are good assumptions for VLF waves in the E and F region nighttime ionosphere, where the electron gyro frequency is 10^6 Hz. The rocket electric field data show that these waves are very nearly right hand circularly polarized in the plane of the magnetic field, \vec{B}_0 .

The dispersion D is found using the whistler spectrograms by first plotting the spectrograms of the VLF electric field data. Next, the arrival times of different VLF frequencies are found from the spectrogram and plotted as the square root of frequency vs. time. The slope of this line, shown in Figure 4.9 in the third panel, gives the value of the whistler dispersion D .

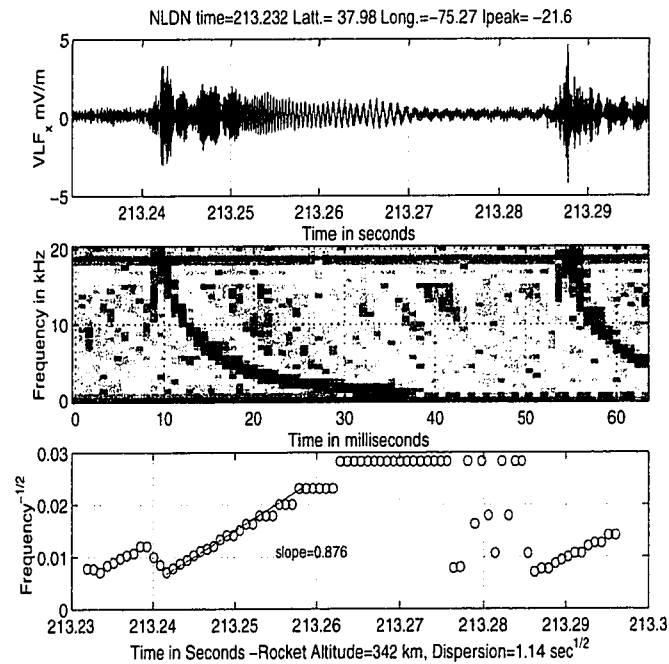


Figure 4.9: Each lightning whistler wave will have a characteristic dispersion D_z which depends on the integrated electron density along the whistler path to the rocket. By plotting the data from the spectrogram in the second panel as a function of $1/\sqrt{f}$, D_z can then be simply found by taking the inverse slope of the line. This was done for more than 190 whistlers from the 3 different storms, two near Wallops Island and one in North Carolina.

It was possible to measure the value of D down to about 210 km altitude. The smallest measured dispersion was $0.08 \text{ sec}^{1/2}$ at 216 km altitude, and a maximum dispersion of $0.3 \text{ sec}^{1/2}$ was measured at the 400 km rocket apogee. Dispersions were measured for more than 190 lightning CG whistlers from the Wallops storm cell and the storm to the Northeast

of Wallops, shown in Figure 4.10. Below 210 km, the waveforms were too short for the dispersion to be analyzed in this way. During conditions of higher electron densities, such as during a solar maximum, this method could be used down to lower altitudes. The parameter

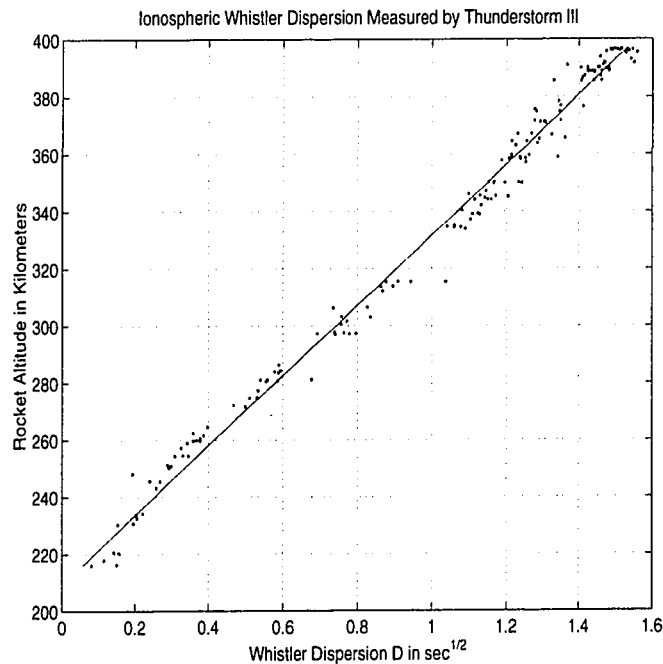


Figure 4.10: More than 190 CG lightning strokes were analyzed to determine the value of the whistler dispersion D at different altitudes during the flight of Thunderstorm III. The dispersion became too small to determine below 210 km altitude. The line is a best fit to the dispersion data using a 3rd order polynomial.

D can also be calculated directly from the IRI95 electron density profile model. This is shown for comparison to the measured dispersions during the flight in Figure 4.11. Here we have used the IRI95 computed electron densities at the time of flight, including the effects of solar cycle conditions, to find the dispersions based on the model profile. The measured dispersions (dots in Figure 4.10) are considerably higher above 240 km compared with the IRI95 results. This suggests that the F region nighttime electron densities were higher during the rocket flight, but that the E region densities may have been lower.

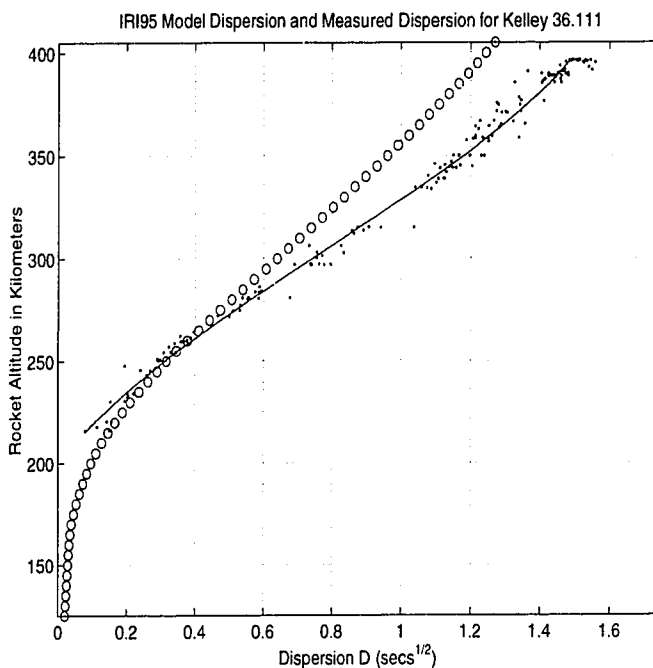


Figure 4.11: The whistler dispersion D was found using the electron density profile from the IRI95 model data and computing the dispersions. These values are plotted here and compared with the measured dispersions from the Thunderstorm III data. Notice the higher values of D from the rocket data suggesting that the electron density must have been higher than predicted by the IRI95 model profile.

The method used here to calculate the F region electron density profile is to take the measured whistler wave dispersions at each altitude level D_{z_n} , and find the change in the dispersion, $(D_{z_{n+1}} - D_{z_n})$, between the different levels. The dispersion difference between two different altitudes will be due to the total electron content in the layer of thickness $(z_{n+1} - z_n)$. In this way, the dispersion D_{z_n} between altitude levels can be used to determine the plasma frequency f_{0n} in each layer. Note that we have made the assumption that the electron density and plasma frequency are constant in the layer. By taking a shorter distance between the altitude points, a better estimate of the density profile can be made, but it is not practical to use this method to determine fine structure densities of say 1 or 2 km or

less. Another limitation is that it becomes difficult to determine D_z below about 200 km, where the dispersions are quite simply too small to be determined from the VLF data.

The easiest way to find the electron densities is to put the problem into a matrix form. The values of D_z are written in matrix form which is set equal to the linear equation corresponding to the integral portion of equation 4.10. This matrix can then be inverted to solve for the plasma frequencies $f_0(z)$ and the electron density in each layer. This is done in the following matrix form of equation 4.10:

$$\begin{pmatrix} D(z_1) \\ D(z_2) \\ \vdots \\ D(z_n) \end{pmatrix} = \begin{pmatrix} m_{11} & m_{12} & \cdots & m_{1j} \\ 0 & m_{21} & \cdots & m_{2j} \\ \vdots & \ddots & & \vdots \\ 0 & \cdots & 0 & m_{ij} \end{pmatrix} \cdot \begin{pmatrix} f_{01} \\ f_{02} \\ \vdots \\ f_{0n} \end{pmatrix} \quad (4.11)$$

Here the elements m_{ij} are:

$$m_{ij} = \frac{\Delta Z}{f_g(z_i)} * \frac{1}{2c} \quad (4.12)$$

and the dispersion D_{z_n} at altitude z_n is given by the summation:

$$D(z_i) = \sum_{j=i}^n m_{ij} \cdot f_{0j} \quad (4.13)$$

The matrix used here consisted of 35 rows, representing the dispersion in layers each 5 km thick, beginning at 225 km up to 398 km. The dispersion data were fit to a 3rd degree polynomial so that values of D_{z_i} could be found at evenly spaced altitude points. The electron gyro frequencies were calculated for each level based on the revised 1995 IGRF magnetic field model, using epoch 1995 [Langel, 1992]. Note that the IGRF calculated field values were compared with the on-board NASA DC magnetometer data and were within 1%.

The inversion of the dispersion altitude profile shown in figure 4.12 shows that the electron density in the F region must have been substantially higher than the values calculated using the IRI95 model. The uncertainty in the values are based on the measured variations in D at any particular altitude in the profile $\pm 5\%$ and in the residuals from the matrix inversion. The total estimated uncertainty is $\pm 15\%$ at each altitude. The PFP electron densities ("*")

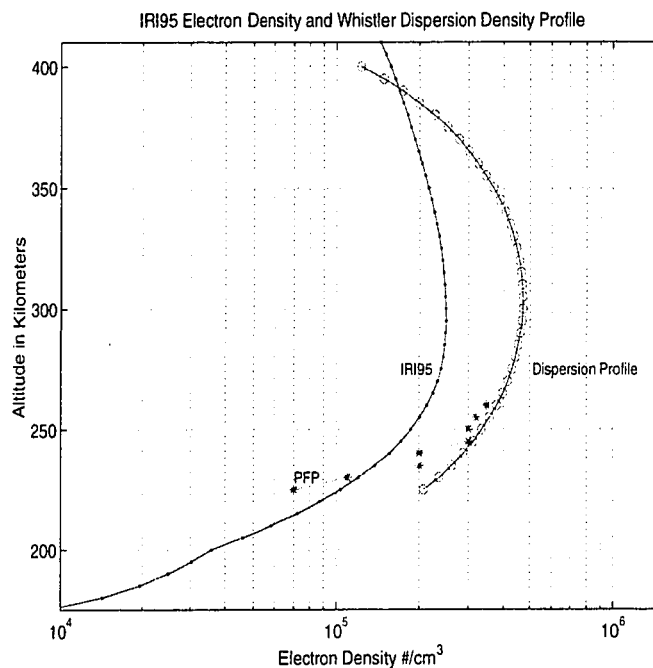


Figure 4.12: The electron density profile was calculated based on the measured changes in whistler wave dispersion with altitude. These values compare well with the Plasma Frequency Probe data. The IRI95 model estimated electron density can not account for the measured whistler dispersion. The actual electron density is found to be considerably higher.

in Figure 4.12) are in good agreement at 240 to 265 km altitudes. At 225 km, the electron densities decrease sharply as shown in the PFP data. The fitting method using 3rd degree polynomial to the dispersion data, and the low dispersion values at the lower altitudes, do not show the decrease in electron density at 225 km. This method also works well at the higher dispersions and electron densities that are found in the F region.

4.6 In-Situ Determination of the Refractive Index

In this section, the calculated index of refraction n is compared with the index of refraction determined from equation 4.5 using the measured values of the electric and magnetic field

magnitudes of the whistler waves. By taking the ratio of the magnetic and electric fields of the whistler waves at different altitudes we can determine $n(z)$ directly at different rocket altitudes using $n(z) = c|B|/|E|$.

This method was originally used to determine the index of refraction using radio waves from a ground VLF transmitter received at a sounding rocket in Antarctica [Kintner *et al.*, 1983] and later at Wallops Island [Siefiring, 1987]. Here we will use the same theoretical method but the source will be the ELF frequency portion of the natural whistlers waves at 1.56 kHz. The whistler magnetic fields were measured by the DSRI AC fluxgate magnetometer. The initial flight magnetometer was replaced earlier in the summer prior to launch. The replacement instrument had an A-to-D latching problem which caused significant noise in the data. The analysis was limited by this noise and by the fluxgate magnetometer sensitivity. Only the largest amplitude whistler waves with relatively "clean" ELF waves were used to make the estimate of the index of refraction based on equation 4.5. The fluxgate frequency response was limited to signals below 4 kHz, and only 5 CG lightning strokes produced sufficiently clean ELF wave forms with reasonably large signals at frequencies between 1 and 2 kHz in both the electric and magnetic field instruments.

The first step was to take the total wave vector magnitudes at 1.56 kHz. This frequency was selected to be approximately in the mid-band of the fluxgate magnetometer. The time and frequency maxima were found from the spectrograms of the waveforms. The wave magnitudes were found by taking the vector sum of the wave fields, after which the magnitudes from the two instruments were compared. The results of the analysis are shown in Figure 4.13. The uncertainties in the analysis are due mostly to the frequency determination from the spectrograms and the noise in the fluxgate magnetometer data. In an earlier study by C. Siefiring, similar problems were encountered with instrument noise causing large uncertainties in the estimated index of refraction [Siefiring, 1987]. In Figure 4.13, the index of refraction n at 1.56 kHz is calculated based on the IRI95 density profile and also calculated for double and triple the IRI95 electron density.

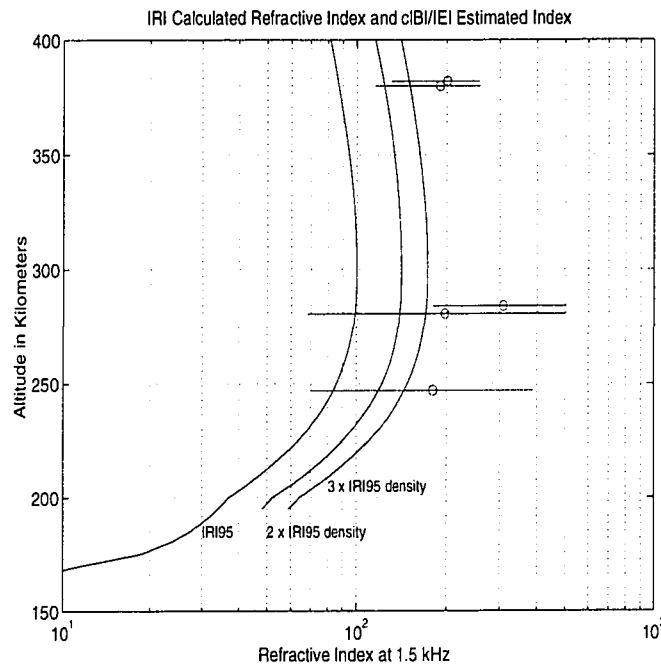


Figure 4.13: The Index of refraction n , was found from the ratio of the whistler wave vector electric and magnetic fields. The magnetic fields were measured by the AC fluxgate magnetometer and electric field from the Cornell University VLF instrument. Only several of the largest amplitude whistlers had sufficiently strong ELF wave intensities at 1.56 kHz. Noise on the fluxgate magnetometer instrument contributed significantly to the uncertainty in the calculated index of refraction.

The peak estimated electron density in the F region, based on the whistler dispersions, is $5 \times 10^5/\text{cc}$, about twice the IRI95 model estimate (see Figure 4.12). The in-situ index of refraction values found for the 5 lightning whistlers in Figure 4.13 are all larger than the n for double density values. Given the large uncertainties found using this method, the dispersion profile densities are in agreement with the the result here. The dispersion calculated electron density was at least double the IRI95 estimated electron density, but this estimate has at least a 15 % uncertainty. The index of refraction based on the whistler dispersion electron densities ($2 \times \text{IRI95}$), agree with at least 3 of the 5 values found using the field ratio index of refraction n .

The method of in-situ electric and magnetic field ratios is difficult to apply in many cases. The method applied to the rocket data uses instruments with different frequency responses. This method shows promise as an additional check on the other methods used to estimate electron densities. The best applications for this method remain at the higher VLF frequencies with the use of fixed frequency transmitters. Continuous source transmitters reduce the problems of timing and frequency estimates from whistler sources.

4.7 ELF Energy in Whistler Waves

Most lightning strokes have their maximum power between 3 and 12 kHz, typically peaking at about 5 kHz [Uman, 1984]. Certain lightning events produce much more energy at lower frequencies, i.e. less than 1 kHz, this type of stroke is associated with a continuing current [Burke and Jones, 1996]. Positive Cloud-to-Ground (CG) lightning events have been associated with strong ELF emissions and continuing currents much more frequently than negative CG events. This type of lightning stroke is also known to trigger Cloud-to-Ionosphere Discharges (CID) or Sprites. The ELF waves in the the earth-ionosphere waveguide with amplitudes which exceed 1.5 mV/m at frequencies below 1 kHz, have been associated with large continuing current events and Sprites [Reising *et al.*, 1996].

Data from the Thunderstorm III rocket flight shows that some of the upward propagating whistler waves produced by CG strokes have much higher than average ELF wave energy. NLDN located lightning strokes, which had low amplitude ELF waves, were usually negative CG strokes with small peak currents, or low current positive strokes. The strokes that produced the higher amplitude ELF waves, in excess of > 1.5 mV/m, were the larger CG lightning events. A large positive CG stroke which produced ELF whistler waves at 3 kHz to 250 Hz frequencies is shown in Figure 4.14. This whistler has ELF wave electric field amplitudes greater than 1.5 mV/m, but it is especially strong at frequencies below 1 kHz compared to other strokes. Positive CG lightning events with continuing currents are less frequent than negative CG lightning strokes, nevertheless they did occur frequently enough

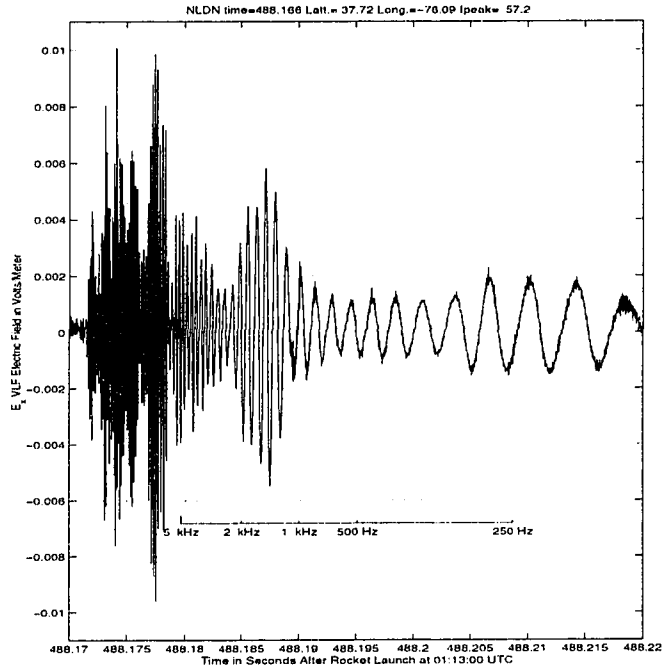


Figure 4.14: This positive polarity CG lightning stroke produced unusually large ELF wave amplitudes. It is possible that there were continuing currents associated with this stroke.

during Thunderstorm III to have been observed several times during the 10 minute rocket flight. This type of lightning stroke is interesting because it may generate much stronger waves at ELF frequencies. ELF waves following within 1 ms or more of CG strokes are associated with Sprite currents above thunderstorms [Marshall *et al.*, 1998].

4.8 Whistler Stimulated Lower Hybrid Waves

The lower hybrid resonant (LHR) electrostatic plasma wave has frequencies in the lower ionosphere which are at the same frequency as some of the most intense VLF whistler energies between 1 and 10 kHz. The problem is whether the whistler wave, which is electromagnetic and polarized perpendicular to \vec{B}_0 can stimulate lower hybrid electrostatic mode waves, which are longitudinally polarized, that is parallel to \vec{B}_0 [Parks, 1991].

Wave energy from the whistler mode has been observed to couple into other plasma wave modes in laboratory experiments, and in some cases it has been observed by satellites such as Alouette-1 and thunderstorm rocket over-flights such as Thunderstorm II [Brice and Smith, 1965; Siefring, 1987]. These types of waves are also seen in the Thunderstorm III rocket data. In this section, some examples of these stimulated waves are shown and we look at the question of whether they are stimulated naturally by the passage of the lightning whistler wave, or if they are an indirect effect caused by the, for instance, plasma wake of the rocket in the vicinity of the whistler wave.

Laboratory experiments have shown that whistler waves can stimulate Lower Hybrid (LH) waves if there are density gradients in the electron plasma along the magnetic field [Rosenberg and Gekelman, 1998]. An obvious question is whether the rocket body itself may produce local density variations which can help stimulate the LH waves. In principal, the LH waves should be difficult to stimulate from the whistler mode, but they have been observed by earlier thunderstorm flights such as Thunderstorm II [Siefring, 1987; Baker, 1998]. Here we will look at the lower hybrid frequencies that should be present in the lower ionosphere, and compare them to what we believe are cases of whistler stimulated lower hybrid waves observed by the Thunderstorm III electric field instruments.

The Lower Hybrid wave should appear at the local LH frequency in the ionosphere. These waves are electrostatic, which means that if they are generated by the passage of a whistler, they should be distinct in appearance in the spectrograms and not show any dispersion. Another feature of LH waves is that the polarization should be in the left handed sense, opposite to the right hand circular whistler polarization. Waves with these properties are observed during the Thunderstorm III flight, an example is shown in Figure 4.15. Notice that the Z axis electric field, which is approximately along \vec{B}_0 , (see middle trace of top panel in Figure 4.15), shows only weak VLF wave activity with the passage of the lightning whistler wave. When the whistler wave frequency reaches 6.8 kHz, which is approximately the local LH frequency, the Z axis electric field increases for about 5 m-sec, (beginning at

the 4th tic mark in the tip panel) and the spectrogram shows that this wave is not dispersed. This means that the wave is being generated close to the point of observation in the ionosphere.

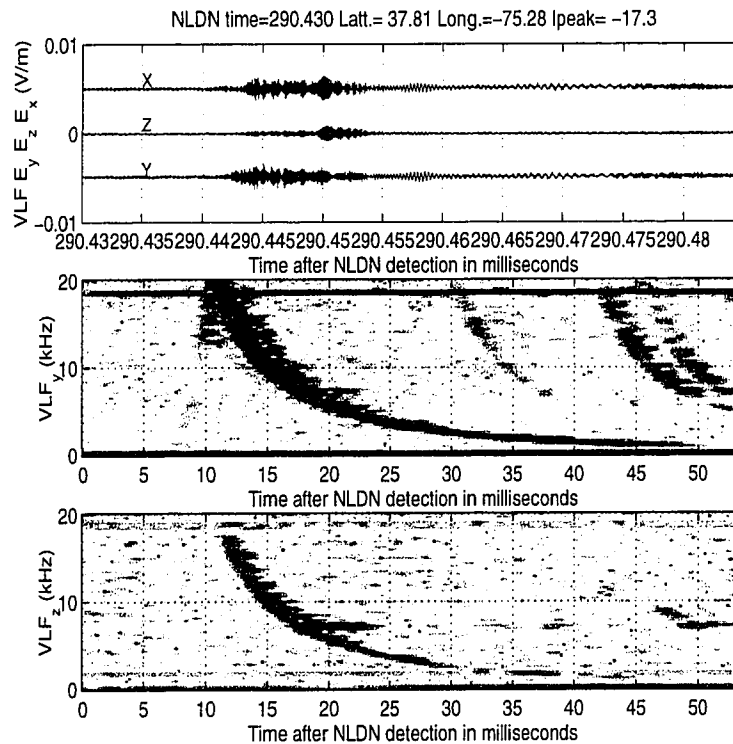


Figure 4.15: A Lower Hybrid wave is stimulated by the passage of a lightning whistler wave from the Wallops thunderstorm. The Thunderstorm III rocket was at 391 km altitude at during the up-leg portion of the flight. Notice the spectrograms of the X-axis and Z-axis electric fields. The field aligned Z axis shows strongest wave energy at 6.8 kHz, and the wave is not dispersed at this frequency, unlike in the spectrogram of the X axis electric field data.

The LH wave mode is a transverse electrostatic wave, yet it is apparently being stimulated by the longitudinal whistler waves above the thunderstorm. Field-aligned irregularities in the local ion and electron density may be sources for the coupling of whistler longitudinal wave energy into LH wave energy [Smith *et al.*, 1960, 1966].

The lower hybrid wave frequencies are estimated from the IRI90 ion density profile. The two dominant ion species between 150 and 400 km altitudes are O^+ and NO^+ . H^+ and He^+ are not present in any appreciable amounts below 400 km. H^+ and He^+ become the dominant ion constituents at 1000 km altitudes, in the Protonosphere, where the ions in this region may block the passage of ELF wave energy out to the magnetosphere. Some researchers believe that unducted ELF whistler waves may propagate outward to the magnetosphere, where they have been tentatively identified by the GEOTAIL satellite [Nagano *et al.*, 1998; Holzworth *et al.*, 1998 -in press].

Based on the model profile of the ion species, the Lower Hybrid wave frequencies were calculated for the rocket altitudes using the method of Brice and Smith [Brice and Smith, 1965]. The equation for the LH wave frequency is:

$$\sum \frac{\alpha_i}{M_i} \frac{1}{f_{lh}^2} = \frac{1}{f_0^2} + \frac{1}{\Omega_e^2} \quad (4.14)$$

The LH frequency f_{lh} is found using the effective mass M_i summed over all of the ion species per their ion fraction α_i . This equation reduces to the LH equation of Stix [1960] for the case of a single ion species.

Using equation 4.14, the calculated peak LH wave frequency, using M_i and α_i from IRI95, occurs at 300 km and is 7.25 kHz. The LH frequency slowly decreases above this altitude to 6.6 kHz at 400 km (Figure 4.16). Below the peak LH frequency at 300 km, the LH frequency decreases rapidly down to 1 kHz at 150 km. LHR noise bands have been observed to be triggered by fractional hop and multi-hop whistlers. These triggered LHR noise bands were recorded by the satellite OGO-4 [Laaspere and Taylor, 1970].

The whistler stimulated lower hybrid waves are produced in the region near the rocket. As the up-going whistler passes the rocket, the LH wave begins when the whistler frequency approaches the local LH frequency. A concern is that the emissions that are measured by the rocket or satellite may be an effect caused by the motion of the vehicle through the plasma. This type of stimulated emission arises from the $V_{rocket} \times \vec{B}_0$ motion. When the perpendicu-

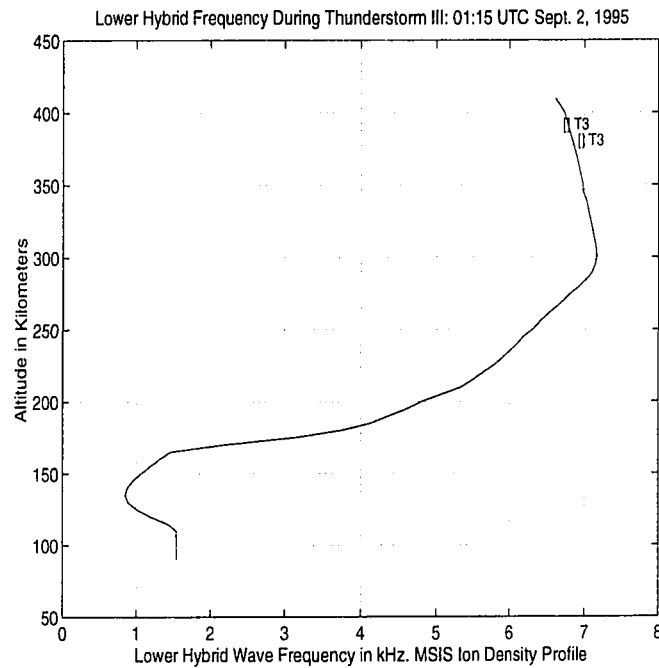


Figure 4.16: The lower hybrid wave frequencies are calculated for the ionospheric conditions at the time of the rocket flight. In the F region, the LH frequency is between 6 and 7.2 kHz. These LH waves were observed during the flight, triggered by the passage of whistler waves.

lar velocity of the rocket is the same order as the group velocity $d\bar{\omega}/d\bar{K}$, it is much easier to stimulate LHR waves in the vicinity of the rocket's plasma wake. This type of wake-effect emissions have been observed on Alouette-1, and were stimulated by whistler mode waves [Al'pert, 1990]. The wake stimulated waves are an unlikely explanation for the observed LH waves on the Thunderstorm III rocket. Unlike Alouette-1, Thunderstorm III was a sub-orbital sounding rocket therefore it had a much lower velocity perpendicular to B_0 , only about 1 km/sec compared to 8 km/sec for Alouette-1. The stimulated emissions on Thunderstorm III occur at frequencies between 5.5 and 8 kHz. Other non-dispersed frequencies occur during the flight, often showing multiple frequency bands which coincide with multiples of the earth-ionosphere waveguide cutoff frequency near 1.5 kHz as seen in Figure 4.6.

The observed multiple band emissions are similar to ground based cutoff waveguide modes measured by [Shvets and Hayakawa, 1998]. The stimulated LHR waves that were measured at higher rocket altitudes on Thunderstorm III are difficult to relate to the calculated LHR frequencies. The wave resonances between 5 and 8 kHz are not monotonic with the change in electron and ion density as the rocket changes altitude. Even if the higher electron densities were used in the LHR model equations, this would still not account for the unordered nature of the LH wave resonances at different altitudes. If these waves are stimulated by the plasma wake around the rocket, there should be a variation which tracks the local plasma density, but this is not what is observed in the data. The F region electron densities were higher on this experiment than on Thunderstorm II, and higher than the IRI95 model profile. It may be that some of the plasma waves are LHR waves, but there is not a consistent change with altitude. Along with what seem to be clear cases of whistler stimulated LHR waves near rocket apogee, as shown in Figure 4.15, there are waveguide tweek frequency harmonics which appear in nearly all of the lower altitude spectrograms below the F region. These generate similar appearing emissions on the spectrograms. Until similar rocket measured resonances are seen on other thunderstorm over-flights, the conclusion is that these may not be LHR waves, but rather a similar appearing emission that is caused locally at the rocket or stimulated by upward propagating tweek frequency harmonics..

4.9 Correlation of Whistler Wave Amplitude and NLDN Peak Currents

Larger currents in the CG lightning strokes should be expected to produce higher amplitude electromagnetic waves. In this section, the whistler wave amplitudes as a function of frequency will be related to the lightning stroke peak estimated current. What is found is that the NLDN estimated peak currents are best correlated with whistler intensity at the lower wave frequencies below 4 kHz. At each of the FFT computed whistler wave frequencies, the correlation between the wave electric field and the NLDN estimated peak currents was computed (see Figure 4.17 for example at 3.1 kHz). The whistlers were grouped by their

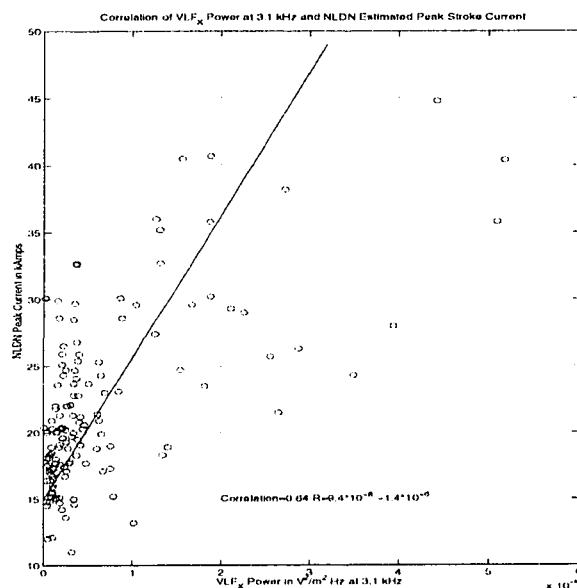


Figure 4.17: The whistler wave electric fields at 3 kHz are correlated with the NLDN estimated peak lightning stroke currents. There is some correlation, though many of the lightning strokes were only average in peak current, and there were not many high current strokes above the average of 22 k-Amps. The correlations were limited to the two nearby thunderstorms, the Wallops storm and the Northeast cell. Positive and negative CG strokes have been included.

source location, one from the main thunderstorm near Wallops Island, the other from the storm to the northeast. The altitude ranges from 208 km to 398 km in the ionosphere. The correlations show that the best relation is found at frequencies below 4 kHz. Note that no correction for the electron density changes to the electric field amplitudes have been made. The correlation determined here makes no assumptions about the ionosphere density, and is a simple comparison between stroke estimated peak currents and measured wave amplitudes.

The whistler wave correlations are best at the lower VLF frequencies as seen in Figure 4.18. It would be difficult to say whether the rocket wave amplitudes are actually a better determination of the peak lightning currents or the NLDN estimated currents. NLDN currents are believed to be within about 70% of the true peak currents based on Florida lightning

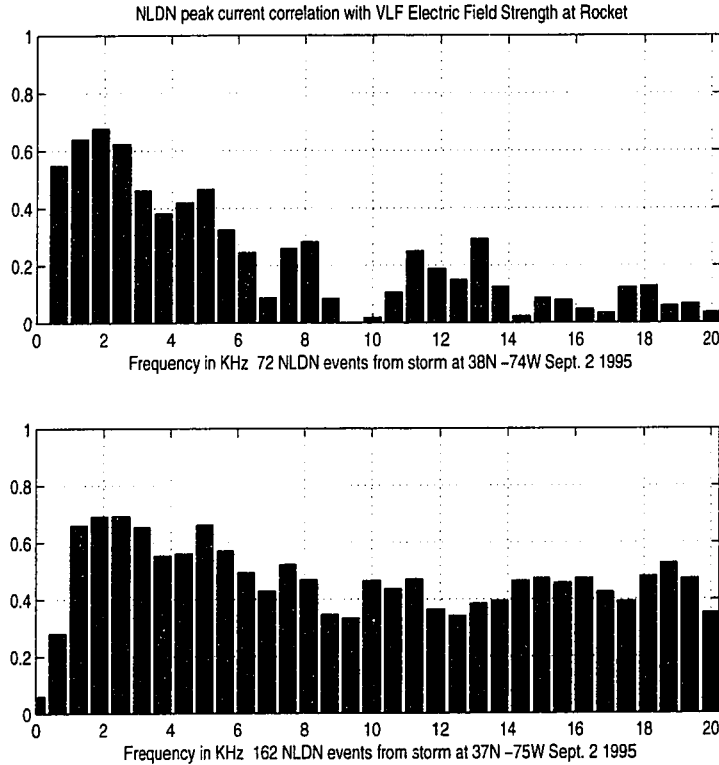


Figure 4.18: Lightning whistler waves from the Northeast thunderstorm (top) and the Wallops Island thunderstorm (bottom) are compared with the NLDN network estimated peak stroke current. Here the correlation between the whistler wave electric field and peak current is highest at the lower frequencies, below 3 kHz.

studies made at Kennedy Space Center and Camp Blanding, Florida. Triggered lightning studies however often have lower peak currents than natural lightning.

We have shown that there is a correlation between the NLDN peak lightning stroke currents and the lower frequency VLF and ELF whistler waves. The linear regression coefficients at each of the frequencies will vary with the source location distance from the rocket subtrack and with conditions in the ionosphere below the rocket. The linear correlation coefficients found by Li are quite different than the ones calculated from this data set. The whistler wave amplitudes measured from lightning strokes near Wallops Island on Thunder-

storm II were 5 to 10 times larger than those measured by Thunderstorm III. The ionosphere electron density was at least 2 to 4 times higher than the density profile during Thunderstorm II [*Jensen and Baker, 1992*]. The measured whistler amplitudes were 5 to 10 mV/m compared to 20 to 30 mV/m that were typical of Thunderstorm II and WIPP [*Li, 1993; Siefring and Kelley, 1991*]. The variation in whistler wave amplitudes caused simply by the electron density profile of the ionosphere will make a direct correlation difficult for an orbiting VLF/ELF sensor. Relative measurement between lightning lightning strokes could be made, but not an absolute correlation between stroke amplitudes and NLDN currents. If the electron density profile were known for the conditions beneath the sensor, it might then be possible to use the whistler amplitudes below 3 kHz to infer the NLDN peak stroke currents.

Chapter 5

FIELD ALIGNED ELECTRIC PULSES

One of the goals of Thunderstorm III was to make measurements of the field aligned electric precursor pulse [Kelley *et al.*, 1990, 1997]. Thunderstorm III used several new instruments to help understand the nature of the precursor pulse. Among these were the SnS (Snatch and Shift) high time resolution burst memory electric field instrument and the electrostatic analyzer. The precursor pulses were seen in the VLF electric field channel at altitudes from 110 km to 220 km. The VLF electric field channel, VLF_{26} or VLF_Z , measures the field parallel to rocket body and to \vec{B}_0 . The precursor pulses were not measured above the point where the rocket entered the base of the F region ionosphere. Note that the pulses are not really precursors of the lightning stroke, and they do not precede the optical flash, for this reason they will be referred to here as field aligned pulses (FAP) rather than precursor pulses.

The observed amplitudes of the pulses on Thunderstorm III were generally smaller amplitude than many of the pulses seen previously on the Thunderstorm II and Thunder Hi rocket flights. Even so, they do seem to be a common feature in the ionosphere. These pulses should have some strong influences on the plasma environment of the nighttime E region of the ionosphere. The results from the measurements on Thunderstorm III show a variety of new features of the pulse. Previous results concluded that the electric field of the pulse was unipolar and directed in the positive (upward) direction. In the data measured on this rocket flight, there are cases in which the pulse polarity is reversed, or even switches during a multiple stroke flash. Distant lightning strokes more than 800 km away in North Carolina are able to stimulate smaller amplitude field aligned pulses. The pulse should ac-

celerate electrons along the earth's magnetic field lines, but no evidence that it does this was found from the measurements of the UNH electrostatic analyzer experiments on Thunderstorm III. There is also a curious absence of any related magnetic field signature in the instruments on Thunderstorm III. These observations and some of the preliminary results from the SnS waveform instrument lead to the following conclusions about the field aligned pulse: It is composed of higher frequency waves, above 20 kHz. The pulse is not actually unipolar, so it does not cause electron particle acceleration along \vec{B} . The source of the pulse is not an electrostatic effect. The pulse is stimulated by cloud-to-ground lightning with strong vertical electric wave fields but not by intracloud lightning strokes which have smaller vertical wave fields. This chapter will be devoted to what has been learned so far about the field aligned electric pulses, and outline what further investigation should be done.

5.1 Properties of the Field Aligned Electric Pulse (FAP)

The Thunderstorm III rocket VLF electric field measurements of lightning electromagnetic fields below the nighttime F region often show a unipolar pulse directed upward along the field line B_0 . The measured pulse shows a positive amplitude in VLF_z , corresponding to a negative electric field change $-\vec{E}_z$. The pulse arrives at the rocket after the optical light of the lightning flash, but preceding the whistler waves at 20 kHz by 1 millisecond or less. The amplitude and the duration of the pulse decreases with rocket altitude, from about 10 mV/m to less than 1 mV/m in the lower F region. The pulse amplitude from distant lightning, more than 800 km ground distance from the rocket were typically small in amplitude. An example of the pulse is shown in figure 5.1.

A curious observation about the pulse is that it is seen for many cases of NLDN recorded negative CG lightning cases, but it was not measured from positive CG lightning. There were 4 positive CG cases during the up-leg of the flight during times when the pulse was measured from negative strokes. These strokes were all small amplitude positive strokes, each less than 22 kA peak currents. Based on this observation, it cannot be conclusively

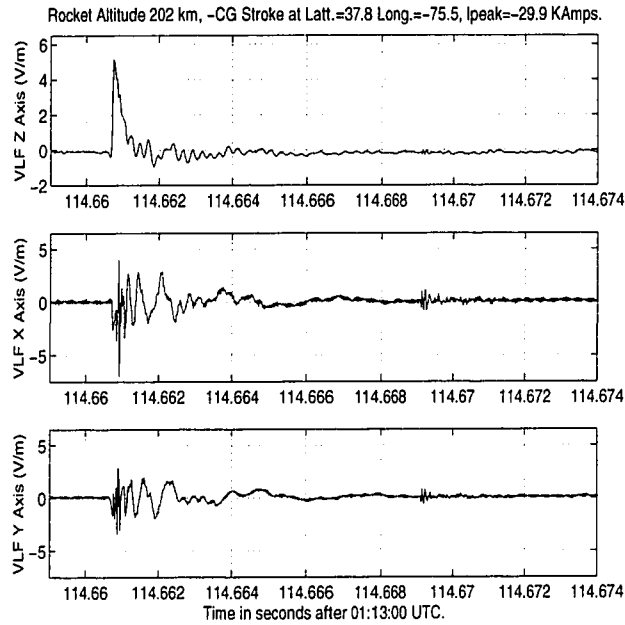


Figure 5.1: Field Aligned Electric Pulses were measured by Thunderstorm III at altitudes below about 220 km in the nighttime ionosphere. The parallel electric field measurements are shown in the first panel and the X and Y perpendicular VLF electric fields are shown in the second and third panels. The parallel pulse amplitude is large enough to drive short duration (1-2 ms) currents along the magnetic field with densities of several nano-amperes per square meter, nearly 1000 times larger than the static currents from the thunderstorm at this altitude. The pulses should be able to increase the electron energies to 20 \times their thermal velocity along the magnetic field in the E region.

stated that positives do not cause the electric pulse since not all negative strokes do either. There is no apparent reason why positive strokes should not cause an electric pulse just as negative strokes do. Until more such cases can be measured, it cannot be conclusively stated that the pulse is not seen for positive strokes.

The electric pulse amplitudes are large enough to drive brief currents along the magnetic field with densities of several nano-amperes per square meter, nearly 1000 times larger than the static currents from the thunderstorm at this altitude. The pulses should be able to increase the electron energies to 20 times their thermal velocity along the magnetic field in the E region. This raises one of the most peculiar results of the Thunderstorm III rocket flight.

If the pulses are truly unipolar field aligned pulses, as measured by the VLF electric field instruments, then the electron energies measured by the electrostatic analyzer instrument should record some change in the particle energies. No such changes were recorded by the electrostatic analyzers on Thunderstorm III.

The lightning pulses cannot be explained by electrostatic fields from the lightning sources. In the Thunderstorm III measured VLF electric field data there are cases of the pulses produced by strokes more than 700 km away over North Carolina, as shown in Figure 5.2. Such lightning strokes are too far away to produce an electrostatic effect of the magnitude seen in the measured vertical VLF channel. Also, if the electric field pulse was caused by the electrostatic fields from the lightning discharge, we would expect the pulse polarity to be negative in the VLF_z electric field channel, corresponding to an upward, positive \vec{E}_z from the negative CG stroke. Instead we find exactly the opposite polarity of the pulse, VLF_z is positive and therefore the pulse has a negative \vec{E}_z . This was also found in the study of the electric pulses by Carl Seifring at Cornell University [Seifring, 1987], the pulses he observed almost always had the same polarity. In the Thunderstorm III data, there were some cases as well where the polarity of the pulse was in the negative direction. Generally though, the observed pulse polarities are positive in most cases, meaning the electric field change.

The field aligned pulses are usually associated with negative CG lightning strokes. There were several positive polarity CG lightning strokes during the times when the electric pulses were seen from other strokes, but based on 4 positive CG strokes, no field aligned pulses were seen. These were not strong +CG strokes, and it may be that stronger +CG strokes will produce FAP, but the conclusion based on our observations is that a positive stroke does not produce an electric pulse.

If the FAP really is a unipolar pulse, it should have a magnetic field signature with frequency components comparable to its pulse width. The expected magnetic field frequencies should be in the 0.5 to 2 kHz range, based on the observed pulse durations. The observations from the 3-axis VLF search coil and the fluxgate magnetometer data simply do not

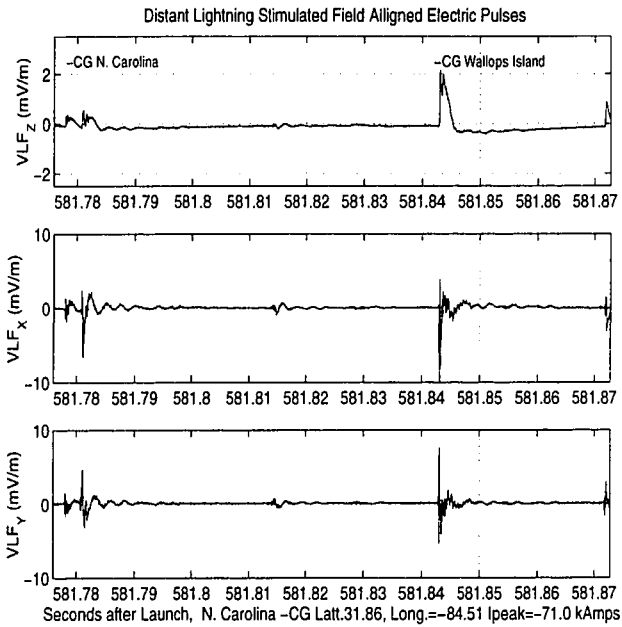


Figure 5.2: The Electric Pulses can be produced by strong, distant -CG lightning strokes such as the example shown here, which was located in North Carolina. Notice that this stroke appears as two distinct pulsations. The channel may have had a second stroke, or an IC stroke may have responded to the initial -CG, but NLDN only recorded a single stroke at this time. A second NLDN detected stroke follows the first one at the same location at $t=581.81$ sec, but it has a much lower peak current of only -26.0 amps. The large electric pulse is from the Wallops Island thunderstorm, this stroke had a peak current of -30.4 k Amps.

show comparable magnetic signatures of the pulse compared with the VLF electric field measurements, as shown in Figure 5.3. These instruments had lower frequency responses than the VLF instruments, but the pulse is primarily composed of ELF frequencies, based on the Fourier analysis of the electric field data.

There are noticeable changes in the pulse with rocket altitude. The amplitude of the pulses decreases with altitude until it is no longer measureable above 240 km, where the rocket enters the F region. Above 220 km, the amplitudes are typically less than 1 mV/m. The field aligned pulses were much smaller than many of the previous observations made by the Thunderstorm II and Thunder Hi rocket flights.

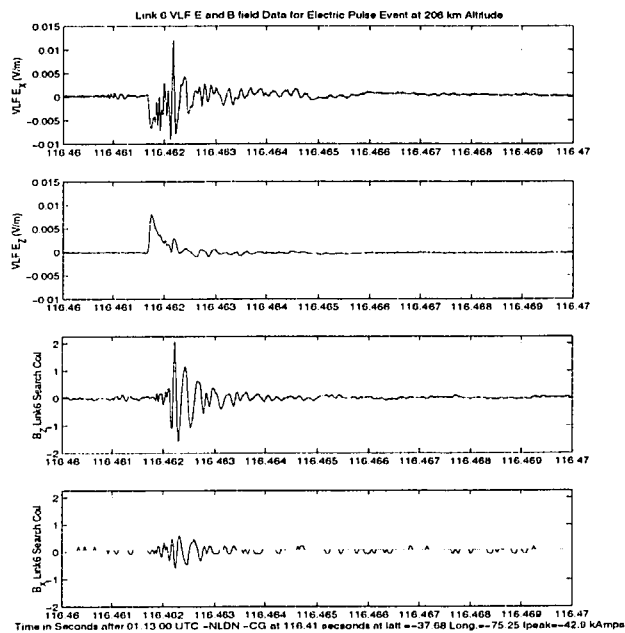


Figure 5.3: Simultaneous Electric (top two panels) and magnetic (lower 2 panels) field measurements of the pulse from data Link 6 show no evidence of the a unipolar pulse in the B field search coil instruments. These had a lower frequency response range than the VLF electric field instrument, peaking at 5 kHz. This lends further support to the evidence that the pulse is composed of higher frequency waves which are vertically polarized but that do not drive field aligned currents.

On the earlier flights the pulses had an average amplitude of 25 mV/m at 150 km on ThunderHI, and nearly the same amplitudes at 290 km on Thunderstorm II [Siefiring, 1987; Kelley *et al.*, 1990]. The electron density of the ionosphere was considerably higher during Thunderstorm III flight. Based on the PFP and Bermuda Digisonde density profiles, it was nearly 4 times higher than on the earlier rocket experiments. This increased electron density does not fully account for the lower amplitudes, since the electric fields should only be about 30% smaller due to the higher densities.

The duration of the electric pulses does decrease with altitude, but the decay of the pulse is not consistent at all with the change in the local conductivity σ_0 . The pulse has average durations of 2 to 0.1 ms between 100 and 240 km altitudes. On ThunderHI, the average

pulse durations were more than 3 ms at 150 km altitudes [Siefring, 1987]. Based on these observations, the pulse duration decreases much more slowly with altitude than the parallel conductivity σ_0 increases. If the pulse duration followed the local electrostatic decay, $\tau = \sigma_0/\epsilon_0$ which is always longer than the actual in-situ relaxation time, the pulse would be less than 1 ms at 111 km altitude and only hundredths of a ms at 200 km.

The pulse seems to decay away into higher frequency whistler waves at higher altitudes, this is shown in Figure 5.4. What seem to be the higher frequency components of the whistler waves appear to be emerging from the pulse. These waves are electromagnetic whistler mode waves at 20 kHz. At 240 km altitude, the pulse seems to be converting into fully electromagnetic waves. The question then is whether or not the pulse really is monopolar, or if instead it consists of unresolved higher frequency waves which are not resolved by the electric field instruments on the rocket.

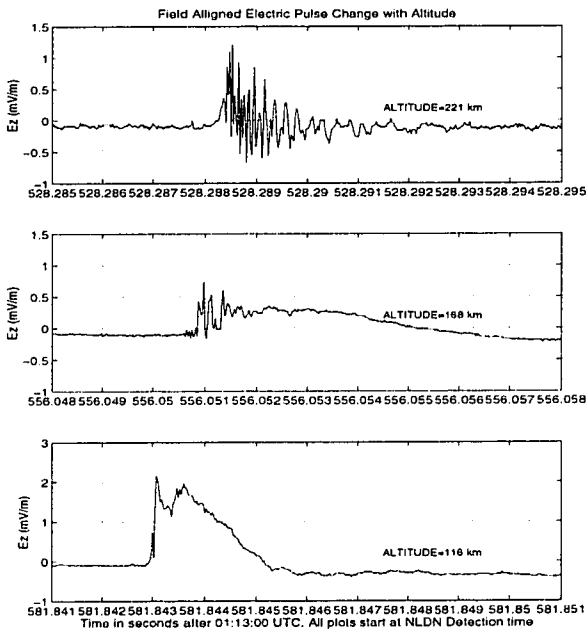


Figure 5.4: The field aligned pulse changes in duration with altitude. It decreases in amplitude and duration. Notice that at higher altitudes the pulse decays into higher frequency components which seem to be dispersed out of the pulse.

The SnS high data rate waveform experiment did capture some lightning whistler events, but the instrument timing and data correlation with the VLF wave data have not yet been matched with specific lightning events. The lightning events that were captured by the SnS instrument at 195 km do not show a unipolar pulse, but only electromagnetic wave energy and an apparent nose whistler in the high frequency spectrograms made from measured waves up to 100 kHz [Kelley *et al.*, 1997]. It is not known if the particular event that the SnS instrument captured was one of several CG strokes that occurred at that approximate time that did produce a pulse, although it seems likely since the SnS instrument did record one of the larger events at 195 km.

The field aligned pulse does not produce any response in the magnetic field instruments, and this is probably the strongest argument that it is not truly a unipolar pulse. If it indeed were such a pulse, the duration and rate of change of the electric fields should have produced measurable magnetic fields at the lower VLF and ELF frequencies. The pulse also did not cause any field aligned particle acceleration, in either direction along \vec{B}_0 .

This observation really leads to some strong questioning about the mono-polar nature of the pulse. The UNH ESA detector was designed to see electron particle energies from 1 eV to 12 KeV. Based on the pulse duration and amplitudes, electron particle energies from 1 eV to 20 keV would be anticipated from the parallel electric field. No particle events were seen during the flight by the ESA experiment above the instrument background noise levels.

Individually each of the observations prove or disprove little, but together the tentative conclusion that can be made is that the electric pulse is made up of higher frequency but unresolved waves, although these may not necessarily be whistler mode waves. If they are high frequency oscillating waves, which are not resolved in the VLF instruments, the electrons would be accelerated both up and down by the passage of the bipolar waves along the magnetic field lines, and experience no bulk acceleration.

5.2 In-cloud and Cloud-to-Ground Lightning Stimulation of the Pulse

Lightning channels can have different orientations, from nearly vertical for CG lightning to mostly horizontal channels observed for IC strokes. The channel orientation should have a large effect on the local electromagnetic wave polarization of lightning. The vertical CG lightning channel will produce stronger vertically polarized waves than in-cloud lightning channels [Rowland, 1996]. Many of the in-cloud lightning channels recorded by LDAR were nearly horizontal, the CG strokes showed some horizontal extent but were dominantly vertical within $\pm 30^\circ$. If the sub-ionospheric (i.e. source) polarization of the lightning electromagnetic pulse plays a role in the generation of the field aligned electric pulse, then there should be a difference in the amplitude and/or the occurrence of the pulse between CG and IC strokes.

The VLF electric field data does show just this type of difference, CG strokes will produce the field aligned pulse, but IC strokes generally do not. An example of two lightning strokes is shown in Figure 5.5. The first stroke, is a negative CG with a peak NLDN estimated current of -18.7 kA. It is followed by a nearly equivalent IC stroke which has nearly the same peak VLF amplitude. Only the negative CG stroke produces a pulse, there is no pulse from the in-cloud lightning stroke. This suggests that the longitudinal or the sub-ionosphere vertical electric fields stimulate the pulse, but horizontal fields simply couple into whistler mode waves and do not produce a measurable pulse.

5.3 Conclusion

The field aligned electric pulse must be made up of higher frequency oscillating electric and magnetic fields. It will only be possible to determine the wave modes when the higher frequency measurements can be correlated with the lower frequency VLF measurements. This study has shown that the pulse is probably not caused by electrostatic fields since lightning strokes as far away as North Carolina can produce weak FAP. As noted by Carl Siefring,

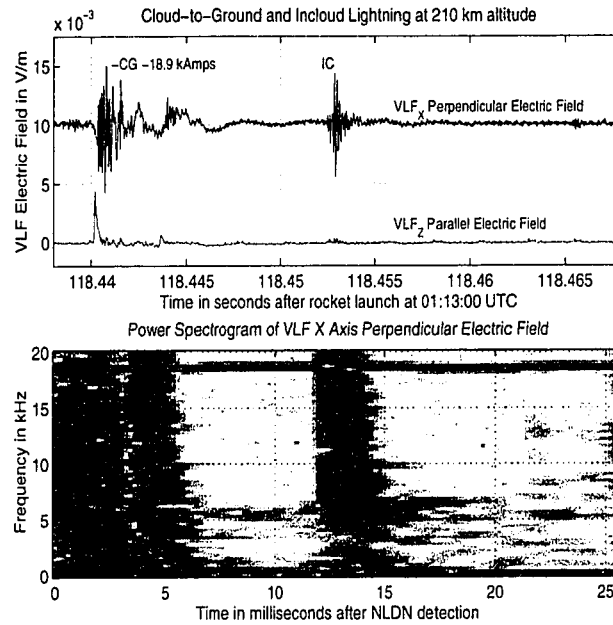


Figure 5.5: There is a dramatic difference in the stimulation of the parallel electric field pulses between cloud-to-ground lightning and in-cloud lightning strokes. In-cloud lightning strokes rarely cause the pulse, which is much more frequent in cloud-to-ground strokes. The orientation of the lightning channel is usually much more horizontal for in-cloud lightning which would produce smaller vertical electric fields than cloud-to-ground strokes.

the usual positive polarity of the pulse is in the wrong direction to be caused by a negative CG discharge [Siefiring, 1987; Kelley et al., 1990]. On Thunderstorm III we also have observed that the pulse sometimes will have a negative polarity. One of the other observations of CG and IC lightning is that IC strokes do not usually produce the field aligned pulse. The lightning channels of in-cloud lightning were generally found to be much more horizontal than cloud-to-ground strokes in the Wallops thunderstorm from the LDAR VHF data in Chapter 6. It seems likely that the pulse is partly an effect caused by the wave polarization, particularly by strong vertically polarized high frequency waves which come from the vertical CG lightning channels.

The next planned rocket experiment has been designed to capture the lightning EMP

in an 8 millisecond high sample rate data frame instrument, similar to the SnS waveform capture instrument. This NASA experiment, called Lightning Bolt, should be able to settle the question of the electric pulse if it is successful. At this time, all of the available data from Thunderstorm III strongly suggests that the pulse is not truly unipolar. It should be kept in mind that the so called "precursor pulse" [Kelley *et al.*, 1990] never preceded the optical pulse, and was coincident with the expected arrival of the higher frequency waves at the rocket. Based on the data from Thunderstorm III, the electric pulse consists of large amplitude waves with field aligned polarizations.

Chapter 6

VHF LOCATION OF THUNDERSTORM LIGHTNING STEPPED LEADER ACTIVITY AND LIGHTNING CHANNEL FORMATION DURING THUNDERSTORM-III

6.1 Introduction

During the flight of the Thunderstorm II rocket experiment, the LDAR VHF system located more than 13,000 VHF pulses known as "triggers". The triggers occur during the formation, or attempted formation, of lightning leader channels. This system has been a tremendous aid in locating electrically active regions of the thunderstorm and for studying the dynamic development of lightning channels.

In this chapter, we will give examples of the leader channels formed by intracloud and cloud-to-ground lightning. The LDAR system can also be used to study the propagation velocity of the stepped leader channels. In our study of stepped leaders using LDAR, we have found that the velocity of the leaders, i.e. the stepping speed, has an apparent decrease with altitude. A similar result was recently reported by Proctor [*Proctor, 1997*]. Later, in Chapter 7, we will compare the stepped leader velocity measured by LDAR to 2 cases of stepped leader velocities inferred by their particular optical signature measured by the rocket. LDAR reveals the form of the lightning channels by the locations of the triggers. We find that intracloud lightning channels are usually horizontally oriented, and CG channels are mostly vertical, with some horizontal extent into the lower charge pool region of the thunderstorm. In this study, LDAR is used to locate IC lightning events so we can compare the VLF wave data measured by the rocket from IC strokes to the wave data from CG

lightning strokes.

The altitude extent of CG and IC lightning channels is important to the interpretation of the lightning optical data in Chapter 7. This study is really the first ever to apply all of the ground based research instruments measuring altitude and extent of lightning channels (LDAR), and stroke current (NLDN), to the space based measurements of lightning.

Lightning Detection and Ranging (LDAR) systems take advantage of the VHF emissions that occur during lightning channel development. There are two distinct types of VHF radiation that are emitted from lightning channels, the first type is a pulsed emission which takes place during the development of step leader channels preceding the initial CG or IC return strokes [Uman, 1984; Kitagawa and Brook, 1960]. The second type, Q burst emission, occurs during changes in the currents in the previously formed leader channels [Proctor, 1988]. The NASA LDAR system only maps the VHF pulsed emissions from the leader channel development. The systems gives an inside look at the processes taking place in the thunderstorm, which would normally not be observable. These systems give valuable information about the location of electrical activity within the thunderstorm. The IC lightning strokes are not recorded at all by the NLDN network, yet these strokes probably occur at least 3 to 5 times more often than CG strokes Uman [1984]; Mackerras [1985]. The LDAR data show the locations and timing of VHF electrical activity related to the leader channels of both types of lightning strokes. The VHF trigger activity also shows how charge is moved within the storm, before and after CG and IC discharges.

Such systems have been in use since their development in the 1970's and have been useful in determining where the electrical activity in the thunderstorm is, how charge is moved, and where the lightning channels develop [Proctor, 1971]. Some of these systems can give very detailed structure of the lightning channels that form near the main charge regions in the storm [Warwick *et al.*, 1979; Rhodes *et al.*, 1994].

During the Thunderstorm-III rocket experiment, the LDAR coverage area was limited by the system software to the region around the main thunderstorm located to the southeast

of Wallops Island. The intensity of the electrical activity in the thunderstorm required additional signal attenuation to be put on each of the LDAR receiving antennas. Even with the limited area coverage and the reduced receiver sensitivity, more than 13,000 individual triggers were recorded during the 10 minute rocket flight. As a result, we have a very clear picture of where the electrical activity is most intense in the storm. There are many cases of CG and IC lightning channel development which are shown by the step-like locations of LDAR detected triggers in the thunderstorm. Many of the triggers are individually occurring triggers. Many of these single, isolated triggers occur above the anvil cloud top of the storms, some as high as 30 km altitude.

6.2 Overview of the LDAR VHF System

Lightning VHF mapping systems have been in use since the 1970's and have been useful in determining the location and timing of electrical activity in the thunderstorm [Proctor, 1971]. Some of these systems can give very detailed structure of the lightning channels that form near the main charge regions in storms [Warwick *et al.*, 1979; Rhodes *et al.*, 1994].

During the summer of 1995, the Lightning Detection and Ranging system (LDAR) at Wallops Island was available for research use. The LDAR system had originally been developed by NASA to study the electrical activity in thunderstorms at Kennedy Space Center (KSC). The older KSC system was moved to the NASA Wallops Flight Facility (WFF). The system then underwent extensive modifications in the software and hardware. This was done by the NASA SPANDAR radar group directed by Dr. Norris Bealsley with Mr. Charlie Etheridge who did most of the redesign and improvement of the electronics and software. These improvements allowed for much better real-time data displays and faster processing of the VHF data from the storm. The system that has been developed is very different from the original LDAR design. The WFF system has much greater flexibility in the processing software and many upgrades to the receivers and signal processing. During the rocket flight, two sets of data were taken, consisting of grouped trigger data and single trigger data, each

with 1 ms time resolution, the same as the NLDN stroke data.

LDAR has moderate time resolution compared with some of the research systems described by [Rhodes *et al.*, 1994], which obtain thousands of single pulses for a single lightning event. A similar system called SAFIR has also been used in thunderstorm studies in France, KSC and Japan [Solomon, 1997]. The LDAR system typically will get 20 or 30 groups of pulses called "triggers" during a single lightning stroke sequence. These triggers can reveal the approximate length and orientation of the lightning channel. This is very useful for modeling comparisons, since the length and channel orientation are believed to have large effects on the radiation fields from lightning [Rowland *et al.*, 1995].

The storm that occurred on September 2nd was ideally situated for the LDAR system and the SPANDAR facility instruments since it crossed over the island and then went to the southeast of the facility over the Atlantic ocean at the time of rocket launch. This data set along with the NLDN data allows a very unique look into the electrical structure of the thunderstorm and the processes associated with CG and IC lightning. Using the data from LDAR, it has been possible to "see" the extent and orientation of the channel forming some of the CG strokes and to look at what takes place electrically before and after the flash.

6.3 Characteristics of Lightning VHF Radiation Producing Triggers

Prior to a CG or a IC flash in a thunderstorm, smaller amounts of charge are moved within the cloud near the main charge levels by the step leader process. When these charges move, the ionization of the air along the path of the charges is a strong source of VHF radio energy. The movements of the VHF sources sometimes occur in a path-like series between regions of charge in the thunderstorm or from the lower level charge regions of the storm extending toward ground, such as for a step leader preceding a first CG stroke. Researchers have identified two distinct types of VHF activity during the development of IC and CG events, these are called Q noise and pulsed emission. Q noise occurs in short bursts of VHF pulses, lasting from 10 to 400 μsec . In contrast, pulsed emissions only last about 1 μsec and do not

have the ragged "spiky" appearance in their waveform; they are quite distinct from Q noise. [Proctor, 1988].

The Q noise bursts occur during K and J type processes which take place during IC and CG events. K processes have been defined as small electric field changes or "Kleineverändering" by Kitagawa. They are weak amplitude field changes which are often not seen by ground electric field instruments unless higher gains are used. The K changes were not seen in the field mill data (EFM) during Thunderstorm III flight, the system sensitivity was not high enough and the strip chart time resolution was too coarse, for the EFM network to reveal this type of process. Junction or J processes occur between CG or IC events, and are believed to be caused by small movements of charge following IC or CG strokes [Kitagawa and Brook, 1960]. The J changes also show up as small field changes in the ground electric field, but were not usually seen in the ground data at Wallops on the low time resolution strip chart recordings.

Lightning VHF pulsed emissions take place during step leaders. Step leaders are common to IC and CG strokes. During the stepping process, each leader step may produce several detectable pulsed emissions. The source of the VHF radiation is believed to occur when the leader tip extends into a new region and the air around the charge extension is ionized [Proctor, 1997]. The duration and rise-time of the pulses are distinct from Q noise activity. The rise times of the pulses is typically on the order of several hundred nanoseconds. The LDAR system at Wallops Island is designed so that only the pulsed emissions are recorded and Q bursts are rejected (C. Etheridge personal communication, 1997). This is done by the signal processing software which puts the received pulses into 376 μ sec long windows. The LDAR software then checks the digitized pulse in the window and compares the signal rise time and duration to the known characteristics of pulsed emissions.

LDAR computes the time of occurrence of the pulsations, their locations in the storm and the grouping of the pulses. If there is a series of discharges in the same region, and close in time, the pulses are grouped into a "multi-trigger" event.

6.4 Location of LDAR Electrical Activity

During the 10 minute flight of the Thunderstorm III rocket, more than 13,300 VHF triggers from the thunderstorm near Wallops Island were recorded by the LDAR system. The altitude distribution of the triggers is clearly bimodal in form, Figure 6.1. There are two peaks in the electrical activity, the lower altitude peak was at 4.5 km, corresponding to the 0°C freezing level, and a second peak at 11 km, or the -45°C temperature level. These temperatures are based on the weather balloon sounding made just prior to the rocket flight. These maxima in the LDAR trigger activity are separated by a relative lull in the trigger activity between 6 to 9 km, at corresponding temperature levels of -15°C to -30°C . Note that the lower altitude electrical activity peaks below the usual charging region identified by the temperature levels between -10 to -20°C .

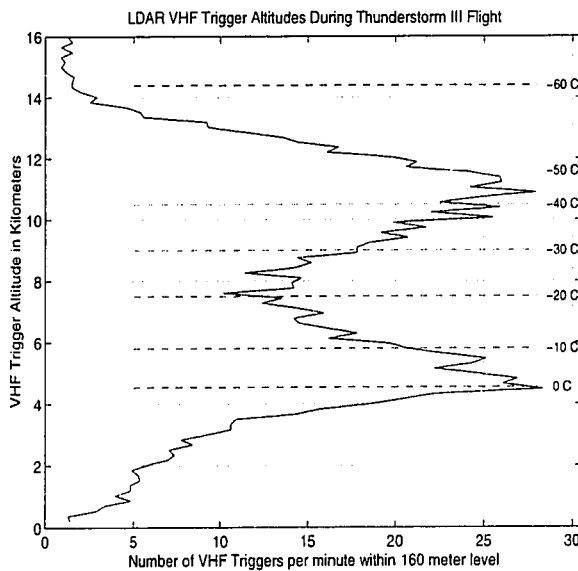


Figure 6.1: All of the LDAR detected triggers occurring during the rocket flight are shown as a function of altitude. More than 13,300 triggers were recorded in the 600 seconds following the rocket launch. Here the trigger activity is grouped by altitude and shown as the average number triggers per minute. Notice that the trigger activity divides into an upper and lower level of electrical activity. Most CG strokes extend from the lower region at 4.5 km.

The LDAR triggers, which preceded many of the CG flashes, usually came from low altitude activity in the thunderstorm below about 5 km. The triggers that LDAR records that are related to CG strokes, are from the stepped leader as it moves toward ground from the lower charge region of the storm as in Figure 6.2. The VHF triggers typically end within 500 meters above the ground. This seems to be a common observation in all of these types of VHF systems [Proctor, 1997]. After the formation of the initial CG channel by the stepped

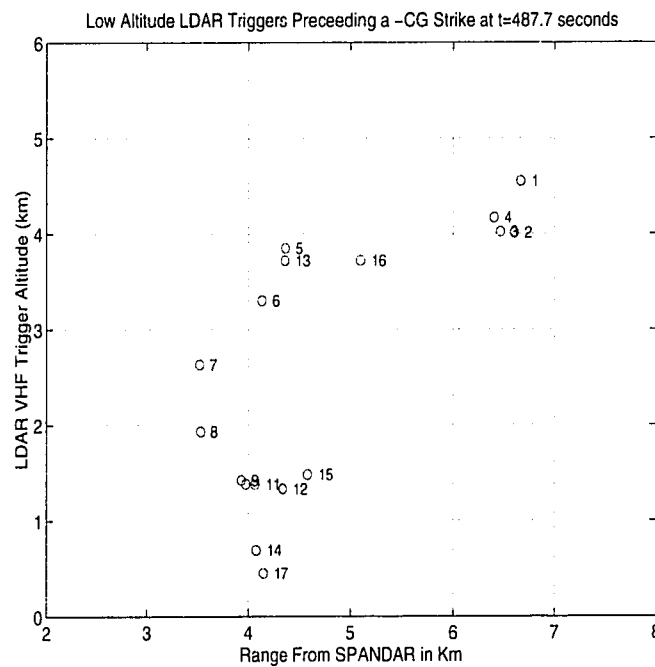


Figure 6.2: The LDAR VHF triggers originating from the lower cloud charge region, extend down to ground forming the stepped leader (SL) channel which precedes the lightning return stroke (RS). All the triggers shown here occurred within 50 milliseconds. Each individual leader step took only a few milliseconds between consecutive triggers.

leader and the first return stroke, there may be VHF activity near the upper lightning channel. This inter-stroke activity in a multiple stroke CG flash, brings more charge into the established lightning channel. This type of activity during the inter-stroke period is known as a Junction process, and can sometimes be seen as a small field change on a ground field sen-

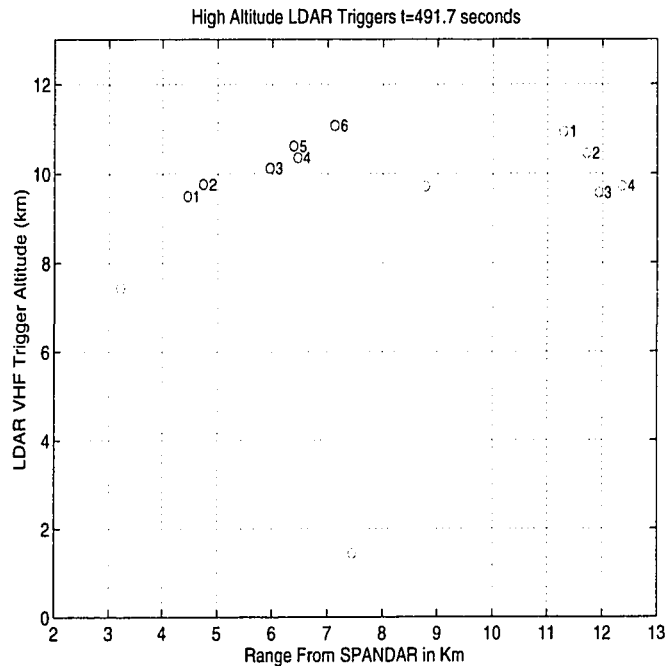


Figure 6.3: High altitude VHF triggers, located in the thunderstorm anvil top, were recorded throughout the rocket flight. These in-cloud channels develop with slower stepped leader speeds than the channels observed at lower altitudes. These high altitude lightning channels show a wide variety of lengths and orientations, and are generally more horizontal than CG channels.

sor such as a field mill or flat plate antenna [Kitagawa and Brook, 1960; Schonland, 1932].

During the thunderstorm, LDAR recorded numerous VHF triggers near the cloud top regions of the thunderstorm. These high altitude triggers show the development of in-cloud lightning channels near the the highest regions of the thunderstorm, an example is shown in Figure 6.3. When these channels encounter regions of positive charge, a recoil streamer takes place. The streamer neutralizes charge in the channel and causes it to illuminate, much like a CG return stroke. There has been less study of these in-cloud processes, but they play an important role in the dynamic movement of charges in the thunderstorm. IC strokes often occur at rates of 3 to 5 times the rate of CG lightning. Middle and high altitude leader channel triggers were recorded throughout the flight. The currents and charge in the IC strokes,

are typically less than CG events [*Uman, 1984*].

Because of the high altitude of these IC channels compared to the usual CG stroke, the light should appear much brighter to a balloon, plane or rocket borne downward looking optical sensor, and dim to a ground based optical sensor. This is what is recorded in simultaneous optical measurements from the ground at Wallops and at the rocket. Many of the IC flashes are never seen by the ground sensor, but appear very bright in the rocket optical instrument. The orientation of the IC channels varies greatly from nearly horizontal to vertical. The horizontal IC lightning channels should have strong radiated fields in the vertical direction, similar to a horizontally oriented dipole antenna. This orientation should produce less vertical electric field radiation than a cloud-to-ground stroke which has a more vertical channel orientation.

6.5 LDAR Stepped Leader Velocities

Some of the LDAR triggers seem to occur as single events which do not appear associated with a regular channel or grouping. The triggers that do make up a coherent channel will often appear as a burst of trigger activity which can occur over hundreds of ms. Often these triggers will group into smaller bursts of short steps which occur within approximately 10 ms or less, and step lengths of several hundred meters. Stepped leader velocities of CG strokes typically range from 10^4 to 10^5 m/s [*Uman, 1984*]. Using the LDAR system, it is possible to examine the speeds of the stepped leader process at different altitudes in the thunderstorm. There has only been one other report of stepped leader velocities measured up to altitudes 11 km. In that study of stepped leader velocities measured in South African storms, D. Proctor found that the mean velocity of the stepped leaders decreased with altitude [*Proctor, 1997*]. Using the improved LDAR system at Wallops, we looked at the Thunderstorm III data to see if there was also a change in leader velocities with altitude measured at Wallops. We also wished to compare the velocity based on the LDAR VHF measurements with the rocket based optical measurements of stepped leader speeds. The

optical measured velocities are based on a particular light signature of the stepped leader that precedes the CG return stroke optical pulse [Brook *et al.*, 1985].

There is a significant decrease in the average velocity of stepped leaders with altitude. From the large numbers of LDAR triggers in the database, the analysis used triggers which occur in groups of activity at 3 different altitudes, those below 5 km, 5 km to 9 km and those which occur above 9 km altitude, which are termed high altitude. Based on the sounding and the SPANDAR radar data, the high altitude triggers occur in or above the thunderstorm anvil. Many triggers were detected by the system above 9 km showing that this region was very active electrically. From the data, there is a significant decrease in the speed of the triggers with altitude shown in the histograms in Figure 6.4. The statistics related to the trigger velocities are tabulated in table 6.1. The most dramatic change is in the median

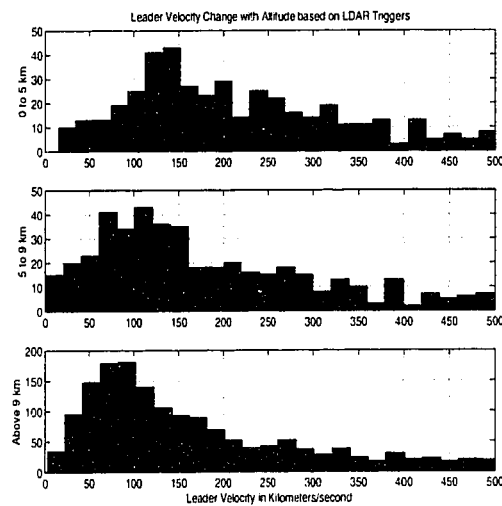


Figure 6.4: LDAR triggers recorded from stepped leader channels show a noticeable decrease in the speed of channel extension with altitude. This effect has also been reported by [Proctor, 1997].

speeds which show a clear decrease with altitude. There is a large standard deviation in all cases. Some of the difficulties in the analysis of trigger velocities are in cases where the channel development is bi-directional, meaning that triggers may propagate away from a

region in space in opposite directions. A second problem is related to branching in lightning channels. If the developing channel develops more branches, the apparent net speed of the overall channel will seem to decrease. Cloud-to-ground lightning channels will tend to have fewer branches in their final development. This could then effectively raise the velocities calculated for the lower altitude CG channels. These difficulties were also noted by D. Proctor in his analysis [Proctor, 1997]. One theory regarding the apparent change in altitude

Table 6.1: LDAR Stepped Leader velocities at different altitudes

LDAR Altitude	Mean Velocity (Km/sec)	Median (Km/sec.)	std of mean
Low 0 to 5 Km	290.5	225.6	217.3
Mid 5 to 9 Km	260.8	174.3	229.0
High > 9 Km	232.8	146.9	219.6

is that the air density directly affects the stepping speed or that the lower magnitude of the breakdown electric fields reduces the forces that cause the stepping [Proctor, 1997]. This explanation was suggested by E. Williams to explain the average velocity decrease found by Proctor in his study of South African thunderstorms mapped by a similar VHF system. The maximum electrical field strengths in thunderstorms decrease with altitude. This reduction is caused by the lower breakdown and break-even electric fields which decrease with air pressure [McCarthy and Parks, 1992]. This reduction in the maximum field strengths has been observed in thunderstorms measured in Oklahoma [Stolzenburg *et al.*, 1998a].

More research is being done with the NASA Wallops NASA LDAR system to look at the higher altitude VHF trigger activity, in particular triggers which take place above the tropopause and into the stratosphere. From this data set there are triggers which occur as high as 30 kilometers, but not many. There are so few of these in this 10 minute data set, during the entire 10 minute data set, more than 127 triggers above 26 km were recorded, 49 of these occurred above 30 km. We can not make any conclusions except to report that these triggers usually were single, unlinked trigger events. These high altitude triggers have been

routinely measured by the NASA Wallops LDAR engineers, but to date, no formal study has been undertaken to determine if they are simply "bad" triggers, mislocated by the system because of poor location geometry, system noise, or due to other causes.

There are cases of high altitude lightning discharges with channels consisting of multiple co-located triggers that extend above the the radar observed cloud top of the thunderstorm. These types of above cloud top lightning channels have also been seen by U2 high altitude aircraft over-flights [*Brook et al.*, 1985].

6.6 Location of LDAR VHF Activity Relative to Radar Reflectivity

The main thunderstorm core is a region of strong vertical wind velocity, rain shafts and hail. The radar reflectivity of this core region gives an indication of the severity of the conditions there. A radar reflectivity of 0 dBz or "dB above 0" is approximately the reflectivity equivalent to the signal return from 1 drop of water per cubic meter in the volume space of the radar beam [*Battan*, 1973]. Radar reflectivity levels above 40 dBz are associated with hail, and above 30 dBz with strong rain. The location of the main thunderstorm core, based on the X-band radar reflectivity is shown in Figure 6.5. Relative to the core region, many of the VHF triggers are located outside of the core, many directly above the core and around it. One explanation for this is that the main charge regions are located around the convective core, not in it. This is because the charging should be most effective in regions with ice, water and graupel in combination. Radar reflectivity from the core will be dominated by water droplets, so the 40 dBz contours locate the rain shafts region of the storm but not the most active charge centers, which lie outside of the rain shafts [*Williams*, 1985; *Proctor*, 1988].

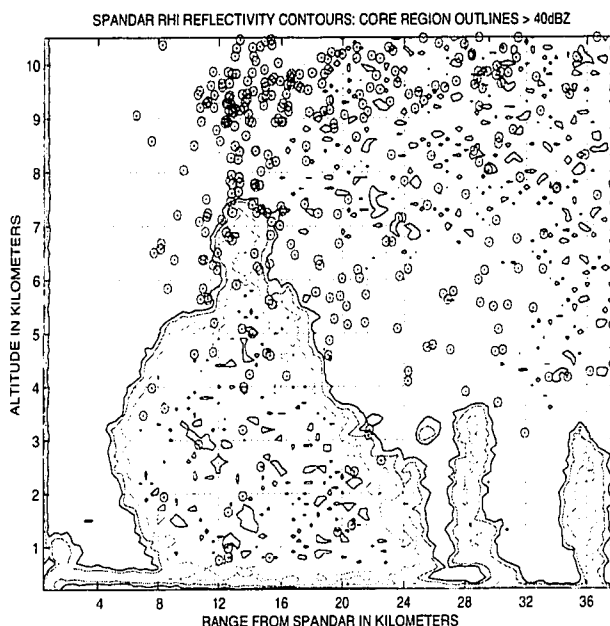


Figure 6.5: The $\geq 40\text{dBZ}$ radar reflectivity contours of the main thunderstorm core region are shown with the LDAR trigger activity. Notice that many of triggers occur above and around the core region. The strong up-drafts and precipitation of the core do not support the development of step leader channels. A similar observation was made by D. Proctor in his study of thunderstorms in S. Africa [Proctor, 1997].

6.7 Comparison of Intracloud and Cloud-to-Ground Lightning Fields Measured in the Ionosphere

As mentioned, intracloud lightning flashes are not recorded by the NLDN system. This type of lightning flash is really the most common form of lightning, occurring at more than 3 to 5 times the rate of CG lightning strokes [Mackerras, 1985]. The intracloud lightning channels revealed by the LDAR system have a variety of orientations and lengths. Many of the high altitude lightning channels were horizontal with lengths of 2 to 5 km. The VLF electromagnetic radiation from in-cloud lightning strokes varied depending on the type of lightning process that was occurring. During the early formation of Cloud-to-Ground strokes, rapid,

higher frequency VLF activity occurs which is associated with the early portion of the lightning channel formation. This stage is known as the "Very Active" or simply "VA" portion of the stroke [Uman, 1984; Kitagawa and Brook, 1960]. In Chapter 7, the VA portion is stud-

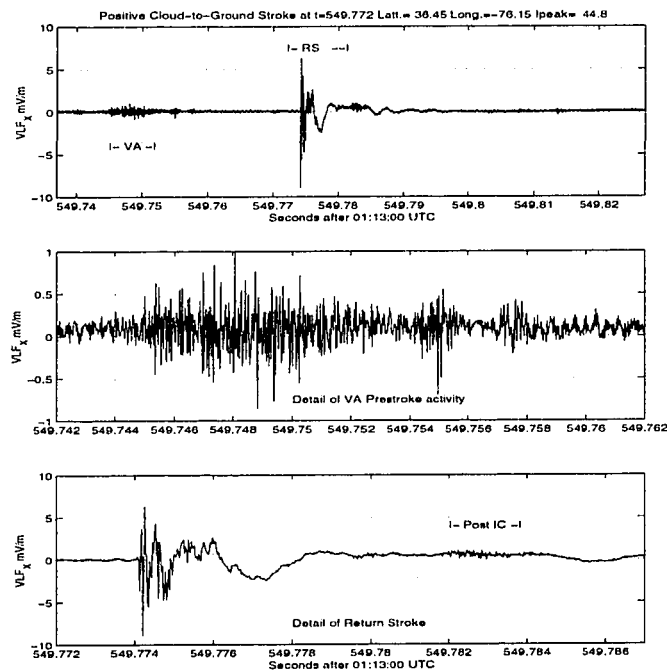


Figure 6.6: Preceding first return strokes, a period of in-cloud electrical activity associated with the lightning channel formation occurs about 20 to 40 milliseconds prior to the first return stroke. This activity is known as the Very Active (VA) portion of CG lightning formation

ied with the result that it often coincides with measurable optical and electrical emissions that are detected by the rocket instruments.

The intracloud lightning strokes that were measured at the rocket had considerable variation in VLF power, and in their VLF power spectra. Weak amplitude whistler waves occur throughout the rocket flight which are seen in nearly all the electric field spectrograms. These small pulses generally are very weak at ELF frequencies, and power densities in the VLF are typically less than $10^{-10} V^2/m^2 Hz$. This type of activity may be caused by short

leader channels that only neutralize small amounts of charge. Such short channels were continuously being logged by the LDAR system, especially in the upper ≥ 7 km regions of the thunderstorm. The trigger activity consisted of several triggers in a small region of the thunderstorm. The triggers would not progress into the organized series seen in CG or long channel IC events.

There was a noticeable difference between the ELF wave power in IC strokes and the CG strokes. The IC strokes usually had much smaller ELF electric fields compared with their VLF power. The cause of this is still a mystery, it could be that continuing currents do not take place in intracloud flash processes, although there does not seem to be any good reason why this should be the case. An example of in-cloud activity and IC lightning power spectra are shown in Figure 6.7; compare this to the CG stroke shown in Figure 6.8. The IC lightning activity that follows CG strokes is usually distinct on the spectrograms because of the smaller ELF power relative to the VLF wave power. In Figure 6.7, the intracloud lightning strokes have varying VLF wave power spectra, but are generally weak in ELF energy below 3 kHz. In the spectrograms of the VLF electric field data measured by Thunderstorm III, it is usually possible to distinguish between IC and CG lightning strokes. IC strokes will often follow a CG stroke, but will have less wave power at the lower VLF frequencies, and almost no measurable wave energy at ELF frequencies. This feature can be useful when NLDN data is not available, or if the CG event was not recorded by the NLDN system. In the study of more than 250 separate CG cases, the only characteristic difference seems to be in the ELF wave intensities. CG strokes will sometimes have very strong ELF wave power. The IC strokes that were measured during the flight never seem to produce large ELF waves. Unfortunately not all CG strokes are strong in ELF intensity, so this feature alone cannot be used as a consistent discriminator between IC and CG.

The current pulse in the conductive lightning return stroke channel should radiate much like simple dipole antenna. Cloud-to-Ground lightning should radiate most strongly in a direction perpendicular to the driving current along the channel. Cloud-to-ground lightning

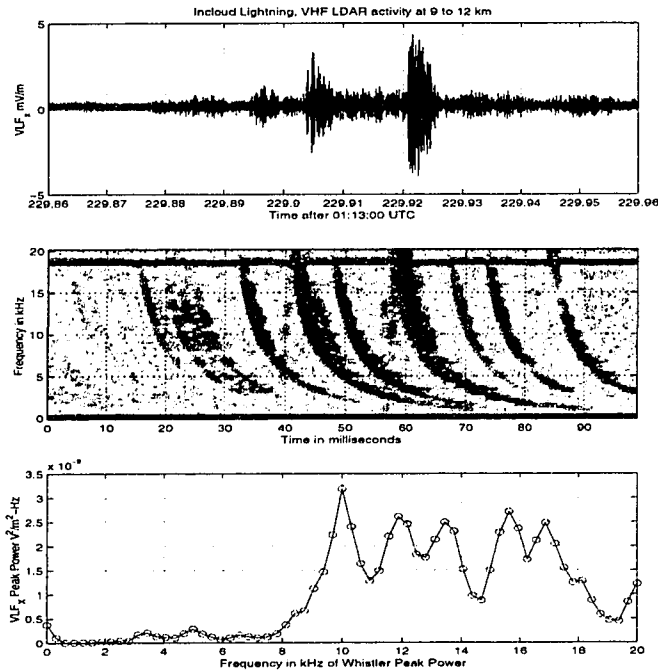


Figure 6.7: LDAR detected VHF trigger activity which was followed by these emissions recorded at VLF frequencies at the rocket. Intracloud lightning tends to have much less ELF wave power relative to the VLF wave power. In the peak power shown in the lower panel, the whistler wave at $t=229.92$ s was analyzed. Strong ELF waves were not measured for the IC strokes during the rocket flight.

channels, being mostly vertical, should radiate most strongly in the horizontal direction. Following a similar line of reasoning, in-cloud lightning channels, with horizontal orientations, should have vertically directed radiated power. Using the LDAR and NLDN data, 24 CG lightning strokes were reconstructed and their length and vertical orientation analyzed. It was found that the lightning channels were within $\pm 30^\circ$ of vertical as measured along a line from the lightning channel base to the top. This gives a crude estimate of the channel orientation and the actual channel is not really straight. Instead, the cloud-to-ground lightning channel forms were usually an inverted L shape, with a nearly vertical section to ground and horizontal channels within the lower regions of the cloud. In a study of Florida

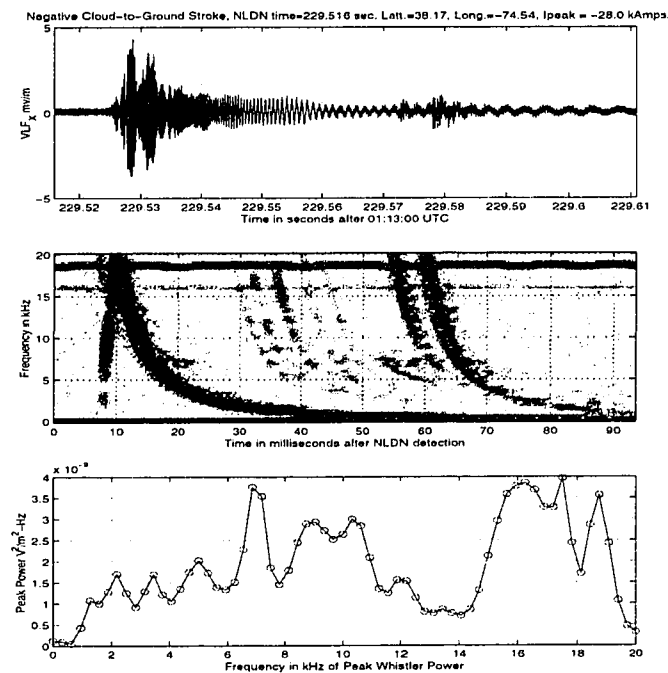


Figure 6.8: Cloud-to-Ground lightning strokes can often be distinguished in the whistler spectrograms by the greater relative amount of power below 3 kHz which is usually at comparable power spectral densities to the peak VLF power present in the stroke.

thunderstorms, Krehbel et al. made a similar observation, that CG strokes developed from the lower charge regions of the storm. Incloud leader channels lowered negative charge from upper cloud regions into the lower charge pool [Krehbiel et al., 1979]. The average

Table 6.2: LDAR Cloud-to-Ground Channel Lengths

Number of Triggers	Vertical Length	Horizontal Length	Angle (degrees)
12 ± 5	$5.3 \text{ km} \pm 5$	$3.3 \text{ km} \pm 1.4$	30.5 ± 10

length of the channels was based on the ground strike location from the NLDN data, and the LDAR triggers which formed the channel above the CG strike location. Note that LDAR triggers become very weak in CG strokes when the leader channel is below 2km. In some

cases triggers are detected down to 500 meters of ground, but this is rare. What is interesting here is that most of the CG strokes have channels that extend from the lower regions (below 5 km) to ground. The leader channels extend horizontally within the lower electrically active regions of the thunderstorm, but not vertically into the upper active charge center above 8 km.

6.8 Conclusion

The rocket measured ELF wave power from LDAR located IC lightning has been found to be much less than the ELF wave power from CG strokes. In order to generate larger, and longer currents that are believed responsible for ELF waves in lightning, a good ground is necessary, which is always available for CG strokes. Strong ELF waves were not measured at the rocket from IC lightning. This can be used in some cases to distinguish between the whistler wave sources, but not all CG lightning strokes had strong ELF wave power. LDAR located IC lightning channels are generally much more horizontal than the CG lightning channels, which are nearly vertical from cloud base to ground. This means that the radiated fields from CG strokes should have much stronger vertically polarized wave energy than IC strokes. This helps to explain why the electric pulse (see Chapter 5) was not caused by IC lightning strokes.

The electrically active regions of the thunderstorm near Wallops Island fall into a clear bimodal distribution with altitude. The peak intensities do not follow the expected charging levels based on models of collisional inductive charging. The models and laboratory based measurements predict the lower electrification region at an air temperature of -10°C to -20°C [Illingworth, 1985]. The observed electrical activity measured by the LDAR VHF activity is clearly seen to occur below this altitude.

The LDAR observations show that the negative CG strokes originated from the lower cloud levels, near the lower electrically active region. The lightning channels formed an inverted 'L' shaped channel in many cases which extended horizontally in the cloud and

vertically towards the ground strike point. Preceding and following the CG strokes, LDAR shows the dynamic processes in the thunderstorm as charge is transported by the movements indicated by the LDAR VHF triggers. Once a CG stroke removes negative charge from a region, negative charge in neighboring regions of the storm are seen to move toward the charge depleted regions.

Numerous LDAR triggers were detected above the thunderstorm anvil. Some of these appear to form leader channels which extend above the thunderstorm anvil. It is possible that some of these cases are similar to the blue jets that were observed by Sentman et al. [Sentman and Wescott, 1993]. They found that the blue jet velocities were on average 98 km/s, ± 14 km/s. The median velocities that we measured for the trigger channels above the storm, 149 km/s, are comparable to the blue jets velocities.

The high altitude triggers that are not associated with extending channels are still a mystery. Many of these high altitude triggers are usually isolated, single, non-sequential events that do not form recognizable channel patterns. These triggers are only hundreds out of 13,000 triggers that were recorded, and we can not rule out that they may be LDAR system location errors. Further research is needed to undertake a serious examination of this type of LDAR activity.

Chapter 7

LIGHTNING OPTICAL EXPERIMENT

7.1 Introduction

In this chapter the data from the ground and rocket optical lightning detection instruments will be compared to investigate the differences between simultaneously recorded lightning strokes. From this study, rocket measured optical and electrical measurements in the ionosphere will be directly compared to the observed ground optical data. In some cases, we will be able to use the LDAR system to tell where the lightning channels were located within the storm. This tells us much more about the lightning events themselves, such as whether there was a continuing current in the stroke, or, if IC lightning channels formed near the main CG stroke channel. From this study, we can better relate lightning stroke processes, both in-cloud and cloud-to-ground, to their optical and VLF signature in the ionosphere. By making studies such as this, data from orbiting lightning sensor scan be better interpreted.

The rocket optical detector was extremely sensitive, within an order of magnitude of a PMT type sensor. This has allowed us to measure in-cloud lightning activity related to the stepped leader of the lightning strokes. This activity is found to produce a higher frequency VLF wave signature, distinct from the CG return strokes.

This study is unique because it combines, for the first time, simultaneous ground and rocket optical measurements of NLDN located CG lightning events. Some of the lightning stroke cases can be studied in detail. By using the LDAR data in combination with the NLDN network, a complete history of the locations of the the lightning channel can be made. The ground and rocket optical data solves the puzzle of the double whistler events which were often seen in the VLF spectrograms of up-going whistlers. It is found that the

second whistler is not an early second return stroke in the CG flash, but instead is closely associated in-cloud lightning occurring above the main CG stroke channel region. In the early part of the data analysis, the second whistler was thought to be a reflected signal. Instead, the data presented here gives a very different interpretation which is that these types of whistlers are the result of triggered in-cloud events following the CG lightning stroke.

This chapter will first cover the design and basic theory of the ground and optical instruments, details of the electric circuit and the circuit diagram and performance data are given in Appendix A. The next section will describe the optical signatures of CG lightning, comparing strokes measured at the ground and at the rocket. The optical pulse widths measured at the rocket and at the ground are summarized.

The pulse widths measured for most of the lightning strokes was 1 ms on the ground, with longer durations of up to 10 ms recorded in a few cases by the ground optical sensor. The rocket optical instrument measured 2 CG strokes with durations of 2.1 ms.

The optical pulse width and the flash brightness are compared to the up-going whistler waves measured by Thunderstorm III. Strokes with longer duration or variations in intensity such as channel brightening and in-cloud events triggered by the initial CG stroke are found to have a direct effect on the form of the whistler waves received at the rocket.

We will also look for a relation between the brightness and the NLDN estimated peak current of the individual lightning strokes. This chapter will also show results of M-channel lightning strokes, in which optical brightness of the CG stroke channel will vary during the stroke. This type of event is typical of CG strokes with continuing currents. For the recorded M events, the whistler waves and the stroke in-cloud dynamics revealed by LDAR will be described.

The propagation velocities of lightning and step leaders, based on the optical signatures are calculated for two CG cases, one a -CG stroke and the other a +CG stroke. The step leader velocities are found to be comparable with the LDAR estimated trigger velocities found in Chapter 6.

In the final section will look at some case studies of CG lightning events which show how the optical signature changes with emission altitude of the stroke and how the optical signatures are related to the measured whistler waves at the Thunderstorm III rocket.

The optical experiments did not work perfectly. An early launch of the rocket, in order to catch this intense thunderstorm, meant that the rocket optical sensor was in sunlight above 200 kilometers altitude. There was also a problem with the DC background cancellation circuit in the rocket optical sensor. The DC circuit problem caused some of the optical data to be lost and made a comparison of the signal amplitudes between the 3 separate sensors impossible. Still, the lightning strokes which were recorded give a unique look at the lightning activity when combined with the ground optical, NLDN and LDAR data.

The ground sensor recorded more than 100 NLDN located CG strokes during the flight and many more in-cloud and CG events that were not recorded by the NLDN network. The rocket optical instrument recorded many optical flashes in the 20 seconds of total usable data, of these 30 were located by the NLDN network, and 12 were also seen by the ground optical sensor.

The ground optical instrument was able to detect many of the CG strokes from the Wallops Island storm cell over the ocean and to the East. The activity from the Northeast thunderstorm cell was too far away to be detected by the ground instrument. Lightning events which were south of Wallops Island were not detected, probably because of poor visibility through the center core of the storm.

7.2 Ground and Rocket Optical Instruments

The rocket optical instrument was designed to detect the optical flashes of lightning and to trigger the SnS burst memory system for data taking. The optical light travels to the rocket much quicker than the LF, MF and VLF waves from the lightning flash, (microseconds vs. milliseconds for the whistler waves). The optical sensor also gives the time of the lightning flash. This time can be compared with the NLDN network time solutions for the detected

CG events. The instrument also gives the times of events that are missed by NLDN such as small ($< 12\text{kA}$) events and all IC events.

The ground optical instrument plays a key role in the stroke analysis for the flight. This instrument had a limited view of the optical lightning events, but it was able to detect many of the strokes around Wallops Island. The instrument response was fast enough to look at some cases of channel brightening, known as M events, which occurred during some of the recorded CG strokes.

The rocket and ground optical instruments used silicon photodiode detectors and both have DC background cancellation circuitry. The methods used for background cancellation differ in each of the instruments as does the speed of response, sensitivity and dynamic range. The basic theory of these two instruments is described in the next section and the details of the instrument performance are given in Appendix A.

7.2.1 Basic Theory of Operation

Optical detectors can use several methods to convert the incident light into a voltage. Two methods are often used on lightning sensors, photo-multiplier tubes (PMT) or photodiodes. PMT's offer extreme sensitivity, even to the single photon level in some applications. They do require much higher operating voltages and are larger than photodiode sensors. Photodiodes have less sensitivity but operate low voltage power supplies typically under 20 volts. Good designs for lightning detection try to eliminate non-transient or DC background light and maintain rapid response to signals over a large dynamic range. This usually means that sensitivity sacrifices response time.

Incident light with wavelengths between 400 and 1100 nm will produce a photo-current on the silicon photodiode. For the photodiode used in the rocket instrument, 1 photo-watt incident at the diode will produce approximately 0.5 amps of output current. This current must be converted into a voltage signal for data output. The photo-current can be very small, several picoamps in the case of the rocket sensor. To convert the photo-current into a volt-

age, a circuit using an opamp with sufficient gain and low noise was designed specifically for this large area silicon photodiode. In the current to voltage circuit, the choice of the feedback resistor is crucial since it will set the response time of the instrument. Some amount of feedback capacitance is needed to keep the photodiode circuit from oscillating. The time response of the sensor is then limited by the feedback resistance R_f and the feedback capacitance, C_f . The roll-off frequency is then given as $2\pi * R_f * C_f$ [Engineering, 1990]. For the rocket instrument the roll-off frequency was 2.2 kHz and 10 kHz for the ground optical system.

The optical sensor must have a time response fast enough to capture the individual strokes in a lightning flash. Individual CG stroke measured from U2 high altitude over-flights of thunderstorms have optical pulse durations averaging 500 μ s, with a standard deviation of $\pm 200\mu$ s [Goodman *et al.*, 1988]. During an individual stroke, the optical brightness may vary, and this is always the case for long duration strokes [Thottappillil *et al.*, 1995; Goodman *et al.*, 1988]. Typical strokes are separated by 10 ms or more, and usually the average time is 40 ms [Uman, 1984]. Longer duration lightning strokes which last longer than 1 ms have variations in optical brightness known as M-events. M-events are observed during a return strokes when the main channel encounters a junction branch in the cloud, or new charge sources connect into the main return stroke channel while it is still conductive. M-event channel brightening are usually observed within 4 ms or less of the return stroke. Return strokes with continuing currents lasting longer than 10 ms never occur without M type current pulses [Thottappillil *et al.*, 1995].

The M events observed in this study occurred within several milliseconds of the main return stroke, sometimes before the optical amplitude of the initial event had decreased by 50 percent. There are other very fast transient events in lightning return strokes that have been recorded in other studies by ground based instruments. These types of pulsations occur in less than 1 microsecond and are believed to be related to the expansion of the main return stroke channel [Jordan *et al.*, 1997].

Another requirement on the flight instrument was sensitivity to very low light level signals. This was done using a voltage biased silicon photodiode with an area of 1 cm^2 . Voltage biasing increases the sensor response because the bias reduces the travel time through the PN junction of the photodiode (silicon) material. The trade-off is an increase in the leakage current through the PN junction which increases the photo-dark-current (noise).

The rocket optical sensor had 3 separate channels which were filtered to detect the color characteristics of the flashes. At the time of design, one of the goals was to look for anomalous optical events or Sprites. By using optical filters, the light from a Sprite might be distinguished from a regular IC or CG flash. The emission lines and spectral distribution of energy were not known for Sprites, but the plan was to find some way to distinguish the sprite discharge from CG or IC events. The early reports were that Sprites were red in appearance. By breaking the total optical response band of the sensor into 3 broad bands, it was hoped that the color distribution of a sprite would be distinguished from an IC or CG event. Wide-band color-glass optical filters were used to divide up the sensor bands. The filter bands for each sensor are given in Appendix A.

For the Thunderstorm III rocket instrument, a sensitive photodiode type instrument was designed by senior electrical engineer John Chin. The schematics and electrical performance characteristics are given in the Appendix A. By careful design and selection of a larger area photodiode, the instrument was able to detect optical signals with incident flux at the sensor as small as $5 \times 10^{-12} \text{ W/cm}^2$.

This level of sensitivity is within an order of magnitude of a PMT instrument. Sensitivity comes at a price, in this case the detector response was slower than the ground optical instrument. The 3 dB roll-off in the rocket optical instrument was at pulse widths less than $500 \mu\text{s}$. The ground optical detector had a 3 dB roll-off at less than $100 \mu\text{s}$, but a minimum sensitivity of $3 \times 10^{-10} \text{ W/cm}^2$.

7.3 Scattering and Intensity of Lightning Optical Signal

The instruments used for the detection of the optical pulses from the lightning flash are non-imaging photodiode detectors. The photodiode receives some amount of light energy on the surface of the diode and produces a current which is then converted to a voltage signal. The energy from the lightning flash radiates its total optical power into 4π steradians. At a distance R away, the optical detector receives a radiant intensity of L_p in Watts per cm^2 .

There is a simple relation between the radiated optical power of the lightning optical channel and the output signal of the optical detector. This relation assumes no scattering from source to observer and the geometrical configuration of the channel source are not considered. The point source relation is given as:

$$P = 4 * \pi * R^2 * L_p, \quad (7.1)$$

where the total radiated power from the lightning stroke P , in photo-watts, is proportional to the irradiance L_p in W/cm^2 at the detector, at a distance of R centimeters [Guo and Krider, 1982].

This energy depends on the area of the photodiode and the the silicon photo-detector response integrated over the optical band of the detector. The output voltage of the lightning optical detector V_{out} , is related to L_p by:

$$V_{out}/R_{fb} * W_p/I_p * 1/a_{det} = L_p, \quad (7.2)$$

R_{fb} is the CVC (current-to-voltage converter) feedback resistance in ohms, W_p/A_p is the photo-watts per ampere constant of the Hamamatsu silicon detector, which at the maximum wavelength intensity of lightning is approximately 2.0 watts per ampere, and a_{det} , is the area of the detector [Engineering, 1990]. The output voltage of the rocket sensor is:

$$V_{out} = \text{sqrt}(L_p * I_p/W_p * a_{det} * R_{fb}) * \text{Gain} \quad (7.3)$$

A thunderstorm is more complicated since light is scattered, reflected and absorbed in the cloud. Lightning channels below the cloud appear bright to the ground sensor but may be dim at the rocket. In-cloud lightning will scatter depending on the height of the channel in the cloud. Channels that are near the cloud top scatter more light upward. Low level channels will be dimmer at the rocket but much brighter at the ground. The thunderstorm cell is optically thick, meaning that a photon will scatter many times before it exits the cloud cell. The scattering of the light is primarily from the liquid water and ice present in the cloud. The absorption is very low in the Near IR where the silicon detector is most sensitive. The single scattering albedo of the droplets is estimated at over 0.99996 at optical wavelengths [Thomason and Krider, 1982]. Realistic values of the distance that a photon would travel before scattering, known as the mean free path λ , are between 8 and 24 meters and an estimated optical depth τ of 80 to 400. This means that the likelihood that a photon of visible or IR light in the sensor's passband would not scatter is $P_{scatt} = e^{-\tau}$, where τ is the distance through the cloud x divided by the mean free path λ . Thus it is a certainty that the photons emitted in the cloud will scatter many times before they exit [Thomason and Krider, 1982].

The light scattering of clouds has been modeled by Thomason and Krider using a Monte Carlo method. Their results for a cylindrical cloud are shown in figure 7.1. The model results show that a source in the center of a cloud will scatter light equally upward and downward. Sources near cloud top will only scatter a few percent of the light to ground, with most of the light energy going out of the cloud top.

In the case of the Thunderstorm III data, sources near the cloud top will appear much brighter at the rocket but very dim or even undetectable at the ground sensor. For the model cloud, an optical depth Λ of 200 was used. These values are probably conservative and the actual optical depth may have been greater. Because of the in-cloud scattering, the optical pulses will be broadened. The maximum time broadening estimated using the cloud model was about $148\mu s$ for a typical lightning stroke [Thomason and Krider, 1982]. This amount of pulse broadening caused by light scattering would not be noticeable in the sig-

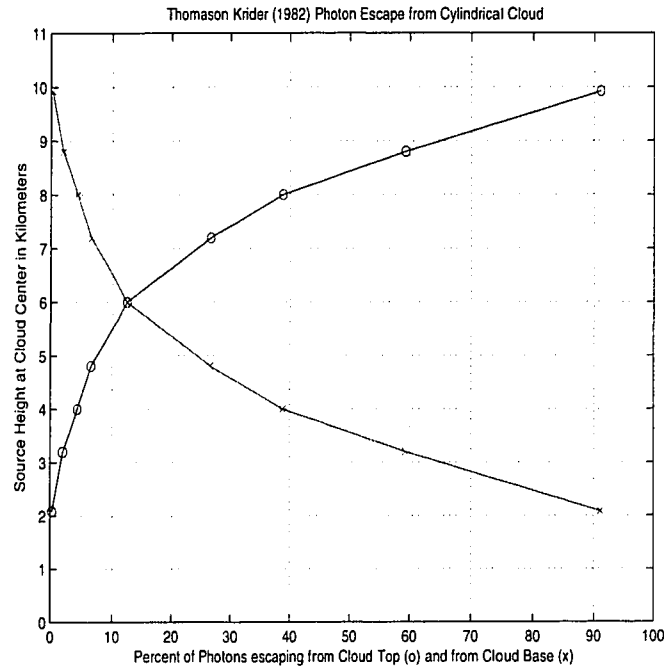


Figure 7.1: A cylindrical cloud modeled with changing optical source height from the cloud axis z is shown using the data of [Thomason and Krider, 1982]. At the base of the cloud, very little light exits the top of the cloud, most exits the sides or is emitted from the base. As the source moves to the center, the top and cloud base will have equal brightnesses. When the source is near cloud top, most of the light is emitted upward. Similar light signatures are seen in CG and IC events where the initial lower altitude CG event appears dim in the rocket sensor. Later, when the IC events occur at higher altitudes, they appear much brighter in the rocket sensor than the GC event.

nals recorded by the Thunderstorm III optical instrument, since it is on the order of 0.1 ms, near the limit of the instrument's time response.

The next section shows cases of CG and IC lightning activity where we have a good estimate of the lightning channel heights based on the LDAR VHF triggers. In agreement with Figure 7.1, the rocket optical instrument typically sees a much dimmer light pulse for the CG lightning, but the IC strokes which take place much higher up in the cloud appear much brighter.

7.4 Analysis of Ground and Rocket Optical Cloud-to-Ground Strokes

The interpretation of the optical data from the rocket is often complicated by problems related to timing and the associated optical activity preceding the CG stroke. Fortunately, we have NLDN stroke resolution data to within ± 1 ms resolution as an aid to interpreting the optical data.

A normal CG sequence will consist of a first return stroke which is preceded by the stepped leader activity. During the stepped leader process, the electrical emissions from the developing channel regions should show the characteristic Very Active (VA) signature, which consists mostly of higher frequency VLF and VHF radiation. This activity usually precedes the return stroke by 20 ms or more [Volland, 1984].

7.4.1 Estimate of Stepped Leader Velocity from Optical Data

The stepped leader channel preceding first return strokes often occurs with VA VLF electrical activity. When observed from above the thunderstorm, the step leader will sometimes produce a measurable optical signal which decreases in intensity when the leader tip exits the base of the cloud and continues to ground. The time from the optical peak and subsequent decrease in light intensity during the VA portion, to the RS optical pulse can be used to measure the step leader velocity, if the cloud base height is known [Brook *et al.*, 1985].

For the example shown in Figure 7.2, we can calculate the step leader velocity for this stroke. The cloud base height, based on the radiosonde data shown in Chapter 3, was 2.2 km. The step leader exits the cloud base, as inferred from the optical signature, at $t=550.807$ s and the optical RS begins at $t=550.813$ s. This gives the stepped leader a travel time from cloud base to ground of approximately 6 ms. The step leader velocity for this -CG stroke is then estimated to be $3.1 \times 10^5 m/s$. This is comparable to the LDAR low altitude mean leader velocity of $2.9 \times 10^5 m/s$ found in 6, Table 6.1.

A second case was calculated for a +CG stroke at $t=549.772$ seconds. This was a single cloud-to-ground stroke as recorded by NLDN with a stroke current of 44 kA. Using the

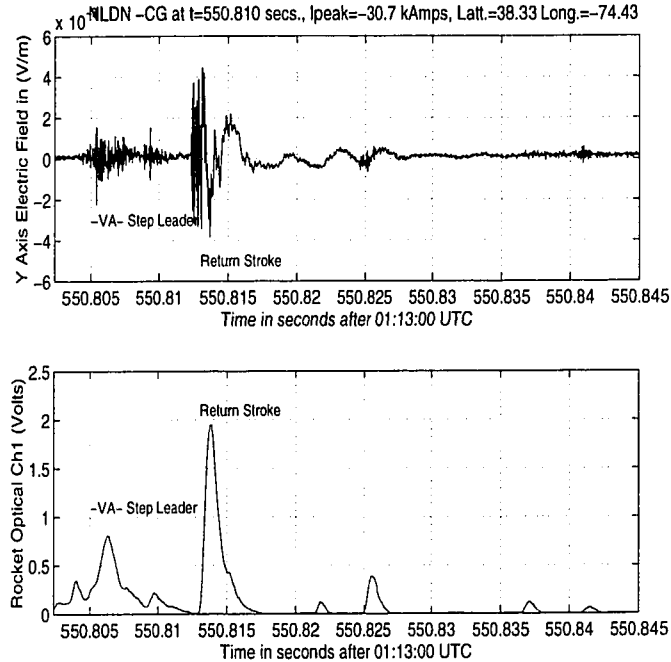


Figure 7.2: This single CG stroke has the characteristic activity which precedes the return stroke. In the electric field waveform, higher frequency activity is measured preceding the RS during the step leader to ground. In the measured rocket optical data, the light during the SL portion disappears about 5 ms prior to the RS. This is probably caused by the luminous leader tip exiting the cloud and heading to ground. This is followed by the return stroke (RS) and some post RS activity, seen in both the electrical and optical channels from the rocket.

same method described here for the -CG stroke, the estimated velocity was $1 \times 10^4 \text{ m/s}$. For the -CG case, the stepped leader time to ground was 6 ms, but in this case, based on the optical signature, the travel time was at least 22 ms. This velocity is slower than the LDAR measured trigger velocities, and we cannot say that positive stepped leaders always have lower velocities than negative stepped leaders. LDAR did not locate any triggers from +CG stroke channels, so we can only compare the negative CG velocities in this case.

We have not compiled a large enough data set from the optical cases to do a statistical analysis, but the -CG case at least, is comparable with the LDAR trigger velocities. This type of optical signature is a convenient tool for identifying first return strokes and new

lightning channels formed by stepped leaders.

7.4.2 *Optical Pulse Analysis of CG Strokes*

The optical lightning strokes that were recorded by the ground sensor at Wallops Island during the flight totaled approximately 125 events. The number of CG events that were cataloged from the rocket instrument during the last minute of the down-leg before reentry was a total of 9 cases.

The stroke analysis follows the method used by Goodman et al. [Goodman et al., 1988]. Each stroke is characterized by the pulse width using the time from the 10% level to 50% and to maximum brightness, also the pulse duration in terms of the full width at half maximum (FWHM). An example of a CG stroke is given in figure 7.3.

The pulse widths measured for most of the lightning strokes were 1 ms, with longer durations of up to 10 ms recorded in a few cases by the ground optical sensor. The rocket optical instrument measured 2 CG strokes with durations of 2.1 ms. The optical pulse width and the flash brightness are compared to the up-going whistler waves measured by Thunderstorm III. Strokes with longer duration or variations in intensity such as channel brightening and in-cloud events triggered by the initial CG stroke are found to have a direct effect on the form of the whistler waves received at the rocket.

The average optical duration of the CG strokes was 0.8 ms, with a maximum duration (FWHM) of up to 8 ms in the case of the M-events described in the next section. These results are similar to the pulse FWHM averages found by Goodman et al. and Guo and Krider for CG strokes [Goodman et al., 1988; Guo and Krider, 1982]. The FWHM mean time for CG strokes was 0.422 ms, with a maximum of 1.4 ms [Goodman et al., 1988], these results are summarized in the histograms shown in Figure 7.4. The maximum durations seen for the Wallops Island thunderstorm are still far less than some of the reported stroke durations of up to 40+ ms from Florida and Oklahoma storms [Rust et al., 1985].

The analysis of the rocket optical and ground data had to account for the telemetry time

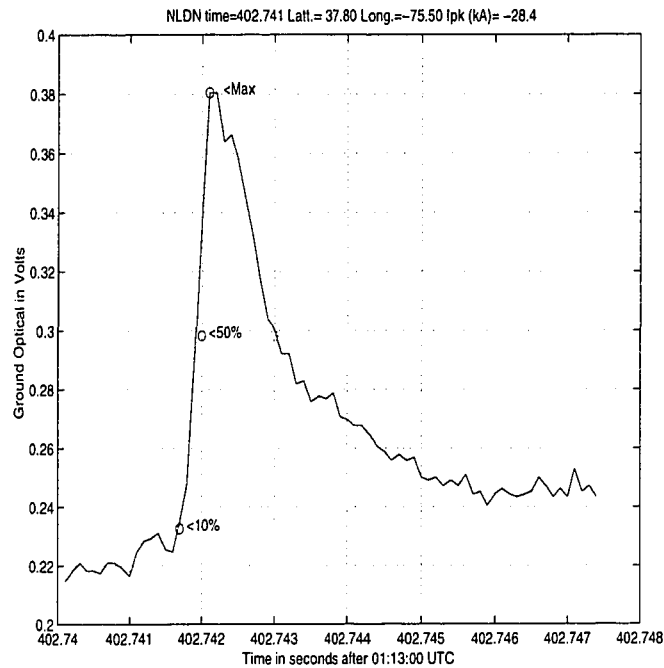


Figure 7.3: Ground optical data was obtained for 125 NLDN located CG lightning strokes. The strokes were analyzed by looking at their duration at the half power level (FWHM) and the time from 10% brightness to 50%, 90% and to peak brightness. The optical sensor used an uncollimated silicon photodiode with background and dark current cancelation circuit.

delay differences during the flight. By $t=522$ seconds the delay time between ground and rocket CG strokes were nearly 3.3 ms. This delay was the sum of the time the lightning optical signal took to travel to Thunderstorm III, and for the rocket telemetry to reach NASA Wallops. The ground sensor was located within a speed of light time difference of the NASA telemetry receiver of $15\mu\text{s}$. Many of the ground flashes had an associated IC lightning stroke that either preceded or followed the CG stroke. The IC strokes usually appeared much brighter than the lower altitude CG strokes. Cloud to Ground strokes with an associated triggered IC flash produced a characteristic double whistler spectrogram. The optical flash signature of such cases is shown in figure 7.5. The initial CG stroke appears bright in the ground optical but dim in the rocket optical sensor, yet the following IC flash is not seen at

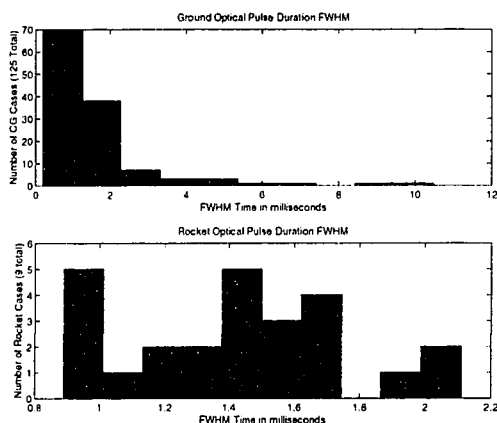


Figure 7.4: Summary of Cloud-to-Ground lightning strokes measured by the ground based optical sensor and the rocket instrument. The average CG stroke had a FWHM duration of less than a millisecond. Several longer events were recorded by the ground sensor (up to 8 ms). The longer duration CG strokes were found to have brighter optical emissions following the initial light pulse indicating that the channels were branching into higher regions of the cloud.

all by the ground optical system but appears very bright to the rocket optical sensor.

This can be understood in terms of the light emitting channel altitude and the scattering of light within the storm clouds. Based on the data from the LDAR system, the lower altitude CG channel extends from approximately 4 km to ground while the IC channel is related to LDAR triggers at higher altitudes. More light reaches the top of the cloud from the IC stroke. The rocket optical system is more sensitive than the ground optical instrument, and is able to capture both CG and IC strokes, but the ground sensor only recorded the main CG stroke in this case. In this case, two whistler waves are produced, one by the CG stroke and one immediately following it by the IC stroke.

7.5 *Cloud-to-Ground M Events*

During the rocket flight the ground optical instrument recorded a few CG strokes which had longer than average (greater than a millisecond) duration. Some of these single strokes lasted for up to 8 milliseconds. During these strokes, the channel brightness recorded by

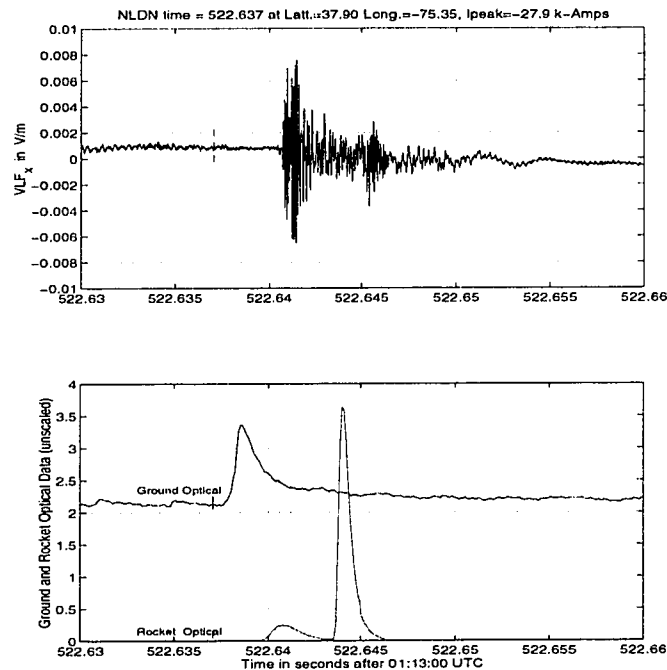


Figure 7.5: The Cloud-to-Ground stroke triggers an IC stroke at a higher altitude in the cloud. The CG stroke appears bright at the ground but dim at the rocket. The IC stroke is very bright at the rocket and probably occurred above the mid-altitude level of the storm cloud. The VLF electric field records two whistler waves, the first from the CG stroke followed within a few milliseconds by a second IC stroke whistler.

the ground instrument had several brightenings. These changes in channel brightness are known as M events and are believed to be caused by in-cloud junction processes which connect new regions of charge into the main conductive lightning channel. In CG strokes that remove large amounts of charge from the cloud, a continuing current flows for longer time during the stroke. The changes in channel brightness during M events are a typical feature reported by other researchers [Schonland, 1932; Uman, 1984]. How do these currents affect the up-going whistler waves in the ionosphere? The continuing currents should only produce electric and magnetic static field changes unless they are slowly varying. It is now believed that the continuing currents in lightning strokes produce larger amounts of ELF

radiation [Reising *et al.*, 1996]. For the cases that were seen during the Thunderstorm III flight, there is some evidence of increased ELF radiation in the whistler waves. The strokes with the largest ELF wave intensity were not recorded by the ground or rocket optical instruments.

During the down-leg of the rocket flight, there were several CG flashes which produced strokes with M-type light signatures. An example is shown in Figure 7.6. In this case, the

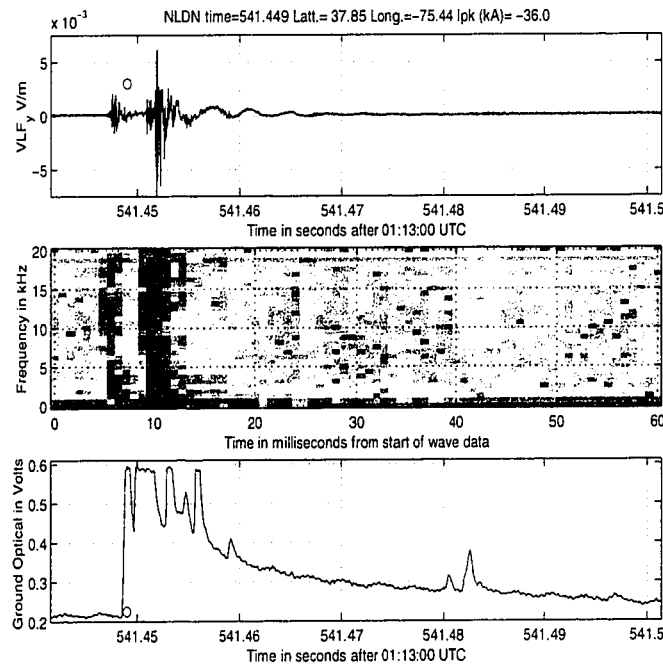


Figure 7.6: The Cloud-to-Ground lightning stroke had a longer than average duration in optical brightness. During the stroke, the brightness of the channel changes. These changes are known as M-events. In the whistler wave recorded by the rocket, the ELF waves are evident as a slow wave following the higher frequencies and are probably produced by the continuing currents in the CG stroke.

lightning optical flash recorded by the ground instrument had an optical duration of nearly 8 ms. During the 8 milliseconds of the flash, there is a decrease in optical amplitude and then several re-brightenings of the channel. During this time, NLDN did not record any addi-

tional CG activity. After the stroke, there is some IC activity which produces weaker VLF waves in the ionosphere. LDAR activity that preceded the CG flash showed widespread triggers at 4 and 5 km altitude occurring up to 5 kilometers away from the ground location. Other triggers were recorded between lightning strokes in the flash. This event was the second stroke of a 2 stroke flash, and it had been preceded by another 2 stroke flash at 540.58 seconds nearby. The two stroke flash with the M event at 540.58 seconds is shown in Figure

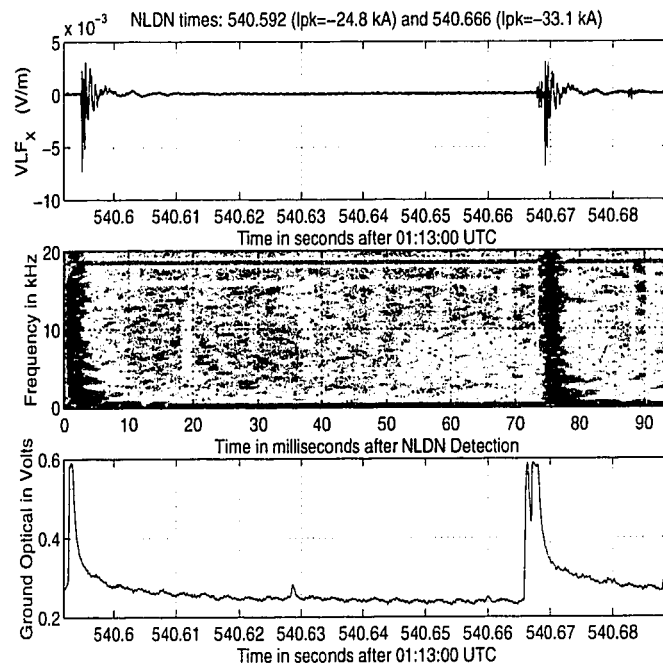


Figure 7.7: The Cloud-to-Ground lightning flash had a longer than average duration in optical brightness during the second stroke. Preceding the flash, LDAR activity shows leader channels lowering charge from the 12 km level down to 8 km, and then channel formation from the 4 km level to ground where NLDN recorded the CG strokes. There was a strong -2kV/m drop in the ground electric fields measured on Wallops Island at the launch pad EFM sensors.

7.7. The first stroke at 540.541 seconds is a normal duration CG stroke, the second stroke at 540.58 has a longer duration of nearly 5 ms. The strongest 1 kHz wave intensity did not occur during the M-event associated stroke in this series, but during the first stroke at 540.592

seconds which had nearly double the 1 kHz wave power ($2 \times 10^{-9} V^2/m^2 Hz$). At the time of this stroke, the ground field mills recorded a large drop in the electric fields of 4.5 kV/m. Oddly, there was only a recovery field recorded during the subsequent strokes. Each of the M-events had significant ELF wave energy but they were not much larger than other CG strokes that produced ELF wave energy without a long optical stroke. The interpretation is that the continuing currents do increase the ELF portion of the whistler wave energy, but not much more than other lightning strokes of normal duration, which also can show significant ELF energy. In all cases with enhanced ELF wave energy measured during Thunderstorm III, the strokes all occurred in a multi-stroke series of a lightning flash.

A more important factor may be the total charge eliminated from the cloud in whatever manner the charge is delivered to ground, be it by a continuing current with an M type signature, or shorter optical duration stroke. The time resolution from the EFM charts is not quite sufficient to clearly resolve each of the individual strokes in this case, but we can see some interesting features. During this two stroke flash, the electric field mill (EFM) measurements from the 3 launch pad sensors, Islands, Pad5 and Pad2, show ground field changes of -2 kV/m. Preceding the CG strokes, the LDAR system shows a series of triggers from 12 km down to 8 km, coincident with an increasing ground electric field measured by the 3 EFM stations. We interpret this as a lowering of charge from the upper cloud region down to mid level causing the increased ground electric fields. LDAR then shows the development of channels between 4 km and 2 km altitudes just prior to the first CG stroke at 540.59 seconds, when the ground fields sharply decrease.

The M event case that has been described did not produce an extremely large ELF wave in the ionosphere. There were sizable changes in the ground electric fields during this two stroke flash, but there does not seem to be a direct relation between M event optical strokes and enhanced ELF wave energy in these cases. The largest ELF measured during the flight, at $t=488.166$ seconds, from a +57 kA CG stroke, actually occurred after a very large negative field change of -6 kV/m measured by the EFM systems at Pad 2 and Island South.

This change was coincident with a series of negative CG strokes, with -17 and -27 kA peak currents.

Enhanced ELF wave energy does not seem to be directly related to the M type continuing current optical events that we have looked at here. The ELF wave energy is not related in an obvious way to the ground EFM changes measured by the Wallops EFM system. The EFM data has been difficult to correlate with the NLDN stroke data since the data is available only on low time resolution strip charts. Also, the proximity of the thunderstorm caused some of the field mills to be saturated. Even so, a direct relation between large amounts of charge removed from the thunderstorm by continuing currents or smaller multiple strokes, do not seem to be the cause of enhanced ELF wave energy. The other option is the lightning channel configuration, i.e. length, that is related to the enhancement of ELF wave energy in whistlers. Here again, using the data from the LDAR system looking at channel lengths and orientation in Chapter 6, no clear relation was found; but, LDAR did not produce any trigger data for the largest cases of ELF wave energy. This was due to the reduced sensitivity, and the fact that some of these cases were positive CG strokes that never seem to produce measurable VHF triggers.

7.6 Case Study of Cloud to Ground Lightning

The question of the "ghost whistlers" was raised in the earlier chapters. By examining some of these cases using the optical data from the ground and rocket their occurrence can be better understood.

A lightning return stroke will sometimes contain more than one current pulse down the main channel in addition to the multiple strokes that occur in a single flash. These pulses brighten the main channel and are known as M-channel events [Uman, 1984]. The dynamics of the M event are believed to be related to K-events occurring in the cloud around the main lightning channel which bring in new sources of charge into the channel. The new charge, once connected to the main channel will discharge to ground. Often these events

do not require a Dart leader to precede the discharge since the main channel is already very conductive, providing that it occurs within 10 milliseconds or less of the main RS [Thottappillil *et al.*, 1995]. It is now believed that the M-event actually does have a dart leader which goes down the already conductive channel. The Dart will propagate differently down the hot channel, and there is a reflected wave at the ground termination which does not occur during dart leaders down older (more than 10 or more milliseconds) channels. This has been modeled using transmission line theory by Rakov *et al.* based on their studies of triggered M events in Florida storms [Rakov *et al.*, 1995].

The removal of charge from the lower regions of the thunderstorm should change the equilibrium of the other charges in the region surrounding it. IC events might be expected to discharge near the region of charge removal in the thunderstorm. This view is supported by the observations made during the Thunderstorm III experiment. We examine a particular case in which a CG discharge is quickly followed by an IC stroke in the region above the stroke to ground. The observations of many CG flashes followed by what appears to be either a reflected or triggered lightning signal are now seen to be in fact triggered IC events. The data from LDAR, NLDN and the ground and rocket optical instruments give a very clear picture of the sequence of events that explains the "ghost whistlers" that have been seen in many cases throughout the whistler data. For the CG event at $t=510.049$ seconds, shown in Figure 7.8, the LDAR system shows triggers above the ground strike point in the lower charge regions of the storm at 2 to 5 km altitudes. There is also trigger development above the region at the mid level of the storm, from 5 to 8 km. This particular event is the second stroke of a 3 stroke flash. During the CG stroke, the ground optical detected a bright pulse but nothing following it (see Figure 7.8). The rocket optical instrument records the CG stroke followed by a much brighter IC event which is not seen by the ground sensor. This shows that the second optical pulse occurred higher up in the thunderstorm and that the channel did not connect to the existing multi-stroke channel to ground. The whistler waves from the IC events are much weaker than the CG stroke, especially at the lower frequencies.

The initial CG stroke appears less bright at the rocket than the later in-cloud activity which occurs high up in the cloud. In this lightning event, the CG stroke produces an initial up-going whistler wave and a bright flash at the ground optical sensor. In the cloud, after several milliseconds, there is optical activity and electrical VHF (LDAR) emissions at the upper in cloud levels. This activity appears much brighter at the rocket because the optical depth is less from the upper part of the cloud to the rocket. The triggered IC activity did not discharge down the CG channel since no brightening was observed by the ground instrument at the times of the light pulses recorded by the rocket.

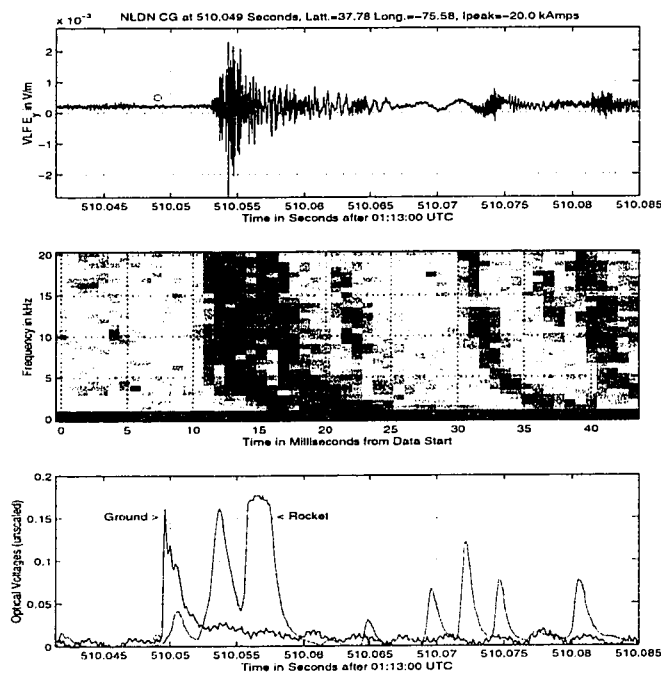


Figure 7.8: The optical flash of a Negative CG stroke measured by the ground optical and rocket instruments at 250 km altitude. Notice that there are two whistler waves, one from the CG stroke, and a second one from the IC stroke which follows it. The IC stroke appears much brighter optically at the rocket than the CG stroke.

The optical signature of the stepped leader and the dart leader are much dimmer than the return stroke. This part of the stroke is usually visible only at close range (less than ≈ 5 km)

on high speed photographic devices. Much smaller currents flow in the channels as they develop. Observations of step leaders indicate that the currents are fairly small but constant in the leader channel. This gives a constant, dim light signature of the dart [*Jordan et al.*, 1997].

The stepped leaders were not usually observed by the ground optical instrument, although some of the in-cloud activity was, especially when it occurred in the lower cloud. The return stroke produces very large currents (kA) and these rapidly heat the channel and ionize the air within the channel into a highly conductive plasma. Temperatures in the channels reach 50,000°K within several microseconds [*Uman*, 1984].

7.7 Comparison of Rocket Optical, VLF and NLDN flash rates

Lightning flash rates are believed to be related to severity of thunderstorm internal convection [*Baker et al.*, 1995]. The flash rate can be measured in several ways. One method is to use the NLDN detected CG stroke data to calculate the rate F in strokes per minute. Flash rates using the rocket optical sensor data will include CG and IC flashes. This rate is found to be 8 to 10 times higher than the NLDN estimate of F. The third way to estimate F is to use the number of whistler waves seen in the spectrograms of the VLF electric field data. This method gives the highest flash estimates, in part because we have not set a threshold level on the whistler wave power.

The NLDN flash rates were calculated using strokes from the Wallops Island storm cell and the storm cell located to the northeast. These flash rates changed during the ten minute flight, from 96 flashes per minute during the upleg of the flight to about 82 flashes per minute during the final 20 seconds preceding re-entry. The rocket flash rates are based on the number of optical pulses exceeding 1.5 volts in the main optical sensor, or a flash intensity at the rocket equal to or greater than $0.8 \times 10^{-7} W/cm^2$. The rocket optical rate includes all strokes, IC, CG from all locations visible to the rocket recorded during the down-leg at $t=520$ to $t=540$ seconds. Optical strokes exceeding the 1.5 Volt sensor level were assumed

to be located from the two thunderstorms nearest Wallops.

The VLF whistler flash rates are even larger, no power restriction was placed on the whistler rates, only that a noticeable trace occurred on the plot of the VLF electric field data. Based on the optical flash rate and the NLDN rate, the ratio of IC to CG strokes, R , can be approximated to be 5-to-1.

Table 7.1: Lightning Flash Rates based on NLDN rocket optical flashes and rocket measured VLF whistlers.

Flash rate F	Number in 20 seconds	Equivalent Flashes/minute
NLDN CG rate	28	85
Rocket Optical rate	107	320
VLF Whistler rate	350	450

7.8 Optical Brightness and the NLDN Current of Cloud-to-Ground Flashes

It seems reasonable to think that the current flowing in the lightning channel during the return stroke should be directly related to the channel brightness. Such a relationship between the stroke current and brightness would give another method to estimate the peak lightning stroke current, if it could in fact be established that such a relation existed. In order to find the relation between brightness and current, laboratory long sparks are used. By controlling the current in the sustained sparks and measuring the optical intensity, a roughly linear relationship can be established. This has been done by several researchers, beginning as early as 1968 [*Uman et al.*, 1968]. The question remains as to whether the characteristics measured in laboratory sparks can be applied to natural lightning. As the history of lightning research has shown, laboratory sparks and natural lightning often have very different behaviors [*Yavetz*, 1996].

Earlier work by Colvin estimated the currents in the lightning channels produced by the IVY-MIKE nuclear bomb test to the lightning channel brightness [*Colvin and Mitchell*,

1987]. Colvin and Mitchell's method was based on lab measurements which controlled the current in long arcs. Their results from the lab work found a simple quadratic relation between the channel brightness per unit length and current. Based on their work, they were able to make a reasonable estimate of the lightning currents for the IVY-MIKE lightning bolts. Unfortunately, there were no other independent means to check the lightning currents. The authors noted that the characteristics of nuclear explosion-induced lightning (NEIL) are very different from natural lightning.

Another study of long laboratory sparks looked at the correlation between the optical signatures and the currents. It was found that the optical pulse of the half meter long sparks did have a linear variation with the current amplitude. Based on this result, it was suggested that the peak current of natural lightning could be measured optically [Gomes and Cooray, 1998].

Idone and Orville, looked at the current and light intensity in triggered lightning. In their study, there did seem to be some relationship between the current and the optical brightness. In their study, there were only two triggered lightning flashes which each had more than 20 return strokes. Most of the strokes had peak currents less than 10 kA, and none greater than 21 kA [Idone and Orville, 1985a]. Triggered lightning can have some very different characteristics from natural lightning. The currents in triggered strokes are often much smaller and the current pulse rise times and duration are often very different as well [Fisher et al., 1993]. In this study, we analyzed the data base of over 100 CG strokes which were measured by the ground optical sensor with coincident NLDN estimated peak currents and location. Because we have all of the NLDN detection data for each CG stroke, it should be possible to check for a relation between the optical brightness and the peak currents. selected cases which have multiple stroke flashes, have normalized to the brightness of the second stroke in the flash and the NLDN peak currents are normalized to the second stroke peak current. The strokes should have approximately the same channel configuration during each CG flash. The differences in the brightness of the strokes in the flash should then be a function only

of the differences in the channel currents, which are estimated by the NLDN peak current. Guo and Krider found in their analysis of Florida thunderstorms that the first stroke was often much brighter than the subsequent strokes. In addition, They did find some apparent relation between the stroke brightness and current, but could not determine if the relation was best described by the brightness L , vs. I_{pk} or $\text{Log}(L)$ vs. I_{pk} or a simple Log Log relation [Guo and Krider, 1982]. The approach used here is somewhat different, we look only at NLDN located flashes with multiple strokes. A total of 8 multi-stroke cases were analyzed to see if there was a correlation between the peak current and brightness. As can be seen in Figure 7.9, which shows 4 of the 8 cases, no clear, consistent correlation was found between NLDN peak current and stroke brightness.

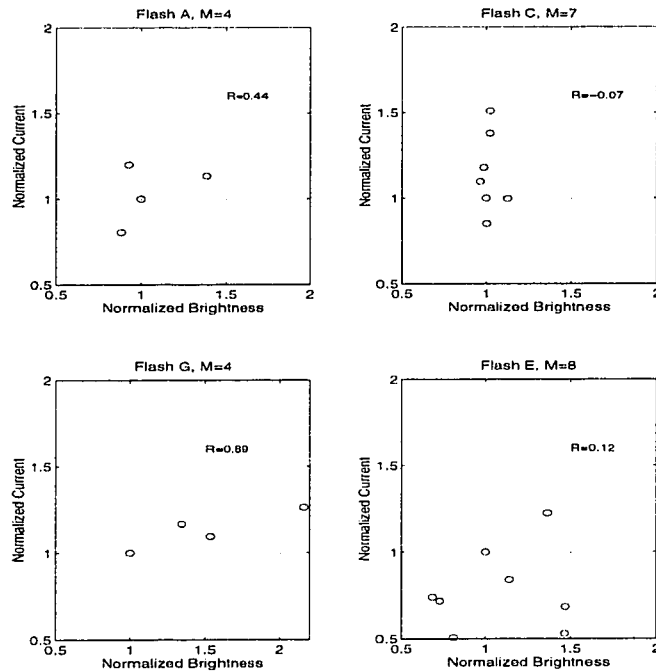


Figure 7.9: For the 8 flashes studied (4 are shown here), no consistent correlation or linear relation was found between the measured optical brightness and NLDN estimated current. In each case, the current and brightness of each stroke in the flash have been normalized to the current and brightness of the second stroke.

In each of the 8 multi-stroke flash cases, the linear correlation varied from 0.9 to -0.07. An examination of the 4 cases shown in Figure 7.9, the relation is very inconsistent, such as in Flash cases C, where the current increases by 50% but the brightness remains the same. Based on these cases of untriggered, natural lightning, it seems that stroke brightness is not related in any simple way to the NLDN peak current. This might have been expected, since the electric fields and the currents in the lightning channel reach their maximum well before the channel has illuminated up to cloud base [Guo and Krider, 1982; Lin *et al.*, 1980]. The NLDN peak currents are received some 20 to 40 μ s before the lightning channel peak brightness. What is apparent in this analysis is that brighter lightning strokes cannot be used in any way to infer larger peak currents in lightning. Each stroke channel seems to be unique in its relation between current and brightness. It might be possible to find some relation based on the brightness characteristics of a portion of the channel rather than the entire channel, but such an analysis would only be possible by fully imaging each event. For space based measurements of lightning, the electric fields have better correlation with the NLDN peak currents in CG lightning but the peak optical brightness from lightning is not a good indicator of peak currents. As we have seen in the case study in this chapter, the rocket measured optical intensity is usually brightest from the IC events following CG strokes and not the return strokes themselves in many cases.

7.9 Conclusion

We now have a better understanding of the close relation between CG and IC lightning. A CG discharge can initiate a stroke in an IC channel that has developed near to it. No doubt, the leader activity detected by the LDAR VHF system is related to the pre-stroke charge reconfigurations of the CG and the IC stroke. Once the CG stroke eliminates the charge, the IC channel responds to the new charge conditions. This type of activity was often observed during Thunderstorm III as the characteristic whistler signature we have called the "ghost whistler".

The altitude of the lightning emissions has been found to have a dramatic effect on the brightness observed at the rocket. CG events normally appear much dimmer than middle and high level IC events. The rocket optical with the simultaneous ground data have been invaluable to determine the timing and the types of lightning stroke that were observed.

There does not seem to be any evidence of a simple relationship between the optical brightness in CG strokes and the NLDN peak currents measured by the ground based silicon photodiode detector. This conclusion is at odds with some of the earlier work of Idone and Krider who found a relation based on photographs of triggered lightning strokes [*Idone and Orville, 1985b*]. In their study, two triggered flashes consisting of 20 strokes each were related to the film exposure densities. The peak currents ranged from 3 to 21 k-Amps. In the analysis done here, the light from the entire lightning channel is recorded, and the stroke currents range from 16 to 38 k-Amps.

The analysis we have done here agrees with the earlier conclusions reached by Guo and Krider [*Guo and Krider, 1982*]. Despite the earlier work by these authors it seems that a linear relation between the optical brightness and the peak currents is still being considered as a plausible research pursuit. The idea of using optical brightness of natural lightning as a proxy of the peak currents is very questionable for the reasons that have been given. The results of the study of multi-stroke flashes also shows no relation between the peak currents and the optical intensity. It is possible that some relation can be found for cases of imaged strokes, particularly near the channel base where the NLDN peak currents might be best related to the initial channel brightness. These would be special case studies, not practical for satellite, rocket or balloon sensors and more comparable to the work done by [*Idone and Orville, 1985b*].

The CG events that we have identified as M events form an interesting class of lightning strokes. The whistler waves generated by this type of lightning usually have higher amplitude ELF waves in comparison to the VLF wave intensities. We still find that the largest ELF intensities were for +CG events, although we do not have the optical record to tell if these

cases did in fact have continuing currents. It is unfortunate that for some of the strongest ELF events we do not have any optical data. This should be a focus of future studies, to characterize the optical signature of strong ELF lightning strokes.

More work needs to be done to see if the optical properties of lightning strokes can be related to the continuing currents of the strokes, and if the continuing currents really are the cause of the ELF lightning electromagnetic wave energy. Further, it remains to be discovered whether or not intracloud lightning strokes can be a source of strong ELF radiation or, if they consistently lack strong ELF wave energy compared to CG lightning.

Chapter 8

3-D LIGHTNING WAVE SIMULATIONS

A lightning simulation code developed by the Department of Electrical Engineering at Kanazawa University, Japan, under the direction of Professor Isamu Nagano, was used to simulate some of the lightning events at Wallops Island. The computer code calculates the full wave electromagnetic fields from a simulated lightning stroke. The radiated components are calculated in 3 dimensions, and the lightning radiation fields can be output at a given location in the ionosphere from a lightning stroke. The model can also show the time development of the radiated lightning fields in 2-D using azimuthal cuts from the 3-D computed solutions. The simulation code is computationally intensive, a single lightning simulation may take several days to run on linked computer workstations. Part of the initial development of the code was to model the electric fields over a thunderstorm in an effort to understand Sprite type emissions [*Miyamura et al.*, 1996].

The Kanazawa simulation results are compared to the measured fields on Thunderstorm III, and some interesting features appear in the simulations. There are harmonic emissions, much like the ones seen in the spectrograms of lower altitude lightning strokes, which are caused by multiple reflections between the earth and ionosphere. The 3-D simulations also give us some idea about how much larger the whistler wave amplitudes would be directly over the lightning strokes. A great benefit of the Kanazawa code is that it computes the electric field amplitudes up to 40 kHz frequencies, and supports some of the early findings from the SnS waveform data, in that the code results show considerable radiated intensity at frequencies above 20 kHz from lightning in the ionosphere [*Kelley et al.*, 1997].

The research using the model and comparing the results to the Thunderstorm III data set

is being continued, even after the writing of this thesis, in an effort to better understand the differences between the simulation and measurements.

8.1 Full-Wave Modeling of Lightning EM Fields

The Kanazawa model uses a transmission line model (TLM) similar to that developed by Lin et al. [Lin et al., 1980]. The lightning stroke that has been compared at different altitudes and ranges in Table 8.1 and Table 8.2 both use a stroke peak current of -50 kA. The lightning stroke currents are computed using a double exponential with two time constants τ_1 and τ_2 . The return stroke is given a velocity of $0.3c$. The lightning discharge current is approximated by the equation 8.1:

$$I(t) = I_0(e^{-t/\tau_1} - e^{-t/\tau_2}) \quad (8.1)$$

Here I_0 is the peak current, which is -50 kA unless otherwise noted. For the cases used here, τ_1 has been set to $50\mu\text{s}$ and τ_2 to $5\mu\text{s}$. The lightning current model does not include the corona field term, but this should not affect the computed results here since it is a slow varying current, with much smaller dI/dt [Uman, 1985; Lin et al., 1980]. The channel length, l is 5 km for all of the cases shown. This length is slightly longer than the average stroke lengths determined by LDAR and does not have the inverted "L" shape channel waveform as in the cases described in Chapter 6. One important characteristic of the vertical dipole radiation fields from lightning is that the maximum wave energy will radiate at angles slightly above the horizontal plane at 65 degrees [Krider, 1992]. This will affect the wave intensities with distance from the lightning, since different sub-ionosphere regions will receive different upward wave intensities, depending on distance from the source.

The model first calculates the source current time domain waveform from the source current described by equation 8.1. The wave fields are then Fourier transformed to the frequency domain and the fields are computed for the near field spherical waves. The spherical waves are then decomposed into plane waves and the electromagnetic fields are calculated

at the boundaries in the horizontally stratified model, matching the boundary conditions at each layer for the upward and reflecting waves. Each of the layers has a thickness of 1 km in the model.

The calculation method used in the Kanazawa model is limited to the electromagnetic field components only. A flat earth and horizontally stratified ionosphere are modeled using an electron density profile described by the IRI90 model. The IRI90 model is used in all of the calculations except for the results shown in Figure 8.1, which used the IRI95 density profile for the time of rocket flight. The IRI90 model has a lower electron density, especially in the F region. In the IRI90 model, the peak electron density, N_c , is 10^5 per cc compared to nearly 2×10^5 per cc in the IRI95 model for the Thunderstorm III flight conditions. The actual densities during the flight were probably more than double the IRI95 densities (see Chapter 4).

8.2 Model Results and Comparison with Thunderstorm III Measurements

The result from one of the model simulations of the whistler wave electric field waveform, E_x is shown in Figure 8.1. In this computer run, the whistler wave field E_x is computed directly above the lightning stroke at an altitude of 370 km. The IRI95 electron density profile was used with the conditions and local time of the rocket flight. The model lightning stroke had a peak current of -50 kA. The whistler wave electric field is shown up to 40 kHz. The results show that the peak whistler wave power is between 6 to 9.5 kHz, and there is a second lower power peak at 22 kHz. The dispersion of the simulation whistler is considerably smaller than was actually measured at 370 km. The model VLF dispersion was $1.0017 \text{ s}^{1/2}$, compared with an average of $1.8 \text{ s}^{1/2}$ measured at this altitude on Thunderstorm III.

The Kanazawa model calculation based on the IRI95 electron density profile, shows that the electron densities must have been higher than IRI95 at the time of flight. The results support the conclusion in Chapter 4 that the actual electron density profile was higher. Based on the IRI95 electron density, the calculated whistler dispersion in Chapter 4 at 370 km was

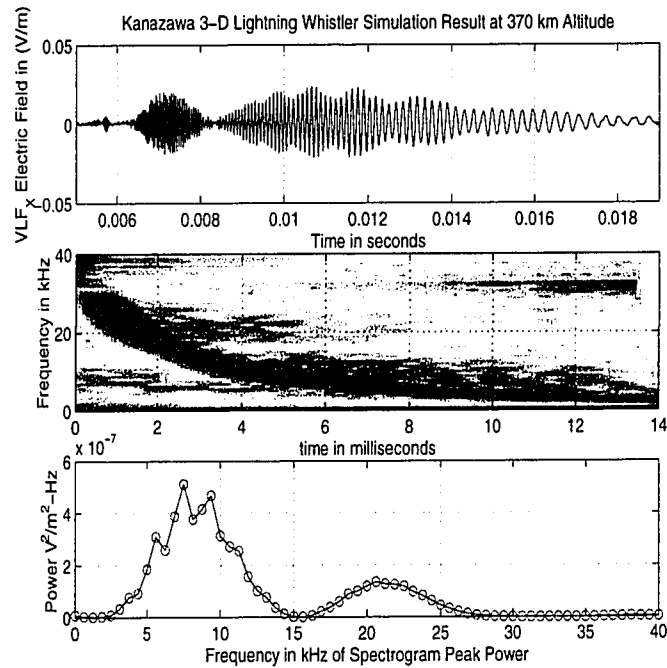


Figure 8.1: The University of Kanazawa computer model was used to simulate a lightning stroke at Wallops Island and to compute the whistler wave electric field E_x at an altitude of 370 km directly over the lightning stroke. The model used here was IRI95 electron density profile using the conditions at 01:00 UT at Wallops Island. The VLF electric field is considerably larger than the measured wave fields at this altitude, and the wave dispersion is less than the measured dispersions.

$1.08 \text{ s}^{1/2}$. The difference between the dispersion in the Kanazawa model whistler and the IRI95 calculated dispersion in Chapter 4 is probably caused by differences in the dip angle estimated for Wallops Island in the Kanazawa model inputs; $\theta = 10^\circ$ instead of $\theta = 20^\circ$. The dip angle would account for a 5% difference in the dispersions, since $D \propto 1/\cos(\theta)$. The larger measured whistler dispersions at the rocket cannot be accounted for by the dip angle input alone, and must be due to the higher electron density.

In the whistler spectrogram, there are bands of wave power at 20 kHz and below 15 kHz. These are caused by multiple reflections between the earth and ionosphere. The model runs using lower altitude cases also show similar multiple reflection effects which look very

similar to some of the measured tweek harmonics seen in the Thunderstorm III whistler spectrograms in Chapter 4.

The simulation results all have lower ELF wave amplitudes than the measured lightning events. By increasing the value of τ_1 and τ_2 , longer duration current moments could be simulated which would increase the ELF wave power in the simulations. This is planned for the future in order to model particular lightning cases such as the intense ELF whistler case at $t=488.166$ seconds.

8.2.1 *Simulations at Different Altitudes at Constant Range*

A number of simulations were made of whistler wave electric fields in the ionosphere at different altitudes and ranges from the lightning stroke. These computer simulations were made using the IRI90 electron density profile, and a stroke current of -50 kA. The whistler wave electric fields are compared to the Thunderstorm III measurements when appropriate in the summary data tables. In Table 8.1, the whistler amplitudes are compared at a range of 143 km from the lightning stroke. This range is most representative of conditions near rocket apogee for strokes originating from the main thunderstorm cell near Wallops. It is interesting that the Kanazawa model results are in good agreement in the F region of the ionosphere with the measured data from Thunderstorm III. Below the F region, the rocket fields are smaller than the model results, especially below 200 km. This is surprising since at the lower altitudes, the differences in electron density between the IRI90 model, and the low densities in this region recorded by the PFP and DC probe experiments suggest that it is the model that has overestimated the wave fields in this region of the ionosphere. The Kanazawa model results are however more comparable to the measured wave fields from Thunder HI and Thunder LO. The measured average wave fields from these rocket flights was 25 mV/m at 150 km with some cases having measured horizontal fields of nearly 50 mV/m at 154 km. The average horizontal fields from Thunder LO below 100 km was 45 mV/m [Siefiring, 1987]. It still seems that the model wave amplitudes are higher than the

measured wave fields from these flights. One of the critical parameters at the lower altitudes is the wave amplitude at the base of the ionosphere. The wave amplitude will vary depending on distance from the lightning dipole, with certain sub-ionosphere entry points receiving much higher wave fields depending on the dipole configuration [Uman, 1985]. A second variable is the conductivity profile used. The conductivity profile of the mesosphere is not well known yet could drastically influence the wave amplitudes at the base of ionosphere [Hale, 1996].

Table 8.1: The model used a 5 km long lightning dipole with a peak current $I_{pk} = -50$ kA. The range is constant at 143 km and the altitude is varied. Notice that the measured electric fields from Thunderstorm III are comparable in the F region at altitudes above 200 km. The values in parenthesis are the peak electric fields between 20 and 30 kHz calculated in the model. Rocket horizontal distances are given in parenthesis.

(a) wave amplitude had 2 main frequency peaks, at 4 to 8 kHz and 18 to 25 kHz, arriving within $500\mu s$ of flash.

(b) wave amplitude had 2 main frequency peaks; 4 to 8 kHz arrived after 8 ms and the 18 to 25 kHz waves given in parenthesis (), arrived prior to 6 ms.

Altitude (km)	Range (km)	Model $E_{x_{peak}}$ (mV/m)	Measured $E_{x_{peak}}$ (mV/m)
350	143	(6) 8_b	4 to 8 (80 km)
300	143	(6) 11_b	5 to 11 (70 km)
250	143	(14) 16_b	5 to 12 (50 km)
200	143	(25) 35_b	5 to 15 (40 km)
150	143	(-) 65_a	5 to 18 (210 km)
100	143	(-) 120_a	5 to 35 (230 km)
50	143	(-) 850_a	reentry (235 km)

8.2.2 Simulations at Different Ranges at a Fixed Altitude

An ideal rocket experiment would be able to place the instruments at different altitudes above the thunderstorm and at different distances. It is important to understand just how much larger the measured whistler wave electric fields might have been if the rocket had

been directly over the storm. The Kanazawa model yields some interesting results about the changes in the whistler wave amplitudes as a function of range, and these are summarized in Table 8.2. The radiation fields from the lightning stroke might be expected to decrease with distance as $1/R$ from the stroke, or at a somewhat slower rate since the wave fields are confined within a cylindrical geometry between the earth and ionosphere. The horizontal whistler electric fields seem to be decreasing at a faster rate than $1/R$, according to the model, though not as rapidly as $1/R^2$ decrease. The decrease in wave field amplitudes with

Table 8.2: The Kanazawa model computed the whistler wave fields at different ranges from the thunderstorm. The model used a vertical lightning dipole simulated with a peak current of $I_{pk}=50$ kA.

(a) wave amplitude had 2 main frequency peaks, at 4 to 8 kHz and 18 to 25 kHz, arriving within $500\mu s$ of flash.

(b) wave amplitude had 2 main frequency peaks; 4 to 8 kHz arrived after 8 ms and the 18 to 25 kHz waves given parenthesis (), arrived prior to 6 ms.

Altitude (km)	Range (km)	Model $E_{x_{peak}}$ (mV/m)	Measured $E_{x_{peak}}$ (mV/m)
150	0	500_a	-
150	60	240_a	-
150	70	235_a	-
150	100	150_a	-
150	143	65_a	5 to 18
350	0	(18) 24_b	-
350	143	(6) 8_b	4 to 8

horizontal distance in the F region is different than the changes in the radiated field amplitudes in the E region at 150 km according to the model results. The whistler wave amplitude above the lightning stroke in the F region at 350 km is 3 times larger than at a range of 143 km. In the E region, at 150 km altitude, the field over the stroke is about 7.5 times larger than at 143 km. According to the Kanazawa model, the horizontal field amplitudes at 100 km altitude increase from 120 mV/m to 750 mV/m directly over the stroke. At 50 km alti-

tudes E_z , also increases by nearly 7.5 times, from 0.95 V/m to nearly 6.5 V/m directly over the stroke. Near the lightning stroke, the static and induction fields from lightning become very important. Even within 150 km of the stroke at the base of the E region the transient electrostatic fields are of measurable intensity (i.e. mV/m vertical fields), as we have seen in Chapter 4.

These model results serve as a guide as to how much larger the whistler amplitudes might be directly over the thunderstorm. The whistler wave amplitudes are least affected by distance from the storm in the F region, and larger changes in amplitude occur in the E region and at lower altitudes. The F region peak whistler wave amplitudes would be expected to increase from 5 mV/m at rocket apogee to 20 mV/m directly over the storm, based on the Kanazawa model results. In the lower E region, the Thunderstorm III measured strokes at 100 km altitude with 30 mV/m fields would increase to 225 mV/m directly over the thunderstorm, if the distance scaling of the model is correct.

The electric field amplitudes are considerably larger in the simulations compared to the measured fields. Some of the cases are comparable to the fields measured by Thunderstorm II, but some of the calculated fields directly over the storm are much larger. The code does show some of the apparent features of the earth ionosphere waveguide tweak harmonics that were seen in many of the lightning spectrograms in Chapter 4. Another feature that is absent in the model are strong wave amplitudes in the lower ELF frequency ranges. These can be modeled using longer duration currents in the input model.

8.3 Conclusion

The whistler electric field amplitudes computed by the Kanazawa model were larger than the amplitudes measured by Thunderstorm III. We believe that some of the differences are due to the electron density profiles that were used in the model, which in all cases were lower than the estimated and measured densities at the time of flight. Some of the model results agree very well, particularly in the F region where the effects of the electron density profile

are not as critical to the computed wave amplitudes. There still is a significant difference in the measured wave dispersions. The dispersion differences are caused by the lower electron density and by the model inputs used for the local magnetic dip angle, 10° , instead 20° at Wallops Island.

The model whistler electric field amplitudes are more comparable at E region altitudes, below 250 km, to the average amplitudes measured by the Thunder Hi and Thunder Lo experiments. *Even so, the computed fields are usually larger than the average measured fields.*

The tweek harmonics seen in the whistler spectrograms in the data from Thunderstorm III are also apparent in some of the lower altitude model calculations. These harmonic emission bands are caused by multiple reflections between the ocean and ionosphere. This ringing effect is enhanced in the model simulations by the higher conductivity of sea water compared to land.

It is interesting that in the other simulations of lightning electromagnetic waves at lower altitudes, the model does not show any evidence of a field aligned electric pulse, but it does show that there is significant whistler wave power above 20 kHz, especially in the region between 20 and 30 kHz. The next step obviously is to re-run the simulations using the electron density profile found in Chapter 4 and to include the vertical wave fields. We also wish to include the source effects of longer duration lightning currents and correct the local magnetic dip angle used in the model inputs.

Chapter 9

CONCLUSION

There have only been a limited number of thunderstorm over-flights by rockets and there remain many puzzles in the in the thunderstorm electrodynamic processes in the mesosphere and ionosphere.

The electric field data has been used to successfully reconstruct an estimate of the F region electron density profile using the measured dispersion of the lightning whistlers. Here we have used fractional hop whistlers recorded by the rocket at different altitudes of the flight. The results are in agreement with the instruments used to measure electron density on the rocket, and with the data from a digisonde profiler in Bermuda.

The study of lightning using the LDAR VHF mapping system has shown much about the way charge moves in the thunderstorm and where the electrical activity takes place. The velocity of lightning channel leaders, inferred from the LDAR measurements, shows a decrease in velocity with altitude. This results is consistent with the recent research work of Proctor in South Africa [*Proctor, 1997*]. The thunderstorm at Wallops Island shows a bimodal distribution in the electrical activity, the low altitude center occurs at temperature levels of 0 to -10°C and the upper charge zone at -40 to -50°C . The lightning channel orientations have been studied using the LDAR VHF system. Incloud lightning channels vary in orientation from nearly horizontal channels observed in many cases for intracloud activity at 7 to 12 km altitudes to vertical channels that move charge in the cloud in response to cloud-to-ground lightning. Cloud to ground channels are typically much more vertical with some lateral extent in the lower cloud regions. The LDAR system did not produce any data on positive cloud-to-ground lightning channels, only the negative cloud-to-ground strokes

produced trigger activity in the channels.

This rocket experiment has been successful in showing more about the nature of the electromagnetic precursor pulse. This pulse was not unambiguously resolved in the SnS electric field waveform capture instruments, but even so, much more is now known about it. The pulse occurs most frequently from negative cloud-to-ground lightning. There were no observed occurrences of the pulse in response to the few observed positive CG lightning strokes which occurred at times when the rocket observed the pulse. So far, there is no satisfactory explanation, but there were only 3 such cases on which the preliminary conclusion is based.

The pulse can be produced by distant lightning strokes and therefore it is not caused by the electrostatic fields. Polarization of the lightning electromagnetic waves seems to play an important role in the formation of the electric pulse. The pulses are usually not produced by strong incloud lightning strokes.

The channels of cloud-to-ground lightning radiate more vertically polarized waves than incloud lightning stroke channels. The field aligned electric pulse is most often stimulated by negative cloud-to-ground lightning strokes, but rarely by incloud lightning. A necessary ingredient to the generation of the electric pulse seems to be strong vertically polarized electric fields. The horizontally polarized fields of incloud lightning do not seem to cause a measureable pulse.

The pulse does not seem to be caused by electrostatic effects from the thunderstorm discharge. The evidence for this is threefold: 1) the direction of the parallel electric field is usually in the opposite direction expected for a negative cloud-to-ground discharge, 2) the pulse is observed for cloud-to-ground lightning strokes as far away as N. Carolina, and 3) the pulse polarity has been observed to be predominantly positive, but some strokes also produce negative polarity pulses.

The data from Thunderstorm III has led us to conclude that the field aligned electric pulse is really made up of electromagnetic waves which do not produce aligned, organized

electron particle accelerations. Even though the VLF pulse appears unipolar, it seems that it does not have the related properties expected of a unipolar pulse of 1 to 4 ms duration. There is no magnetic field response in the fluxgate or the VLF search coil instruments during the time of the pulsations. The pulse should drive a sizable parallel current since it would be able to accelerate the electrons to at least 20 to 30 times their thermal velocity, but this is not observed in the UNH electrostatic analyzer experiments.

Simultaneous measurements from the ground and rocket of NLDN located cloud-to-ground lightning strokes show that incloud lightning often occurs immediately following the discharge to ground. These strokes are distinct in their appearance in the VLF electric field spectrograms and have a double whistler trace . The rocket optical signature shows a dimmer optical flash from the CG stroke followed by a much brighter IC flash. The brighter flash from the IC stroke is the result of the higher altitude of the stroke in the cloud and subsequently less light attenuation and scattering to the rocket. LDAR measurements show that these IC stroke channels often form over regions of the lower CG lightning channel activity.

Ground based optical flash data of more than 100 strokes were recorded during the experiment. We looked at individual lightning flashes that were recorded by the NLDN network and compared the stroke brightness with the NLDN estimated peak current in each stroke. In the cases studied, we did not find a relation between the stroke optical brightness and the NLDN peak current.

This result along with the more complex structure measured at the rocket of lightning optical characteristics in individual strokes causes us to question whether orbiting satellite instruments will be able to determine stroke currents from optical intensity alone. We also question whether CG and IC flash rates can be discriminated by satellite instruments. VLF electric field measurements in conjunction with optical data might offer a means of such a discrimination between IC and CG strokes.

BIBLIOGRAPHY

- Al'pert, Y. L., *Space Plasma*, vol. 2, Cambridge University Press, 1990.
- Baker, M. B., H. J. Christian, and J. Latham, A computational study of the relationships linking lightning frequency and other thundercloud parameters., *Quarterly Journal of the Royal Meteorological Society*, 121(527), 1525–48, 1995.
- Baker, S. D., Sounding rocket electric and magnetic field measurements above thunderstorms, Ph.D. thesis, Cornell University, 1998.
- Battan, L. J., *Radar Observation of the Atmosphere*, University of Chicago Press, Chicago, IL, 1973.
- Brice, N. M., and R. L. Smith, Lower hybrid resonance emissions, *JGR*, 70(1), 71–80, 1965.
- Brook, M., C. Rhodes, O. Vaughn, O. R. E., and V. B., Nighttime observations of thunderstorm electrical activity from a high altitude airplane, *JGR*, 90(D4), 61111–6120, 1985.
- Brown, G. M., ed., *Progress in Radio Science 1960-1963*, vol. III, Elseier Publishing Company, 1965, review papers presented at Assembly of URSI, Tokyo, September 1963.
- Burke, C. P., and D. L. Jones, On the polarity and continuing currents in unusually large lightning flashes deduced from elf events, *JATP*, 58(5), 531–534, 1996.
- Cain, J. C., I. R. Shapiro, J. D. Stolarik, and J. P. Heppner, A note on whistler waves observed above the ionosphere, *JGR*, 66(9), 2677–80, 1961.
- Colvin, J., and C. Mitchell, An empirical study of the nuclear explosion-induced lightningseen on ivy-mike, *JGR*, 92(D5), 5696–5712, 1987.

- Dowden, R. L., and C. D. Adams, Size and location of lightning-induced ionisation enhancements from measurement of vlf phase and amplitude perturbations on multiple antennas, *JATP*, 55, 1335–1359, 1993.
- Dowden, R. L., L. Brundel, and W. L. Lyons, Detection and location of red sprites by vlf scattering of subionospheric transmissions, *GRL*, 23, 1737–40, 1996.
- Engineering, H., *Silicon Photodectors*, Hamamatsu Corporation, Tokyo, Japan, 1990.
- Fisher, R. J., G. H. Schnetzer, R. Thottappillil, V. Rakov, M. Uman, and J. Goldberg, Parameters of triggered-lightning flashes in florida and alabama, *JGR*, 98(D12), 22887–902, 1993.
- Fleagle, R., and J. Businger, *Atmospheric Physics*, Anthenium Press, 2nd edn., 1981.
- Goldberg, R. A., S. A. Curtis, J. R. Barcus, C. Siefiring, and L. Hale, Detailed structure of magnetospheric electron bursts of precipitated by lightning, *JGR*, 92, 2505, 1987.
- Gomes, C., and V. Cooray, Correlation between the optical signatures and current wave forms of long sparks: applications in lightning, *Journal of Electrostatics*, 1998.
- Goodman, S., H. Christian, and D. Rust, A comparison of the optical pulse characteristics of intracloud and cloud-to-ground lightning as observed above clouds, *JATP*, 27, 1369–1381, 1988.
- Guo, C., and E. P. Krider, The optical and radiation field signatures produced by lightning return strokes, *JGR*, 87(c11), 8913–8922, 1982.
- Hale, L. C., On the coupling of energy in parallel pland waveguides, *IEEE Transactions on Electromagnetic Compatibility*, 1996.
- Helliwell, R., *Whistler Waves*, Simon and Schuster, 1964.

- Hepburn, F., Atmospheric waveforms with very low frequency components below 1kc/s known as slow tails, *Journal of Terrestrial and Atmospheric Physics*, 10, 266–287, 1957.
- Holzworth, R. H., and Y. T. Chiu, *Sferics in the Stratosphere in Atmospheric Electricity*, H. Volland editor, vol. 1, chap. 2, pp. 235–264, CRC Press, Boca Raton, FL, 1982.
- Holzworth, R. H., R. Winglee, B. Barnum, and Y. Li, Lightning whistler waves in the high latitude magnetosphere, *JGR*, 1998 -in press.
- Idone, V., and R. Orville, Correlated peak relative light intensity and peak current in triggered lightning subsequent return strokes, *JGR*, 90(D4), 6159–6164, 1985a.
- Idone, V. P., and R. E. Orville, Correlated peak relative light intensity and peak current in triggered lightning subsequent return strokes, *JGR*, 90(D4), 6159–6164, 1985b.
- Illingworth, A. J., Charge separation in thunderstorms: Small scale processes, *JGR*, 90(D4), 6026–6032, 1985.
- Imhof, W. L., E. Gaines, and H. Voss, Results from the seep active space plasma experiment: Effects on the ionosphere, *RS*, 1985.
- Jackson, R., *Classical Electromagnetics*, Berkely University Press, CA, 2nd edn., 1980.
- Jensen, M. D., and K. D. Baker, Measuring ionospheric electron density using the plasma frequency probe, *Journal of Spacecraft and Rockets*, 29(1), 91–95, 1992.
- Jordan, D., V. Rakov, W. Beasley, and M. Uman, Luminosity characteristics of dart leaders and return strokes in natural lightning, *JGR*, 102(D18), 22025–22032, 1997.
- Kelley, M. C., et al., Electrical measurements in the atmosphere and the ionosphere over an active thunderstorm: 1) campaign overview and initial ionospheric result, *JGR*, 90(D6), 9815, 1985.

- Kelley, M. C., J. G. Ding, and R. H. Holzworth, Intense ionospheric electric and magnetic field pulses generated by lightning., *GRL*, 17(12), 2221–4, 1990.
- Kelley, M. C., S. D. Baker, R. H. Holzworth, and P. A. and S. A. Cummar, Lf and mf observations of the lightning electromagnetic pulse at ionospheric altitudes., *GRL*, 24, 1111, 1997.
- Kintner, P. M., R. Britain, M. C. Kelley, D. L. Carpenter, and M. J. Rycroft, In situ measurements of transionospheric vlf wave injection, *JGR*, 88(A9), 7065–73, 1983.
- Kitagawa, N., and M. Brook, A comparison of intracloud and cloud-to-ground lightning discharges, *JGR*, 65(4), 1189–1201, 1960.
- Krehbiel, P. R., M. Brook, and R. McCrory, An analysis of the charge structure of lightning discharges to ground, *JGR*, 84(C5), 2432–2456, 1979.
- Krider, E. P., On the electromagnetic fields, poyting vector and peak power radiated by lightning return strokes, *JGR*, 97(D14), 15913–15917, 1992.
- Laaspere, T., and H. A. Taylor, Comparison of certain vlf noise phenomena with the lower hybrid resonance frequency calculated from simultaneous ion composition measurements, *JGR*, 75(1), 97–106, 1970.
- Langel, R. A., Igrf, 1991 revision, *EOS Trans.*, 73(182), 1992.
- Li, Y., Electrical and optical phenomenon over thunderstorms, Ph.D. thesis. Univeristy of Washington, 1993.
- Lin, Y. T., M. A. Uman, and R. B. Standler, Lightning return stroke models, *JGR*, 85, 1571–1583, 1980.
- Mackerras, D., Automatic short range measurement of the cloud flash ratio in thunderstorms, *JGR*, 90(D4), 6195–6201, 1985.

- Marshall, L. H., L. C. Hale, C. L. Croskey, and W. A. Lyons, Electromagnetics of sprite and elve-associated sferics, *JATP*, 60, 771–786, 1998.
- McCarthy, M. P., and G. K. Parks, On the modulations of x ray fluxes in thunderstorms, *JGR*, 97, 5857–5864, 1992.
- Miyamura, K., I. Nagano, S. Yagitani, and Y. Murakami, Full wave calculation of 3d vlf/lf wave fields radiated from a lightning discharge, in *Proceedings of ISAP*, pp. 701–704, Chiba, Japan, ISAP, ISAP, 1996.
- Nagano, I., X. Wu, S. Yagitani, K. Miyamura, and H. Masumoto, Unusual whistler with very large dispersion near the magnetopause: Geotail observations and ray-tracing modeling., *JGR*, 103(A6), 11827–40, 1998.
- Orville, R., A. Weisman, R. Pyle, R. Henderson, and R. Orville, Cloud-to-ground lightning flash characteristics from june 1984 through may 1985, *JGR*, 92(D5), 5640–5644, 1987.
- Parks, G. K., *Physics of Space Plasmas*, Addison-Wesley, Redwood City, CA, 1991.
- Pinto, O., R. B. Gin, I. R. Pinto, and O. M. Jr., Cloud-to-ground lightning flash characteristics in southeastern brazil for the 1992-1993 summer season, *JGR*, 101(D23), 29627–29635, 1996.
- Poehler, H. A., and C. L. Lennon, Lightning detection and ranging system lidar system description and performance objectives, Technical Memorandum 74105, NASA, 1979.
- Proctor, D. E., A hyperbolic system for obtaining vhf radio pictures of lightning, *JGR*, 76(6), 1478–1489, 1971.
- Proctor, D. E., Vhf radio pictures of lightning flashes to ground, *JGR*, 93(D10), 12683–12727, 1988.
- Proctor, D. E., Lightning flashes with high origins, *JGR*, 102(D2), 1693–1706, 1997.

- Rakov, V., R. Thottappillil, M. Uman, and P. Barker, Mechanism of the lightning m component, *JGR*, *D12*(100), 25701–25710, 1995.
- Ratcliffe, J. A., *The Magneot-Ionic Theorey and its Apppllications to the Ionosphere*, Cambridge University Press, 1959.
- Reising, S. C., U. S. Inan, and T. F. Bell, Evidence for continuing current in sprite-producing cloud-to-ground lightning, *GRL*, *23*(24), 3639–42, 1996.
- Rhodes, C., X. Shao, P. Krehbiel, R. Thomas, and C. O. Hayenga, Observations of lightning phenomena using radio interferometry, *JGR*, *99*(D6), 13059–13082, 1994.
- Rosenberg, S., and W. Gekelman, Electric field measurements of directly converted lower hybrid waves at a density striation, *GRL*, *25*(6), 865–868, 1998.
- Rowland, H. R., J. Fernsler, J. Huba, and P. Bernhardt, Lightning driven emp in the upper atmosphere, *GRL*, *22*, 361–364, 1995.
- Rowland, R. F. F. H. L., Models of lightning-produced sprites and elves, *JGR*, *101*(D23), 29653–29662, 1996.
- Rust, W. D., D. MacGorman, and W. L. Taylor, Photographic verification of continuing current in positive cloud-to-ground flashes, *JGR*, *90*(D4), 6144–6146, 1985.
- Rustan, P. L., M. A. Uman, D. G. Childers, and W. H. Beasley, Lightning source locations from vhf radiation data for a flash at kennedy space center, *JGR*, *85*(C9), 4893–4903, 1980.
- Sao, K., M. Y. S. Tanahashi, and W. Taylor, Genesis of slow tail atmospherics deduced from frequency analysis and association with vlf componenets, *JATP*, *32*, 1147–1151, 1970.
- Schonland, B. F., *Atmospheric Electricity*, Methuen Co. ltd., London, 1932.

- Sentman, D. D., and E. Wescott, Observations of upper atmosphere optical flashes recorded from an aircraft, *GRL*, 20, 2857–2860, 1993.
- Shvets, A. V., and M. Hayakawa, Polarisation effects for tweek propagation, *JASTP*, 60(4), 461–469, 1998.
- Siefring, C., Upward propagating electric fields from thunderstorms and vlf transmitters, Ph.D. thesis, Cornell University, 1987.
- Siefring, C., and M. C. Kelley, Analysis of standing wave patterns in vlf transmitter signals: effects of sporadic E layers and in situ measurements of low electron densities, *JGR*, 96(A10), 17813–26, 1991.
- Smith, R., R. A. Helliwell, and I. W. Yabroff, A theory of trapping of whistlers in field-aligned columns of enhanced ionization, *JGR*, 65(3), 815–823, 1960.
- Smith, R. L., I. Kimura, J. Vigneron, and J. Katsufakis, Lower hybrid resonance noise and a new ionospheric duct, *JGR*, 71(7), 1925–27, 1966.
- Solomon, R. N., Modelling of thunderstorm charging and flash rates, Ph.D. thesis, University of Washington, 1997.
- Stolzenburg, M., D. Rust, and T. Marshall, Electrical structure in thunderstorm convective regions 2. isolated storms, *JGR*, 103(D12), 14079–96, 1998a.
- Stolzenburg, M., D. Rust, B. Smull, and T. Marshall, Electrical structure in thunderstorm convective regions 1. mesoscale convective systems, *JGR*, 103(D12), 14059–78, 1998b.
- Taranenko, Y., U. Inan, and T. Bell, Interaction with the lower ionosphere of electromagnetic pulse from lightning, heating, attachment, and ionization, *GRL*, 1993.
- Taylor, W. L., and K. Sao, Elf attenuation rates and phase velocities observed from slow components of atmospherics, *Radio Science*, 5(12), 1453–1460, 1970.

- Thomason, L., and E. Krider, The effects of clouds on the light produced by lightning, *JAS*, 39(9), 2051–2065, 1982.
- Thottappillil, R., J. Goldberg, V. Rakov, M. Uman, R. Fisher, and G. Schnetzer, Properties of m components from currents measured at triggered lightning channel base, *JGR*, D12(100), 25711–25720, 1995.
- Uman, M. A., *Lightning*, Dover, 1984.
- Uman, M. A., Lightning return stroke electric and magnetic fields, *JGR*, 90(D4), 6121–6130, 1985.
- Uman, M. A., R. E. Orville, A. Sletten, and E. P. Krider, Four meter sparks in air, *J. Appl. Phys.*, 39, 5162–5168, 1968.
- Vaughan, O., M. L. Curtner, and D. Yeates, Circuit detects faint flashes against bright background, *NASA Tech Briefs*, pp. 19–21, 1991.
- Volland, H., *Atmospheric Electrodynamics*, Springer-Verlag, New York, 1984.
- Voss, H. D., et al., Lightning-induced electron precipitation, *Nature*, 312, 740, 1984.
- Wait, J. R., On the theory of the slow-tail waveform, *JGR*, 65(7), 1939–1946, 1960.
- Wait, J. R., *Electrodynamics of VLF Waves*, Pergamon Press, 1967.
- Warwick, J. W., C. O. Haynga, and J. Brosnahan, Interferometric directions of lightning sources at 34 mhz, *JGR*, 84(C5), 2457–62, 1979.
- Williams, E., S. Rutledge, S. Geotics, N. Renno, and E. Ramussen, A radar and electrical study of tropical "hot towers", *Journal of Atmospheric Sciences*, 40, 1386–1395, 1992.
- Williams, E. R., Large-scale charge separation in thunderclouds, *JGR*, 90(D4), 6013–6025, 1985.

Wilson, C. T. R., A theory of thundercloud electricity, *Proc. Phys. Soc.*, 37(32D), 1925.

Yavetz, I., Between high science and practical engineering: two studies of lightning by simulation, *Physis*, 33(1-3), 221–258, 1996.

Appendix A

APPENDIX A: ROCKET OPTICAL INSTRUMENT

The rocket optical instrument is shown in Figure A.1. The instrument consists of 3 separate silicon photodiode detectors. The instrument is designed to automatically subtract the DC background light and dark current which is inherent in this type of system. The center channel, referred to as the white light or wide-band detector, is used as an optical trigger for the SnS waveform burst memory system [Baker, 1998]. The two other channels have wide-band color glass optical filters which are used to discriminate the broadband color differences between optical Sprite events and CG and IC strokes.,

The instrument uses a large area photodiode sensors which have a photo-sensitivity within an order of magnitude of a photo-multiplier (PMT) type system. An optical irradiance at the sensor input of only 1 pW/cm^2 will produce a minimum detectable output signal of 1.2 mV. The instrument automatically subtracts the dark current and the DC background under most low light levels and nighttime conditions. The circuit diagram for the rocket optical instrument is shown in Figure A.2.

Each of the three Hamamatsu photodiodes has a surface area of 1 cm^2 and is reversed biased in the circuit to increase sensitivity and response time. Large area photodiodes have larger inherent capacitance which must be matched in the current-to-voltage conversion portion of the circuit that is directly connected to the photodiode. A 2 pF capacitor is used in parallel with the feedback resistor. This combination controls the maximum RC time response of the system, which is about 4.1 kHz. There is a trade off between photo-sensitivity and speed of response of the system. In the current-to-voltage conversion portion of the circuit, the feedback resistance can be selected to give greater sensitivity, but this is finally

limited by the photodiode noise or dark current level, about 5 picoamps for a resistance of $100\text{ M}\Omega$.

The subtraction of the DC background light from the output signal is a difficult problem in the design of lightning optical flash detectors. The circuit design used for Thunderstorm-III subtracts the DC background and photodiode dark current after the current to voltage converter section of the circuit. A second method of background subtraction is to subtract the background signal at the photodiode itself by inverting the DC background signal and feeding it directly into the photodiode output. This is the method that has been used in the NASA Optical Transient Detector [Vaughan *et al.*, 1991]. This method increases the sensor range and makes possible daylight detection of optical lightning signals.

The background cancelation is done using a fast MOSFET switched DC background subtraction circuit. Prior to a light impulse, dark current and low frequency (i.e. 2 Hz) levels are continuously monitored and subtracted from the output. During a lightning flash, the background levels are clamped at the pre-stroke DC level and subtracted from the transient output signal. After the optical transient, the DC level is updated.

The optical detector achieves a 30 dB dynamic range by using a square rooting circuit to compress the output signal voltage which ranges from 1.5 mV to 15.8 V, compressed into a 0 to 4.8 V range. The full circuit schematic for a single detector channel is shown in Figure A.2.

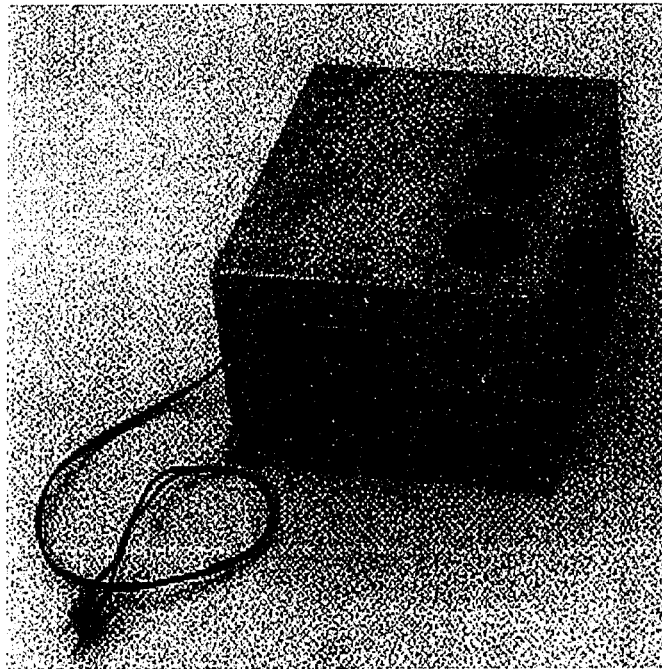


Figure A.1: The University of Washington rocket optical experiment used 3 separate channels. The center optical detector was used for triggering the SnS burst memory system. The two other channels used wide band color glass filters to discriminate CG and IC strokes from Sprite associated activity.

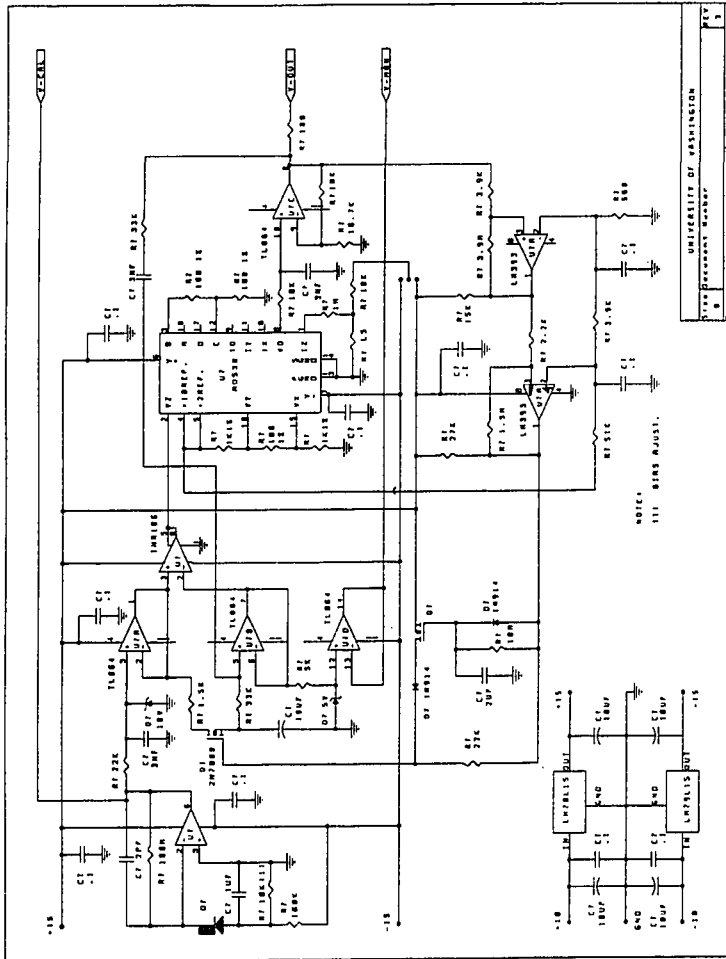
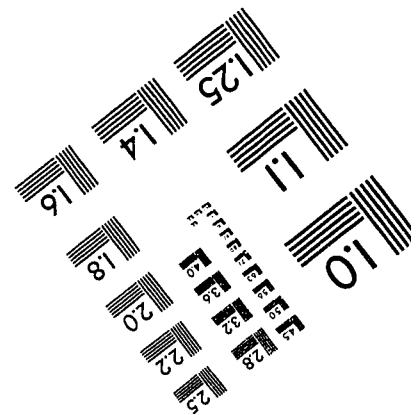
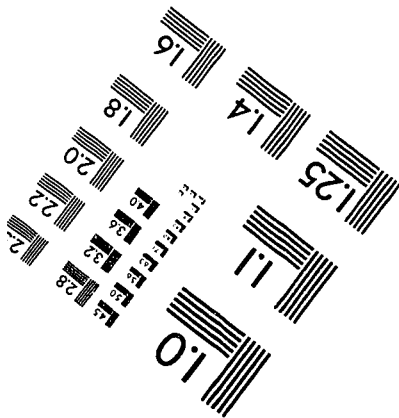
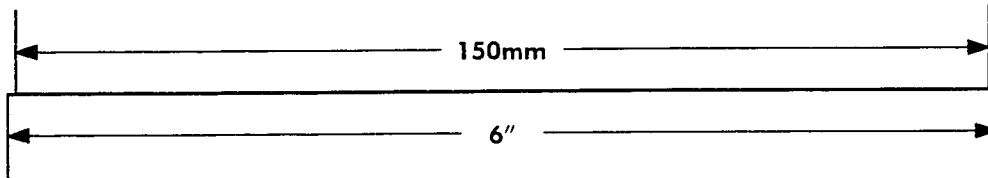
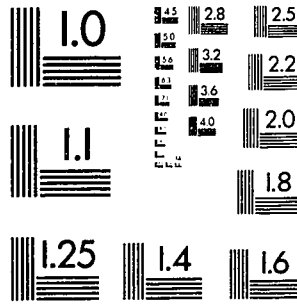
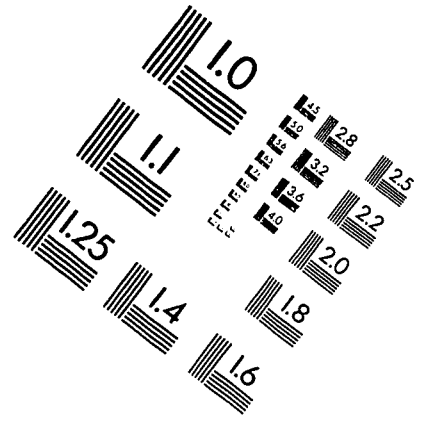
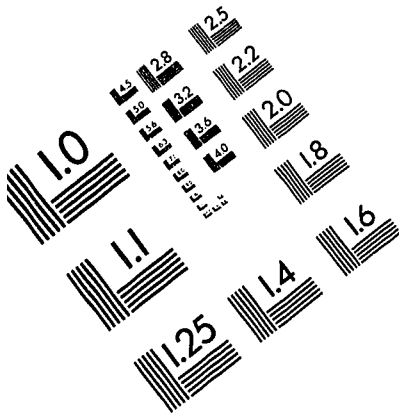


Figure A.2: The University of Washington rocket optical experiment used a new method of DC background cancellation. The quasi DC background and photodiode dark current are automatically subtracted from the output.

VITA

Benjamin Heath Barnum was born in Syracuse, New York on February 9, 1957 to Priscilla and Theron Crouse Barnum. He graduated from the Putney School in Vermont in May 1975. After working as an electronics technician in Boston, he attended the University of Colorado in Boulder and graduated with a BA in Physics and minors in Computer Science and Mathematics and Anthropology in 1983. After graduation, he worked at NOAA in the Wave Propagation Lab in Boulder working on radar wind profiling systems and microwave temperature systems. In 1984, he moved to Seattle to work for the Boeing Company as an engineer. In 1989 he moved to San Diego, California to work at McDonnell Douglas. After many years away from school, he returned to Seattle to be a full time Graduate Student at the University of Washington, Seattle, Washington, in the Geophysics Program. He received a Master's Degree in Geophysics in May 1993.

IMAGE EVALUATION TEST TARGET (QA-3)



APPLIED IMAGE, Inc
1653 East Main Street
Rochester, NY 14609 USA
Phone: 716/482-0300
Fax: 716/288-5989

© 1993, Applied Image, Inc., All Rights Reserved